Arming, pseudotyping, and enhancing the efficacy of oncolytic measles virus for a better cancer therapeutic

Serge Neault

Thesis submitted to the University of Ottawa in partial fulfillment of the requirements for the Doctorate in Philosophy degree in Biochemistry

Department of Biochemistry, Microbiology, and Immunology

Faculty of Medicine

University of Ottawa

Ottawa, Ontario, Canada

TABLE OF CONTENTS

ABSTRACT

Everyone knows someone affected by cancer. It is a heterogeneous malignancy requiring different approaches depending on the source, aggressiveness, and stage of the disease. To this end, innovative cancer therapies are required to conquer the unique obstacles posed by each type of cancer. One emerging therapeutic avenue employs the use of oncolytic viruses. Oncolytic viruses are predominantly attenuated viruses that specifically replicate in cancerous cells, which often have defective anti-viral responses, while leaving normal tissue unaffected. The inability of certain cancers to counter viral infections stems from a defective interferon pathway utilized by the malignant cells for unregulated proliferation. This ingenious exploitation of the cancer's double-edged attribute led to numerous oncolytic virus clinical trials presently culminating in an approved oncolytic virus therapy, Talimogene laherparepvec, for the treatment of advanced melanoma. Oncolytic measles virus is currently being evaluated in several pre-clinical and clinical cancer trials. This virus offers many advantages as a replicating cancer therapeutic such as an excellent safety profile, oncotropic traits, and permissiveness for enhancement via genetic engineering. Even so, further improvements of oncolytic measles virus may be required to overcome the various complexities that each type of cancer poses. Some concerns are also inherent to the use of measles virus itself, such as pre-existing neutralizing antibodies towards the virus from routine immunization. This thesis outlines three distinct projects which aim to improve oncolytic measles virus as a cancer therapeutic. Firstly, a novel pseudotyping platform for oncolytic measles virus is described as an efficient and robust system for viral envelope exchange for the purpose of evading neutralizing antibodies. Secondly, oncolytic measles virus armed with granzyme B displayed increased oncolytic and proinflammatory activity. Finally,

synergizing oncolytic measles virus with viral sensitizers enhanced the replication and cancer cell killing ability of the virus in both human and murine cancer models. Each project uniquely demonstrated advances in improving oncolytic measles virus so it may surmount the current challenges facing it as a cancer therapeutic.

ACKNOWLEDGEMENTS

Completing this degree would not have been possible without the help and support of my colleagues. Firstly, I would like to thank Dr. Jean-Simon Diallo and his team for including me as a member of his lab. The accomplishments achieved by combining viral sensitizers and oncolytic measles virus were only realized because of their professional and financial support. Specifically, Dr. Rozanne Arulanandam for her expertise in experimental design and for her edits of Chapter 5, and Andrew Chen for his invaluable experience with the *in vivo* experiments. I would like to underscore my gratitude for Dr. Jean-Simon Diallo as my time as a graduate student at the Ottawa Hospital Research Institute would not have been possible without him.

Next, I would like to thank Dr. Guy Ungerechts for the inspiration, mentorship, and expertise he offered during my time as a graduate student. His endless motivation and compassion towards cancer research makes him a true role model that I strive to emulate. I would like to thank Dr. Sascha Bossow (aka: crazy German guy) for being a great mentor. The expectations were always very high but, in turn, this drove me to be a better scientist. Likewise, I would like to thank Dr. Mathias Leber for his incredible attention to detail and meticulous organizing ability; while others were out of reach, Mathias was always there holding down the fort. Also, I would like to especially thank him for the arduous task of revising my entire thesis. I would like to thank Dr. Carole Achard for her insight and expertise in the lab, and for always being available to lend an ear at moment's notice. Additionally, I would like to thank the countless colleagues that I have met throughout the years that I can now call friends. Thank you to the funding and donation organizations for their financial support, without which, none of this research would have occurred.

Thank you to my parents René and Josée Neault, and my sister Carine Neault for their support during the course of my degree. You have always made an effort to appreciate my work and support my career. It was a reassuring reminder that no matter what happened, you would support me and that everything will work out in the end.

Finally, thank you to my wife Dr. Nafisa Neault for her sacrifice, empathy, and support during the course of my degree. I cannot emphasize enough how none of this would have been possible without you. Your professional and personal contributions were countless and guided me in the right direction. I could not ask for a more loving individual who shares my passion for science. Last but not least, I would like to thank my son Zayan for the inspiration to continue to achieve my goals. While I could have passed on the constant banging on the upper floor while I was writing my thesis in the basement, you were a constant reminder of why I needed to strive for success. Thank you.

LIST OF ABREVIATIONS

ahGZMB	Active human granzyme B
ANOVA	Analysis of variance
ATU	Additional transcription unit
BSA	Bovine serum albumin
cDNA	Complementary deoxyribonucleic acid
CDV	Canine distemper virus
CEA	Carcinoembryonic antigen
CIU	Cell infectious units
CPE	Cytopathic effect
CTL	Cytotoxic lymphocytes
cy	Cytoplasmic
DMEM	Dulbecco's modified Eagle's medium
DMF	Dimethyl fumarate
DNA	Deoxyribonucleic acid
ec	Ectoplasmic
ECM	Extracellular matrix
EGFP	Enhanced green fluorescence protein
EGFR	Epidermal growth factor receptor
F	Fusion protein
FDA	Food and Drug Administration
FLUC	Firefly luciferase
GAPDH	Glyceraldehyde 3-phosphate dehydrogenase
GM-CSF	Granulocyte macrophage colony-stimulating factor
GZMB	Granzyme B
H	Hemagglutinin protein
HDAC	Histone deacetylases
HSV	Herpes simplex virus
ICD	Immunogenic cell death
IFN	Interferon
IPA	Ingenuity pathway analysis
ISG	Interferon-stimulated gene
IT	Intratumorally
JAK	Janus kinase
L	Large Protein
M	Matrix protein
MCS	Multiple cloning site
MeV	Measles virus
MOI	Multiplicity of infection
mRNA	Messenger RNA

N	Nucleocapsid protein
N.Ctrl	Negative control
NDV	Newcastle disease virus
NF-κB	Nuclear factor κB
NK	Natural killer cells
ORF	Open reading frame
OV	Oncolytic virus
P	Phosphoprotein
PCR	Polymerase chain reaction
PDV	Phocine distemper virus
RFP	Red fluorescence protein
RNA	Ribonucleic acid
RT-PCR	Reverse transcription-PCR
scFv	Single-chain antibody
SLAMF1	Signaling lymphocyte activation marker
STAR	Six-his-tagging and retargeting
STAT	Signal transducer and activator of transcription
TCID50	50% tissue culture infective dose
tm	Transmembrane
TPM	Transcripts per kilobase million
TPMV	Tupaia paramyxovirus
T-Vec	Talimogene laherparepvec
uBahGZMB	Ubiquitin active human granzyme B
VP	Viral passage
VS	Vanadyl sulfate
Vse	Viral sensitizer
VSV	Vesicular stomatitis virus

LIST OF FIGURES

LIST OF TABLES

CHAPTER 1: GENERAL INTRODUCTION

1.1 AN INTRODUCTION TO CANCER

It is estimated that, in 2020, there were 225,800 newly diagnosed cancer cases in Canada alone, consequently classifying it as one of the most prevalent group of diseases in the country. Moreover, an estimated 83,300 people in Canada have died in 2020 from this disease[1]. A more in depth look at any particular type of cancer reveals the complexity of the disease with multiple biochemical pathways responsible for driving the progression of that specific class of malignancy. A combination of factors arising from various sources, such as environmental elements and genetic predisposition, can contribute to the dysregulation of key regulatory pathways such as metabolic or cellular processes[2] . These include upregulation of growth signals and angiogenesis, evading apoptosis, and desensitization to anti-proliferative signals[3]. By derailing the fundamental mechanisms that ensure a coherent coordination within a biological system, these dysregulations can induce a cancerous malignancy.

The type 1 interferon (IFN) signaling pathway is a major regulatory component involved in the malignancies of certain cancers[4]. In normal conditions, IFNs can activate a vast panel of signaling pathways such as antiviral, anti-proliferative, immunomodulatory, and pro-apoptotic responses[4,5]. Hence, the dysregulation of the IFN response can have disastrous systemic effects. For example, a defective IFN signaling pathway has been attributed to increased cellular proliferation with a rise in susceptibility to spontaneous tumor formation[6].

The IFN signaling pathway is a component in the cellular antiviral response and, through the activation of interferon-stimulated genes (ISG), leads to an anti-viral response which, in turn, blocks viral translation, replication, and budding[7]. A defect in the IFN signaling pathway has been attributed to an increase in local susceptibility to viral infection and propagation[8]. The IFN signaling pathway consists of multiple chains of regulators with each link being essential to the eventual ISG activation. Dysregulation of this pathway may occur at multiple levels of the chain including the IFN receptors, the downstream regulatory proteins, and at the transcriptional stage[7]. These defects have unexpectedly offered an opportunity to take advantage of a driving characteristic of cancer; a defective IFN system found in some cancers can be exploited by using viruses that would otherwise be ineffective in non-cancerous cells to eliminate the disease from the system.

1.2 ONCOLYTIC VIRUSES AS A CANCER THERAPEUTIC

The use of viruses to combat cancer is aptly termed oncolytic virus (OV) therapy, or simply virotherapy. This innovative approach utilizes viruses that can readily replicate in tumors and eliminate cancerous tissues devoid of a functional IFN signaling pathway while leaving healthy cells untouched[9]. The result is propagation of a virus specifically within the malignancy, lysis of the cancerous cells, and ensuing cell death. Viruses used for OV therapy are not necessarily the pathological strains known to cause human disease but are rather attenuated versions. For example, current pre-clinical and clinical OV therapies employing measles virus (MeV) are using engineered variants of the Edmonston or Schwarz commercial vaccine strains[10–12]. Clinical trials employing oncolytic MeV include phase I or II trials for glioblastoma multiforme,

ovarian cancer, multiple myeloma, squamous cell head and neck cancer and breast cancer[10-12]. The attenuated MeV vaccine strains developed mutations in its V and C non-structural proteins, which result in a reduced ability to counteract cellular IFN signaling when compared to the wild-type virus. The exact mechanism of the IFN signal blocking has not been fully elucidated. Preliminary studies have demonstrated that the V wild-type protein blocks the activation of the signal transducer and activator of transcription (STAT) protein which, in turn, limits the down-stream transcription of ISG's[13]. Nevertheless, these attenuating mutations give a certain specificity to OVs to preferentially replicate in cancer cells deficient of IFN signaling.

To promote their own survival, cancer cells have adapted themselves to escape existing cell death mechanisms, such as apoptosis, a process of programmed cell death. CD46 is a complement inhibitory factor which blocks the complement system, which is a key component for the mediation of apoptosis, and thus blocks programmed cell death[14]. Overexpression of CD46 has been demonstrated in many cancer types, such as prostate and breast cancer cells, which, in turn, protects the cancerous cells from this apoptotic induction[15]. However, this adapted immune-evasion tactic also offers an opportunity to preferentially target these malignant cells. During the generation of MeV vaccine strains via serial passaging, the attenuated virus gained the ability to enter cells via the CD46 receptor.[16] Therefore, overexpression of CD46 on cancer cell surfaces would promote this MeV strain to preferentially target these tumor locations. Consequently, in addition to IFN signaling deficiency, overexpression of a recognised cellular receptor may increase the oncotropic nature of OVs.

Multiple ongoing clinical trials for OV therapy are currently underway. One OV, talimogene laherparepvec (T-Vec), which is a variant of herpes simplex virus I (HSV) expressing

granulocyte macrophage colony-stimulating factor (GM-CSF), has been approved by the US Food and Drug Administration in 2015 for the treatment of advanced melanoma[17,18]. With a continuously growing list of OVs being expectedly approved for various cancer treatments, it is evident that the field is progressing rapidly. However, many hurdles remain before OV therapy is a staple alongside chemo- and radiation therapy for the treatment of cancer. For example, following systemic administration of an OV, the patient's adaptive immune system will develop neutralizing antibodies against the oncolytic vector[19]. Consequently, this would likely depreciate the efficacy of the same OV for future rounds of treatment. The same effect would occur in individuals who have been in contact with a specific serotype of a virus prior to the first therapeutic administration of a synonymous OV, as in the case of MeV.

1.3 VACCINE STRAIN MEASLES VIRUS AS AN ONCOLYTIC VIRUS

The measles virus is a non-segmented negative-sense single stranded ribonucleic acid (ssRNA) virus belonging to the *Paramyxoviridae* family. It is characterised as an enveloped pleomorphic virus ranging from 300-1000 nm in size[20]. The MeV genome is comprised of six structural genes which code for the nucleocapsid protein (N), phosphoprotein (P), matrix protein (M), fusion protein (F), hemagglutinin protein (H), and large protein (L). The nucleocapsid protein plays a role in binding and stabilizing the genomic ssRNA of the virus[21]. This protein binds the ssRNA at a ratio of exactly one protein for every six nucleotides. The MeV genome is consequently always an exact multiple of six and any deviation from this ratio, dubbed the rule of six, will result in the lack of viral particle formation[22]. The phosphoprotein is a polymerase transcription co-factor working with the large protein, the viral RNA-dependent RNA polymerase.

These three proteins, N, P and L, form the MeV ribonucleotide protein complex responsible for transcription and genome replication of the virus[23]. The P gene encodes two additional non-structural proteins, C and V, which each play a role in enhancing viral propagation through host immunomodulation[13]. The matrix protein has been demonstrated to be a key component in virus assembly and budding and is a regulatory factor for the viral RNA synthesis[24]. The hemagglutinin protein is one of two envelope glycoproteins found in MeV particles. It is responsible for viral entry into the cells through binding to signaling lymphocyte activation marker (SLAMF1), nectin-4, in addition to CD46 in vaccine strain MeV[25,26]. Moreover, the tropism of MeV is regulated by the H binding and is restricted to primate and human cells via these recognised receptors[27–29]. The other envelope glycoprotein, the fusion protein, is responsible for fusing the viral envelop with the cell membrane upon virus entry and for intercellular MeV propagation via fusion of plasma membranes of neighbouring cells[27]. Through this mechanism, the cytoplasm of an infected cell is joined with that of another cell, consequently propagating the virus. The fusion of cells together through this mechanism results in the formation of syncytia, defined as a large cell consisting of a single cytoplasm with multiple accumulated nuclei, which is a prominent cytopathic effect (CPE) of MeV[30,31].

Measles virus has been extensively studied as an OV and many adaptations have been developed to increase its effectiveness as an oncolytic agent. The measles oncolytic virus strains currently being researched as a cancer therapy include the Edmonston vaccine strain as well as the further attenuated Schwarz variant. These attenuated strains limit the MeV replication to deficient IFN signaling cell lines. The excellent safety record of the vaccine strain has been closely monitored with no documented reversion of the attenuated form back to the pathogenic MeV[32].

Additionally, genetically engineered vaccine recombinants have been generated in order to increase its affinity for cancerous cells. For example, MeV has been retargeted towards tumor cells by linking a single-chain antibody (scFv) to the H protein. Furthermore, the H epitopes for binding to CD46 and SLAM were blinded, thus limiting the targeting of the modified MeV to the antigen recognized by the scFv attached to the H glycoprotein[33]. Fragments that have affinity for, e.g., human epidermal growth factor receptor (EGFR)[34], CD20[35] and carcinoembryonic antigen (CEA)[33] have all demonstrated successful retargeting of the MeV towards cancer cells. Moreover, by having CEA ectopically expressed in a murine tumor cell line (MC38-CEA) and implanted in a murine model (C57BL/6), the modified anti-CEA MeV was shown to be able to specifically infect, albeit to a limited degree, the murine carcinoma cells which was previously difficult to achieve with the MeV parental strain[33]. By effectively retargeting the MeV, a specific tropism is established, hence opening up the possibility of studying the effects of the MeV in novel cell lines and *in vivo* models.

1.4 RATIONALE AND RESEARCH OBJECTIVES

While there have been many advances in utilizing oncolytic measles virus as a therapeutic option for cancer, some obstacles remain to be overcome to advance oncolytic MeV to routine clinical oncology. In this thesis, three major topics regarding the current state of oncolytic measles virus will be addressed and novel findings pertaining to their improvements in the field will be demonstrated and discussed. They are as follows:

1. Developing a robust genetic platform for MeV pseudotyping for evading pre-existing MeV antibodies.

2. Enhancing the potency of oncolytic measles virus by encoding granzyme B for increased cancer killing and cytokine production.

3. Increasing MeV replication and tumor killing ability with co-treatment of viral sensitizer molecules in both human and murine cancer models.

CHAPTER 2: GENERAL MATERIALS AND METHODS

2.1 CELL CULTURE

The 4T1 (CRL-2539), DF-1 (CRL-12203), and BxPC-3 (CRL-1687) cells were obtained from ATCC (Virginia, United States). PBMCs were sourced from Stem Cell technologies (British Columbia, Canada). The Vero and Vero α-His cells were a generous gift from Stephen Russell at the Mayo Clinic. The TC-1 cells were a generous gift from Brian Lichty at McMaster University. The HCT-15, B16, HT-29, A549, MCF7, and U87 cells were generous gifts from John Bell at the Ottawa Hospital Research Institute. Cells were maintained in Dulbecco's modified Eagle's medium (DMEM; Life Technologies, Darmstadt, Germany) supplemented with 10% fetal bovine serum (Hyclone Laboratories Inc, Utah, United States) unless otherwise stated. Cultured cell lines were incubated at 37 °C in a humidified atmosphere with 5% CO_2.

2.2 VIRUS RESCUE AND PROPAGATION

Measles viruses were rescued from complementary deoxyribonucleic acid (cDNA) using the MeV reverse genetics system[36,37]. Briefly, Vero cells were transfected with 500 ng of MeV-N, 100 ng of MeV-P, 500 ng of MeV-L and 100 ng of red fluorescence protein (RFP) plasmid (as a positive transfection control) in addition to 5 µg of genomic MeV cDNA. Transfection reagent used was Fugene HD (Promega, Wisconsin, United States) at a ratio of 3 µl of Fugene HD per µg of plasmid transfected. The transfection was done as outlined in the manufacturer's protocol. The virus stock was propagated by infecting Vero cells at an MOI of 0.03 and incubating for 48

hours at 37 °C in a 5% CO_2 humidified incubator. At viral passage 2, for non-ultra-centrifuged samples, cells were scraped in media, moderately vortexed, and centrifuged at 5000xg for 15 min at 4 °C to remove debris. Clarified samples were aliquoted and stored at -80 °C. At viral passage 3, for ultra-centrifuged samples, cells were scraped in media, moderately vortexed, and centrifuged at 5000xg for 15 min at 4 °C to remove debris. Clarified samples were then deposited on a 20% sucrose cushion and centrifuged at 117,000xg for 35 min at 4 °C. The supernatant was removed, and virus pellets were subsequently re-suspended in Opti-MEM, aliquoted and stored at -80 °C. The virus titer was determined by 50% tissue culture infective dose (TCID50) endpoint method according to Spearman–Kärber on Vero cells[38,39].

2.3 FLUORESCENCE MICROSCOPY

All microscope images were taken with an AMG EVOS Fluorescence microscope (Advanced Microscopy Group, Washington, USA) at the indicated exposure time.

2.4 ALAMARBLUE ASSAY

AlamarBlue assay was done using the alamarBlue™ Cell Viability Reagent (Invitrogen, Massachusetts, United States) according to manufacturers instructions. Indicated cell lines were treated 24 hours post-seeding with the specified virus or drug and readings were taken with the BioTek Synergy HT reader (Biotek, Vermont, United States).

2.5 STATISTICAL ANALYSIS

Statistical significance was calculated using either an unpaired t-test, one-way, or two-way analysis of variance (ANOVA) test as indicated in the figure legend. Log-rank Mantel-Cox test was used for the survival curve. Post hoc analysis was performed using the Bonferroni method. For all statistical analyses, differences were considered significant when a P value was below or equal to 0.05. If no indication is shown, the results are non-significant. Error bars represent standard deviation of the mean. Statistical analyses were performed using Graphpad Prism 5.0.

CHAPTER 3: ENVELOPE EXCHANGE IN ONCOLYTIC MEASLES VIRUS FOR NEUTRALIZATION ESCAPE

3.1 BACKGROUND AND RATIONALE

3.1.1 Pre-existing neutralizing antibodies towards measles virus

Pathogenic measles virus is a highly contagious pathogen that can cause coughing, rash, fever, immune amnesia, subacute sclerosing panencephalitis, and death[40–42]. As a result, a vaccine for MeV was developed and cases in immunized populations dropped drastically[43,44]. Administration of the vaccine led to immunized individuals developing highly specific antibodies that neutralize incoming MeV particles. While this is excellent for preventing pathogenic MeV infection, this poses a serious impediment for the systemic administration of a therapeutic oncolytic measles virus for the treatment of cancer. Past studies have documented the neutralization of systemically administered oncolytic MeV and highlighted this obstacle as a major predicament that must be addressed. Briefly, the therapeutic agent is neutralized prior to it being able to home to the tumor location, rendering it ineffective[11,45,46]. Although systemically administering an exceptionally large amount of MeV can overcome the pre-existing neutralizing antibody response, this is not a feasible strategy for future use in the clinic as manufacturing costs become exceedingly expensive[46]. It is evident that strategies other than brute force must be looked at to overcome this hurdle. Therefore, the aim of this project was to develop a robust envelope exchange platform facilitating rapid pseudotyping of oncolytic MeV to prevent neutralization by pre-existing anti-MeV antibodies.

3.1.2 Pseudotyping measles virus

Neutralization of MeV by pre-existing neutralizing antibodies is predominantly achieved via antibodies binding to the F and H surface glycoproteins of MeV, effectively preventing the virus from entering host cells. An innovative approach in avoiding the neutralizing response is to remove the targeted MeV F and H glycoproteins and exchange them with glycoproteins of other viruses that the general population has not come in contact with and thus, does not possess neutralizing antibodies against. Substitution of viral glycoproteins, termed envelope exchange or pseudotyping, has been previously accomplished with oncolytic MeV with mixed results. Examples of pseudotyping MeV include viral glycoprotein donors like Tupaia paramyxovirus (TPMV)[47], vesicular stomatitis virus (VSV)[48], and canine distemper virus (CDV)[49]. Pseudotyping MeV with CDV proved to be successful in yielding chimeric particles capable of evading anti-MeV antibodies while displaying similar viral kinetics to the endogenous MeV oncolytic[49–51]. On the other hand, pseudotyping MeV with TPMV yielded no viable particles while doing so with VSV generated a highly attenuated construct that achieved 50-fold less titers than MeV[47,48]. It has become increasingly evident that envelope exchange in MeV is a complex undertaking and requires careful considerations in order to achieve a viable construct.

3.1.3 Rationale for generating a genetic MeV pseudotyping platform

Attempting to pseudotype MeV can be a laborious project involving complex cloning procedures. Furthermore, although literature review and genetic analyses can improve the likelihood of finding a suitable viral glycoprotein donor, the confirmation of a successful construct is only obtained after the viral rescue is performed. Therefore, the generation of an

efficient and robust genetic MeV pseudotyping platform to readily assess proposed envelope exchange partners would be of great benefit to this field of research. To this end, we describe herein this chapter a platform that fulfils these criteria. The design of this platform consists of the introduction of unique but complimentary restriction sites, *AscI* and *MauBI*, which replace the open reading frames (ORF) of the F and H glycoprotein genes of MeV, respectively. This allows for a seamless exchange of the donor glycoprotein in either ORF slot if the gene of interest is amplified using flanking primers that contain an *MluI* and *AscI* site for the 5' and 3' primer, respectively. Furthermore, the backbone of the glycoprotein negative MeV (MeV ΔF ΔH) follows the rule of six[22], which allows for a straightforward strategy when generating the donor glycoproteins. This platform allows for a simple two-step cloning procedure for inserting envelope glycoproteins in MeV: firstly, amplification of the target gene with appropriate primers, secondly, insertion of the amplicon in MeV ΔF ΔH via a basic restriction enzyme digestion and ligation.

The genetic MeV pseudotyping platform was used to attempt to produce three different constructs. The first viral glycoprotein donor candidate chosen was VSV. The prior moderate success of pseudotyping MeV with this virus[48] in addition to the broad tropism VSV has for utilizing LDL-R as its host cell entry receptor, a protein that is expressed ubiquitously and present across species[52], made it an interesting candidate. MeV is restricted to infecting primate cells as it can only gain entry via primate expressed nectin-4, SLAM150, and CD46 (vaccine strain only)[25,26]. Therefore, a broadening of the MeV tropism by pseudotyping with VSV would be a useful improvement for testing out *in vivo* murine models in a more straightforward methodology. Additionally, pseudotyping MeV with Newcastle disease virus (NDV) and canine

distemper virus (CDV) was attempted. Both NDV and CDV are of the same family as MeV, *Paramyxoviridae*, with CDV also being of the same genus, *Morbillivirus*, while NDV belonging to the *Orthoavulavirus* genus. Their close phylogenetic proximity to MeV in addition to them both employing F and H (HN for NDV) glycoproteins to spread via syncytia formation analogous to MeV were strong indicators for a valid pseudotyping match. We hypothesize that by developing a straightforward and efficient MeV pseudotyping platform, we can offer a useful tool for screening viral glycoprotein donors for the goal of overcoming MeV neutralizing antibodies. In this chapter, we show the establishment of a novel MeV pseudotyping platform and the intricacies around selecting appropriate viral glycoprotein donors to generate a viable pseudotyped MeV construct.

3.2 MATERIALS AND METHODS

3.2.1 Generation of MeV ΔF ΔH plasmid.

MeV Schwarz vaccine strain (GenBank no. AF266291) used is as follows: order *Mononegavirales*, family *Paramyxoviridae*, genus *Morbillivirus*, species measles virus. The plasmid pCG-10MCS, a pCG plasmid with an introduced *MluI* unique cut-site in its multiple cloning site, was used for all transgene cloning and expression. The sequences of all cDNA cloned constructs were confirmed via DNA sequencing (Applied Biosystems 3730 DNA Analyzer). MeV cDNA genomic plasmids follow the rule of six[22]. The MeV subgenomic region of interest stretches from *SpeI*3373 in P 3'UTR to *SpeI*9175 in H 3'UTR and was subcloned in pUC19 with the digestion of *SalI* and *XhoI* flanking the MeV *SpeI* sites. Two polymerase chain reaction (PCR) amplicons are generated which are then fused together in an overlap extension PCR. PCR1 goes from the *SpeI*

in P 3'UTR to the F 5'UTR adding *AscI* (replacing F ORF). Primers used are as follows (sequence in uppercase form indicate complementary sequence to the template): fwd 5'-CCAGTCGACCCAACTAGTACAACC-3', rev 5'- AGAGGggcgcgccGGATGAGTCTTGATTCTGGGATTC-3'. PCR2 spans from *AscI* to *SpeI* in H 3'UTR and covers the F 3'UTR, H 5'UTR, while adding *MauBI* (replacing H ORF). Primers used are as follows: fwd 5'-GAATCCCAGAATCAAGACTCATCCggcgcgccCCTCTACAACTCTTGAAACACAAA-3', rev 5'-ccttctcgagACTAGTGGGTATGCCTGATGTCTGGGTGACATCATGTGATTGGTTCACTAGCAGC cgcgcgcgGTGGATGATCTTGCACCCTAAGTTTTG-3'. The overlap fusion PCR of the two fragments was done with the following primers: fwd 5'-CCAGTCGACCCAACTAGTACAACC-3', rev 5'-ccttctcgagACTAGTGGGTATGCCTGATGTCTG-3'. The subgenomic region was inserted in a pUC19 plasmid via *SalI* and *XhoI* digestion. After, the subgenomic ΔF-AscI ΔH-MauBI region was exchanged with the existing corresponding loci in the MeV backbone via *SpeI* digestion, thus creating the MeV ΔF-*AscI* ΔH-*MauBI* genomic backbone.

3.2.2 Generation of MeV ΔF+F ΔH+H plasmid.

MeV F and H glycoproteins were cloned from purified MeV cDNA and subcloned into the pCG mammalian expression vector via flanking unique restriction sites (underlined), *MluI* and *AscI*, using the following primers: for F, fwd 5'-cccttt**acgcgt**ATGTCCATCATGGGTCTCAAGGTG-3', rev 5'- cccttt**ggcgcgcct**AGAGCGACCTTACATAGGATTTTG-3'; for H, fwd 5'-cccttt**acgcgt**ATGTCACCACAACGAGACCGG-3', rev 5'-cccttt**ggcgcgcct**ATCTGCGATTGGTTCCATCTTC-3'. The glycoproteins were subsequently inserted in either the *AscI* (MeV F) or *MauBI* (MeV H) site of the MeV ΔF ΔH backbone to generate the reconstructed full-length MeV genome.

3.2.3 Generation of MeV-VSV plasmid.

VSV Indiana strain used is as follows: order *Mononegavirales*, family *Rhabdoviridae*, genus *Vesiculovirus*, species vesicular stomatitis virus. The glycoprotein regions (ec: ectoplasmic, tm: transmembrane, and cy: cytoplasmic) were determined via the Uniprot database: P03522 (GLYCO_VSIVA) for VSV G and Q77M18_MEASW for MeV F. Full length VSV G glycoprotein was cloned from purified VSV cDNA and subcloned into the pCG mammalian expression vector via flanking unique restriction sites (underlined), *MluI* and *AscI*, using the following primers: fwd 5'-ccctttacgcgtATGAAGTGCCTTTTGTACTTAGCC-3' (same fwd primer for all VSV G constructs), rev 5'-cccttt**ggcgcgcc**TACTTTCCAAGTCGGTTCATCTC-3'. The VSV Gec+tm fused to the MeV F cytoplasmic tail was generated in a two-step fusion PCR. Firstly, for VSV G ecto- and transmembrane domain, the reverse primer used was 5'-gttacaacgccccctGAGAACCAAGAATAGTCCAATGAT-3'. The primers used for MeV F cytoplasmic tail were: fwd 5'-cttggttctcAGGGGGCGTTGTAACAAAAAGGGA-3', rev 5'-cccttt**ggcgcgcc**tAGAGCGACCTTACATAGGATTTTG-3'. Secondly, the VSV Gec+tm domain was fused to MeV Fct via fusion PCR. Both PCR products were fused together with the following primers: fwd 5'-cccttt**acgcgt**ATGAAGTGCCTTTTGTACTTAGCC-3', rev 5'-cccttt**at**AGAGCGACCTTACATAGGATTTTG-3'. The VSV Gec fused to the MeV Ftm+ct was generated in a two-step fusion PCR. Firstly, for the generation of the VSV G ectodomain, the reverse primer used was 5'- ggatgtagactatTTTCCAACTACTGAACCAACCTTC-3'. The primers used for the MeV Ftm+ct fragment were: fwd 5'-gtagttggaaaATAGTCTACATCCTGATTGCAGTG-3', rev 5'- cccttt**ggcgcgcc**taTCAGAGCGACCTTACATAGGATTT -3'. Secondly, the VSV Gec domain was

fused to MeV Ftm+ct via fusion PCR. Both PCR products were fused together with the following primers: fwd 5'- ccctttacgcgtATGAAGTGCCTTTTGTACTTAGCC-3', rev 5'-cccttt**ggcgcgcc**taTCAGAGCGACCTTACATAGGATTT-3'. The glycoprotein transgenes were all subcloned in the pCG plasmid and then inserted in the MeV ΔF ΔH backbone, either in the *AscI* or *MauBI* slot. Enhanced green fluorescence protein (EGFP) was subcloned into the pCG mammalian expression vector via flanking unique restriction sites (underlined), *MluI* and *AscI*, using the following primers: fwd 5'-ccctttacgcgtATGGTGAGCAAGGGCGAGGAG-3', rev 5'-cccttt**ggcgcgcc**TTACTTGTACAGCTCGTCCATG-3'. The transgene was subsequently inserted in either the *AscI* or *MauBI* site in the MeV ΔF ΔH backbone.

3.2.4 Generation of MeV-NDV plasmid.

NDV Hitchner B1 strain used is as follow: order *Mononegavirales*, family *Paramyxoviridae*, genus *Orthoavulavirus*, species Newcastle disease virus. NDV F and HN glycoproteins were cloned from purified NDV cDNA and subcloned into the pCG mammalian expression vector via flanking unique restriction sites (underlined), *MluI* and *AscI*, using the following primers: For F, fwd 5'-ccctttacgcgtATGGGCTCCAGACCTTCTAC-3', rev 5'-cccttt**ggcgcgcc**ACATTTTTGTAGTGGCTCTCATC-3'. For HN, fwd 5'-ccctttacgcgtATGGACCGCGCCGTTAG-3', rev 5'-cccttt**ggcgcgcc**TAGCCAGACCTGGCTTC-3'. The NDV F monobasic cleavage site (GRQGRL) was reverted to the oligobasic sequence (RRQRRF) with a point mutation using the following primers in a divergent PCR in pCG-NDV Fv: fwd 5'-aggagacagcggcgctTTATAGGCGCCATTATTGG-3', rev 5'-

aaagcgccgctgtctcctCCCTCCAGATGTAGTCAC-3'. Following sub-cloning and mutagenesis, the NDV Fv and HN transgenes were cloned in the *AscI* and *MauBI* slots, respectively.

3.2.5 Generation of MeV-CDV plasmid.

CDV Onderstepoort strain used is as follow: order *Mononegavirales*, family *Paramyxoviridae*, genus *Morbillivirus*, species canine distemper virus. CDV F and H glycoproteins were cloned from purified CDV cDNA and subcloned into the pCG mammalian expression vector via flanking unique restriction sites (underlined), *MluI* and *AscI*, using the following primers: for F, fwd 5'- cccttt<u>acgcgt</u>ATGCACAGGGGAATCCCCAAAAG -3', rev 5'- ccctttGGCGCGccTATCAGAGTGATCTCACATAGG -3'; for H, fwd 5'- cccttt<u>acgcgt</u>ATGCTCCCCTACCAAGAC-3', rev 5'- ccctttGGCGCGccTATTAACGGTTACATGAGAATC-3'. Following sub-cloning, the CDV F and H transgenes were cloned in the *AscI* and *MauBI* slots, respectively.

3.2.6 RT-PCR on MeV-CDV infected samples.

Vero cells were seeded in a 6-well plate at a density of 2.5 x 10^5 cells per well and infected 24 hours later at an MOI of 0.03 with either MeV P-EGFP, MeV-CDV or negative control of MeV-CDV (mock infection with a viral rescue sample lacking MeV L plasmid). Total RNA was harvested 48h later using the RNeasy Plus Mini Kit (Qiagen, Hilden, Germany) according to manufacturer's instructions. Reverse-transcription PCR was performed on 1 µg of purified RNA to make cDNA using the SuperScript® III One-Step RT-PCR System (Thermo Fisher Scientific, Massachusetts, United States) according to manufacturer's instructions. Amplicon sizes: MeV H

340 bp, CDV H 1800 bp, and β-actin 355bp. Primers used for MeV H amplification were as follow: fwd 5'-CTTCCAGGGTTGAACATGCTGTG-3', rev 5'- TTAATTCTGATGTCTATTTCAACT-3'. For CDV H amplification: fwd 5'- ccctttacgcgtATGCTCCCCTACCAAGAC-3', rev 5'- ccctttGGCGCGccTATTAACGGTTACATGAGAATC-3'. For β-actin amplification: β-actin sense and anti-sense from the Superscript RT-PCR kit. Using an Eppendorf Mastercycler Gradient 5331 thermocycler (Eppendorf, Hamburg, Germany), the condition for the RT reaction was 50 °C for 1 hour followed by denaturing at 94 °C for 2 minutes. For the PCR, the steps were 94 °C for 30 sec, 60 °C for 30 sec, 72 °C for 2 min (30 cycles).

3.3 RESULTS

3.3.1 Successful generation of a robust MeV pseudotyping platform

As most MeV neutralizing antibodies are primarily recognizing its two glycoproteins, they were substituted for two unique restriction sites where glycoproteins of other viruses can be inserted. The MeV F and H glycoprotein ORFs were looped out via PCR and then *AscI* and *MauBI* restriction sites were inserted in their place. The MeV ΔF ΔH construct was completed and verified via DNA sequencing (Figure 3.1). In order to ensure that the cloning strategy was properly designed with the rule of six in mind, the F and H glycoproteins of MeV were re-introduced in their original slots. The newly reconstituted MeV ΔF+F ΔH+H displayed successful viral replication and the usual cytopathic effect of syncytia induction whereas the negative control of MeV ΔF ΔH-EGFP, a MeV with no glycoproteins but with an EGFP transgene inserted in the H slot, showed no viral replication (Figure 3.2).

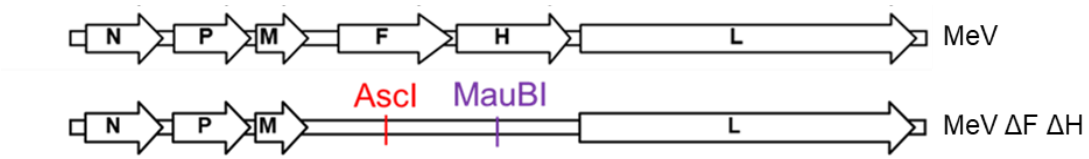

Figure 3.1. Schematic Representation of the MeV and MeV ΔF ΔH Genome. Schematic of the MeV genome with the viral ORFs on the top with the MeV ΔF ΔH construct on the bottom. The F and H glycoprotein ORFs of MeV have been substituted by two unique restriction sites, *AscI* and *MauBI*, respectively, for MeV ΔF ΔH. Genomic map is not to scale.

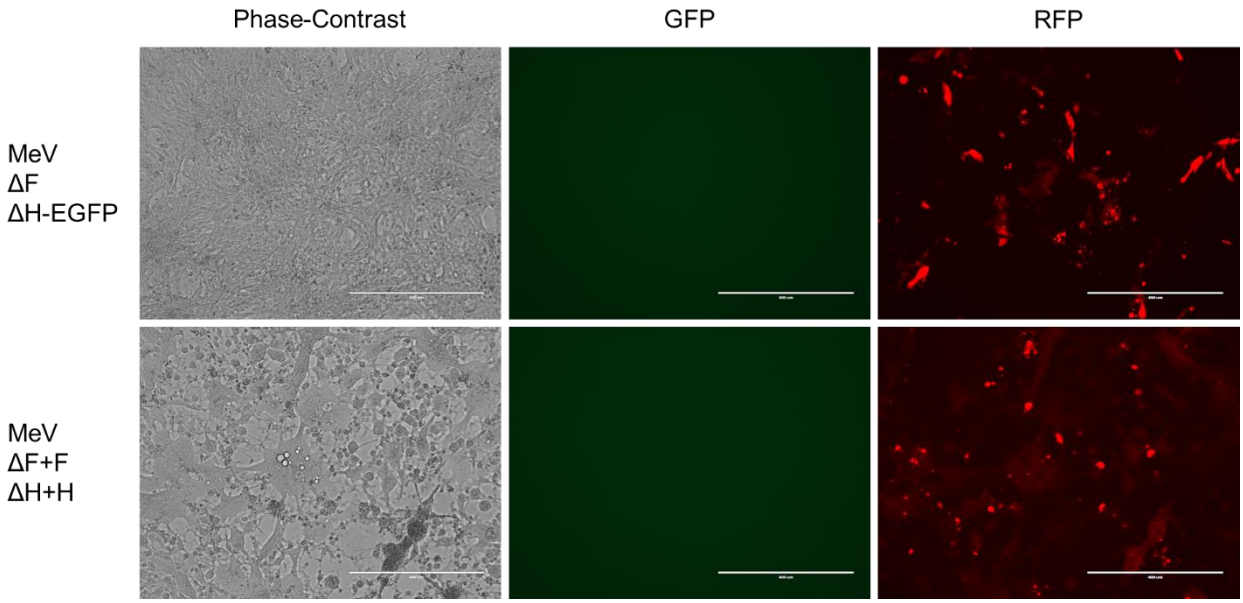

Figure 3.2. MeV glycoprotein re-introduction validates this genomic platform's proof of concept. Images 7 days post transfection (4X) in Vero cells. MeV ΔF ΔH-EGFP acts as a negative control as this construct does not contain any glycoproteins; consequently, no GFP is observed in the green channel. MeV ΔF+F ΔH+H is a construct with reconstituted glycoprotein ORFs following their removal as a proof of concept for the cloning strategy. Major syncytia formation is observed in the reconstituted construct while the Vero cells remain intact following 7 days post transfection. Red fluorescent protein plasmid was co-transfected with the genomic DNA as a transfection control. Exposure times were 250 ms and 120 ms for the GFP and RFP channel, respectively. Bar represents 1000µm.

3.3.2 Limited production of a pseudotyped measles virus with vesicular stomatitis virus G.

The delta-glycoprotein MeV was firstly pseudotyped with the G glycoprotein VSV. Various chimeras of VSV-G and MeV-F were constructed, such as VSV-G ecto and transmembrane domains fused to the cytoplasmic tail of MeV-F as well as VSV-G ectodomain fused to the transmembrane domain and cytoplasmic tail of MeV-F (Figure 3.3). These two chimeric proteins in addition to the full length VSV-G were inserted in the F or H slots of the MeV ΔF ΔH backbone with the other slot being filled with EGFP as a viral replication marker. A representative image of the rescue of the MeV-VSV-G pseudotype is seen in Figure 3.4; the viral replication is marginal compared to the positive rescue control of an MeV encoding EGFP. This was the case for each of the MeV-VSV-G pseudotypes. Further viral passaging of the construct yielded no replicating particles. Co-transfection of the MeV-VSV-G construct with MeV F and H during viral rescue, also known as trans-complementation, was performed in an attempt to initially boost the virus for subsequent passaging. While virus replication was evident as indicated by large EGFP signals (Figure 3.5), subsequent passaging also yielded no replicating viral particles.

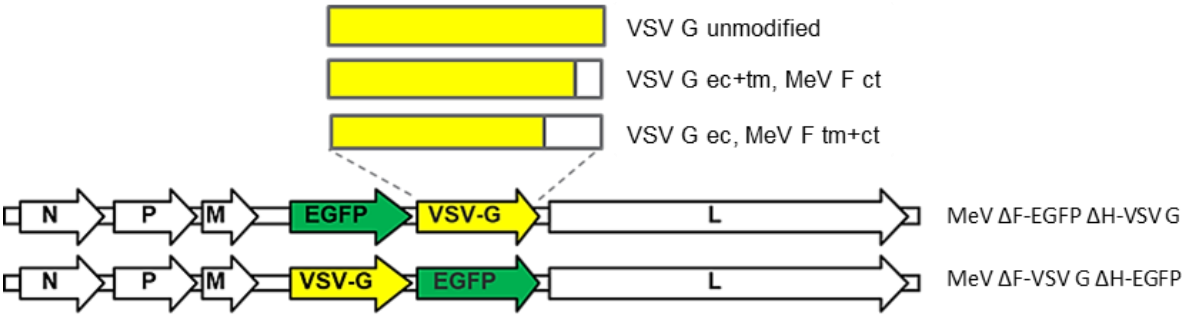

Figure 3.3. Schematic representation of the genomic map of the MeV-VSV G pseudotype and its chimeras. The VSV G protein can be inserted in either the F or H slot of the MeV ΔF ΔH backbone while EGFP can be inserted in the open ORF as a viral replication marker. Various chimeras of MeV F and VSV G are also shown as options for insertion. Genomic map is not to scale.

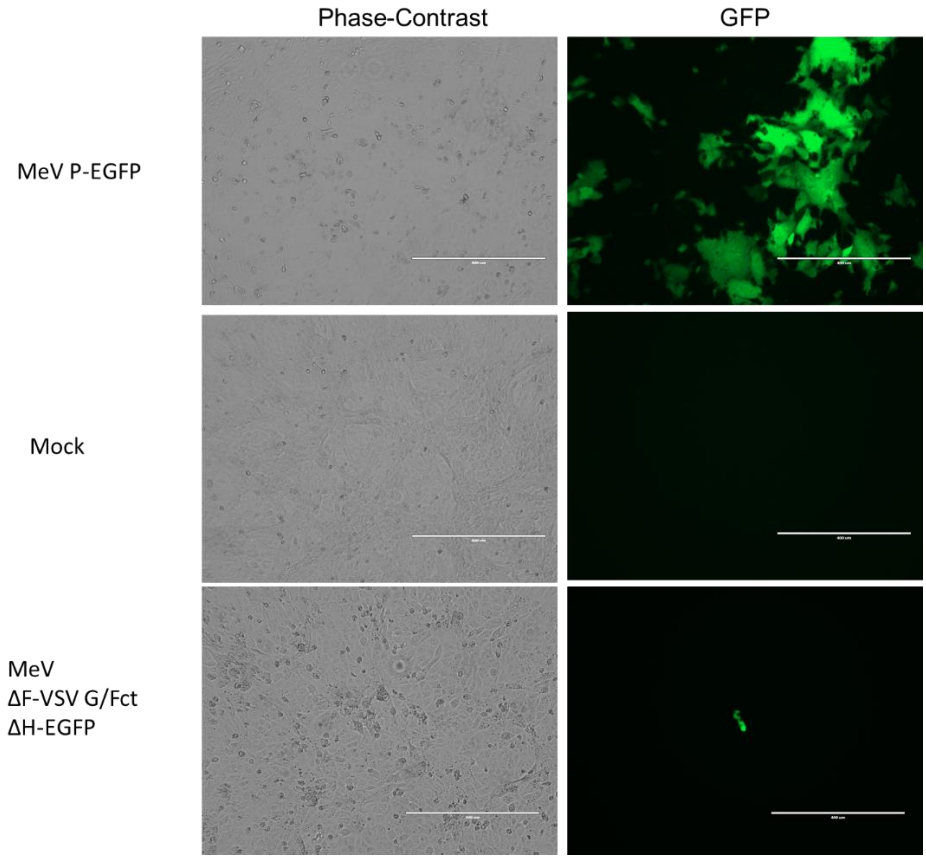

Figure 3.4. MeV-VSV pseudotype virus rescue proves unsuccessful. Images 7 days post transfection (10X objective) in Vero cells. MeV P-EGFP acts as a positive control for viral infection. Mock viral rescue (lacking L plasmid) is shown in the mid panels. The MeV ΔF-VSV G/Fct ΔH-EGFP construct is the pseudotyped MeV with VSV G ecto- and transmembrane domains fused to the F cytodomain in the F gene slot and EGFP in the vacant H slot. Exposure time was 250 ms for the GFP channel. Bar represents 400 µm.

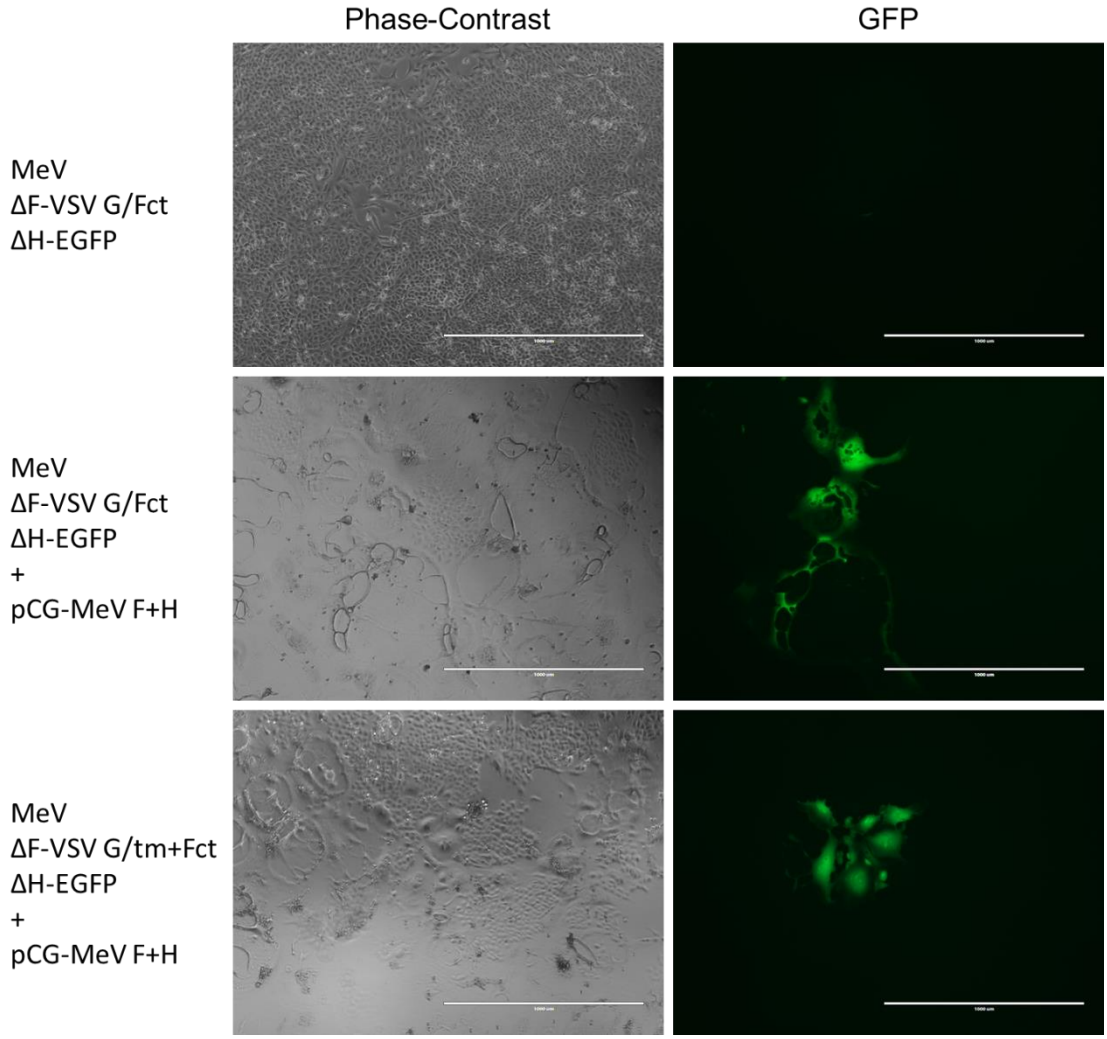

Figure 3.5. MeV-VSV G trans-complementation viral rescue assay demonstrates phenotypic viral rescue. Images 4 days post transfection (4X objective) in Vero cells. Pseudotyped MeV-EGFP with a chimeric VSV G+F cytoplasmic tail construct was transfected in Vero cells alone or with MeV-F and H expression plasmids in a trans-complementation assay. Massive syncytia formation was observed with the MeV F+H combination whereas no CPE was observed in the pseudotyped construct alone. Green events from genome replication were observable from the co-transfection, indicative of a phenotypic rescue of the original MeV, while the MeV-VSV-G alone demonstrates very weak EGFP signal. Exposure times were 250 ms and 120 ms for the GFP and RFP channel, respectively. Bar represents 1000 µm.

3.3.3 Incompatibility of pseudotyping measles virus with Newcastle disease virus

The NDV F and H glycoproteins were chosen to be inserted in the MeV ΔF ΔH backbone because of its similarity in viral spread kinetics and its close genetic relationship to MeV as NDV is also part of the *Paramyxoviridae* family. The NDV Hitchner B1 avirulent strain was used, which meant the F glycoprotein had a monobasic cleavage site requiring external reagents for activation and subsequent viral replication. Therefore, this cleavage site was converted to an oligobasic cleavage site via site-directed PCR mutagenesis. The fusogenicity was evaluated via co-transfection of the newly generated NDV Fv (oligobasic/virulent) and H glycoproteins in Vero cells and compared to the monobasic NDV F (non-virulent) and H glycoproteins. Cells were also co-transfected with a red fluorescent protein (RFP) as a transfection control to observe the syncytia more clearly. Syncytia formation was observed following NDV Fv+H co-transfection while none was seen from NDV F+H (Figure 3.6). The syncytia were, however, much smaller, and fewer in number than the ones observed following MeV F+H co-transfection. Multiple rescue attempts of the MeV-NDV pseudotype were unsuccessful with no CPE observed while the positive controls were always successfully rescued (Figure 3.7). The lack of replicating MeV-NDV viral particles was confirmed via reverse transcription-PCR (RT-PCR) (Figure S3.1).

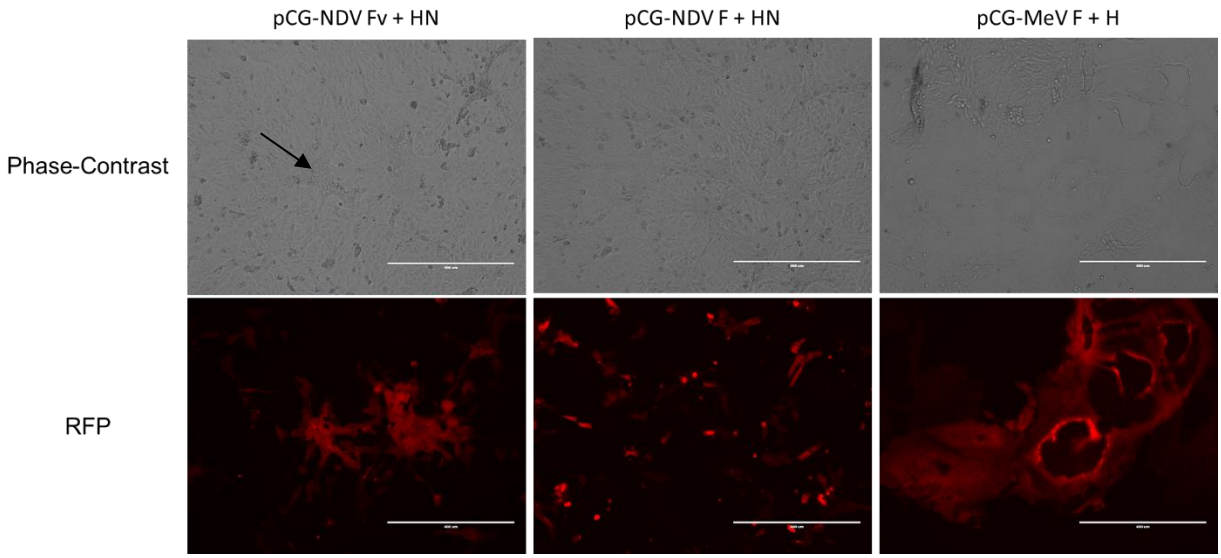

Figure 3.6. NDV envelope glycoprotein fusion assay displays reacquisition of fusogenic properties from F glycoprotein engineering. Images 5 days post transfection (10X objective) in Vero cells. Fusion assay of co-transfected expression plasmids (pCG) of either NDV or MeV glycoproteins plus an additional red fluorescent protein plasmid (RFP). The NDV F and HN glycoproteins originate from the lentogenic Hitchner B1 strain with the F protein having a monobasic cleavage site. The NDV Fv glycoprotein was engineered to possess an oligobasic cleavage site. The MeV F+H glycoproteins were of the Schwarz strain variants. As denoted by the arrow, syncytia formation with NDV occurs solely with the co-transfection of the virulent Fv + HN combination and is comparable to the MeV cytopathic effect which is easily seen by the RFP distribution. Bar represents 400 µm. Exposure time was 120 ms for the RFP channel.

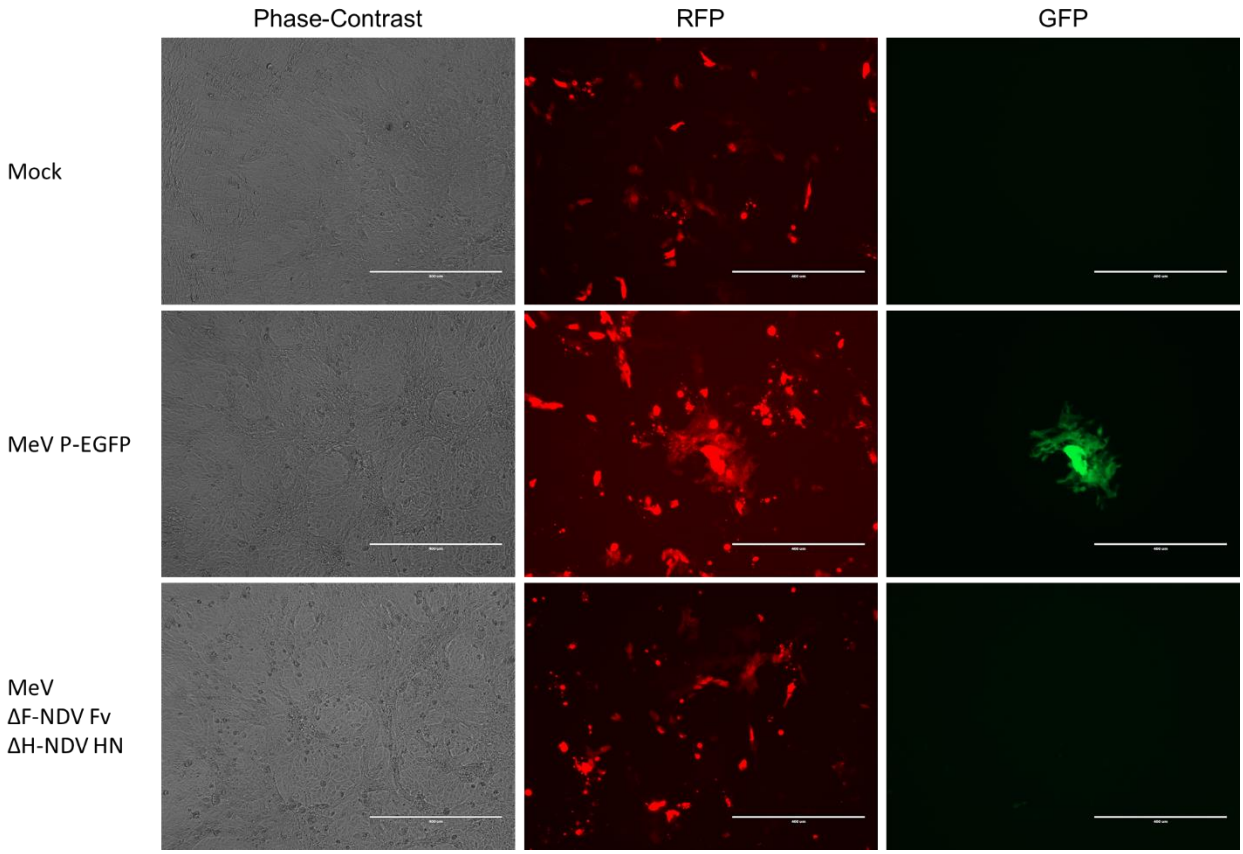

Figure 3.7. MeV-NDV pseudotype virus rescue proved unsuccessful. Images 6 days post transfection (10X objective) in Vero cells. MeV ΔF-NDV Fv ΔH-NDV HN, the measles virus pseudotyped with virulent NDV glycoproteins was co-transfected with a red fluorescent protein plasmid (RFP), as a transfection control, in bottom panels. Mock viral rescue (lacking L plasmid transfection) is shown in the top panels with RFP as a transfection control. MeV P-EGFP, was rescued as shown by GFP events in the center panels with RFP as a transfection control. Syncytia were observed in the red channel for the positive control of MeV P-EGFP but none for the pseudotyped construct. Exposure times were 250 ms and 120 ms for the GFP and RFP channel, respectively. Bar represents 400 µm.

3.3.4 Successful pseudotyping of measles virus with canine distemper virus F and H

The CDV glycoproteins were cloned into the MeV ΔF ΔH backbone using the same strategy as the NDV pseudotyping. As seen in Figure 3.8, the MeV-CDV pseudotype viral rescue was successful as indicated by the presence of massive syncytia. No cytopathic effect was observed in the negative control (N.Ctrl). The N.Ctrl viral rescue consisted of a typical MeV rescue procedure; however, the L plasmid, an essential viral rescue component, was omitted from the transfection. Passaging of the supernatant of the viral rescue 7 days post-transfection onto new cells was performed. This was also successful with observation of syncytia 3 days post infection (Figure 3.9). No cytopathic effect was observed in the N.Ctrl passage. To determine whether the observed cytopathic effect was induced by the pseudotyped MeV-CDV or if there were lingering MeV contaminants in the sample, an RT-PCR was done on the viral passage samples. The exclusive presence of the MeV-CDV construct was validated via RT-PCR (Figure 3.10) where CDV H was detected in the virally passaged sample but not MeV H. No glycoprotein messenger RNA (mRNA) was detected in the N.Ctrl sample. Following growth kinetic experiments, MeV-CDV replicated at a similar rate and quantity as the MeV parental strain (Figure 3.11).

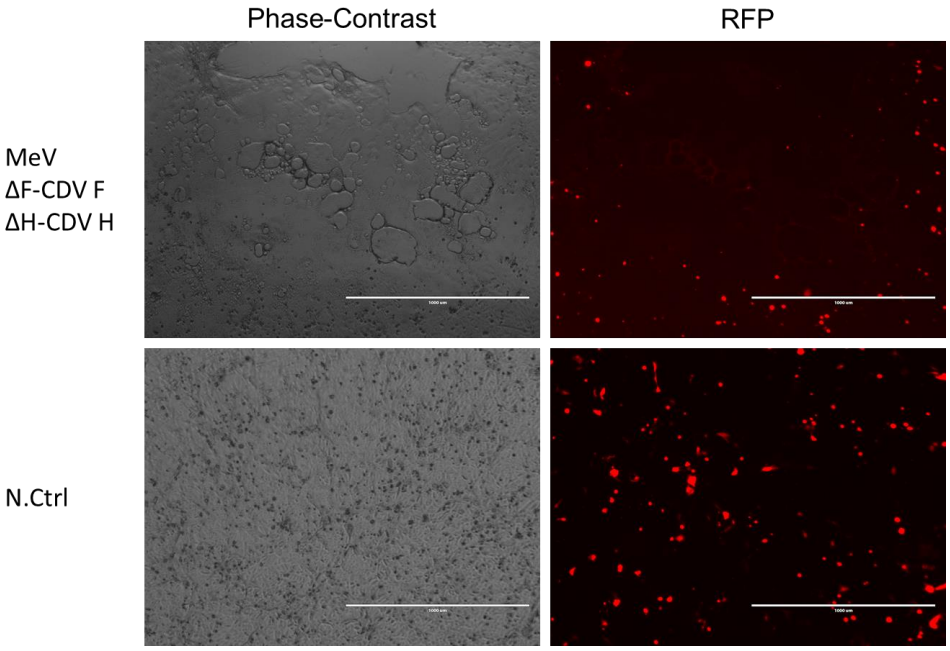

Figure 3.8. MeV-CDV pseudotype virus rescue was successful. Images 7 days post transfection (4X objective) in Vero cells. MeV ΔF-CDV F ΔH-CDV H, the measles virus pseudotyped with CDV glycoproteins was co-transfected with a red fluorescent protein plasmid (RFP) as a transfection control. Mock viral rescue (lacking L plasmid transfection) is shown in the bottom panels with RFP as a transfection control. Syncytia was observed in the phase contrast and red channel for the MeV-CDV construct but none for the negative control. Exposure time was 120 ms for the RFP channel. Bar represents 1000 µm.

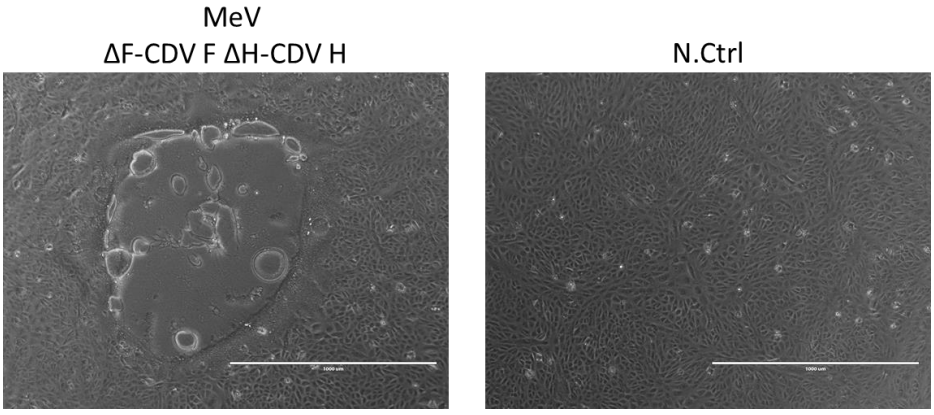

Figure 3.9. MeV-CDV pseudotype viral passage displayed syncytia cytopathic effect. Vero cells 3 days post infection (4X objective, phase contrast) of viral passage 1 (VP1), blind titer passaging. Syncytia was observed from the pseudotyped MeV ΔF-CDV F ΔH-CDV H construct whereas none was observed in the negative control rescue which is the passage of the mock rescue (lacking L plasmid transfection). Bar represents 1000 µm.

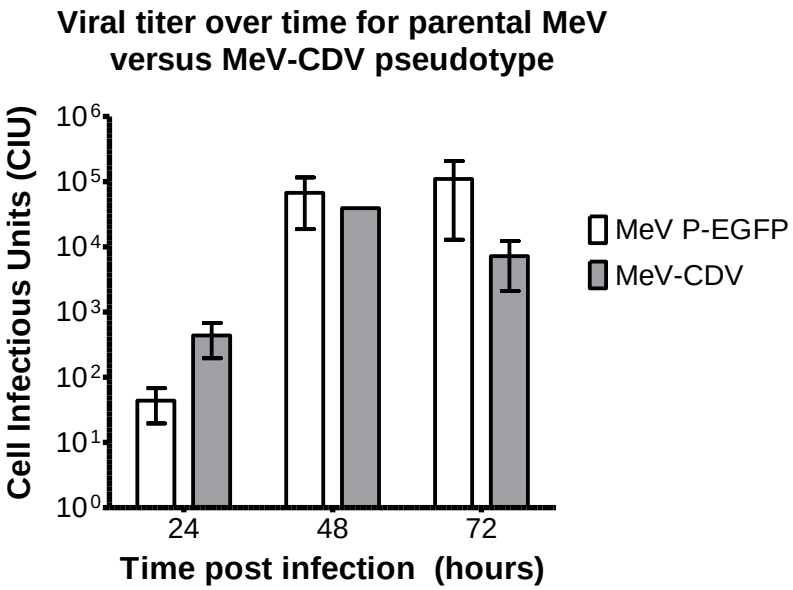

Figure 3.10. MeV-CDV replication kinetics are analogous to MeV. Viral titer over time of the parental MeV versus the MeV-CDV pseudotype. Vero cells were infected at an MOI of 0.03 with either virus and an aliquot was taken at the indicated time point. No major difference in titer was observed at any timepoint. (n=3, mean ± SD, two-way ANOVA)

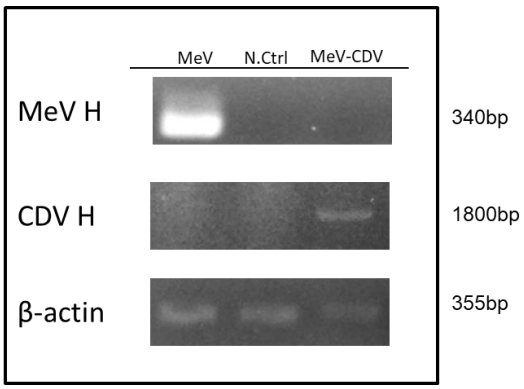

Figure 3.11. MeV-CDV RT-PCR validates the exclusive presence of MeV-CDV from the rescue procedure. RT-PCR was done on VP2 virus samples. RNA was harvested from Vero cells 48 hours post-infection at MOI 0.03 followed by RT-PCR processing using the SuperScript III First-Strand Synthesis System by Invitrogen SOP. N.Ctrl was an MeV-CDV rescue without MeV L Co-transfection. β-actin was used as a housekeeping gene. Amplicon size is shown on the right of the figure.

3.4 DISCUSSION

This chapter highlights the generation of a novel oncolytic MeV pseudotyping platform as well as the viability of several viruses as viral glycoprotein donors for this system. Evading pre-existing neutralizing antibodies is a necessary obstacle to overcome in order to use oncolytic measles virus via systemic administration for novel cancer therapy. This major hurdle is due to the fact that the vast majority of people have been vaccinated against measles virus in the Western population. Anti-measles antibodies target predominantly the two glycoproteins (F and H) at the virus' surface, which then inhibits the virus from binding to its cellular receptor and gaining entry. Consequently, since the MeV glycoproteins are the antibody neutralization targets, they were removed and replaced with surface glycoproteins of other viruses. This technique, termed pseudotyping, has been previously attempted with MeV and VSV, TPMV, and CDV resulting in constructs with varying viability. While this strategy is effective when a suitable glycoprotein donor is matched with MeV, the cloning process to generate these constructs is time-consuming and inefficient. Furthermore, a successful and viable formation of these chimeric viruses is only revealed subsequent to an attempted viral rescue and passage. Therefore, we aimed to generate a cloning platform for a straightforward and efficient pseudotyping for MeV. This would allow for a rapid way to test for suitable viral glycoprotein donor candidates for pseudotyping MeV.

The pseudotyping platform system was engineered to allow for the insertion of viral glycoproteins where the MeV F and H glycoproteins are typically situated via a simple cloning procedure. To this end, the MeV F and H glycoprotein ORFs were removed and substituted with *AscI* and *MauBI* restriction sites, respectively (Figure 3.1). These restriction sites were chosen

due to them being compatible, which means that, when digested, they produce identical nucleotide overhangs. With this in mind, transgenes destined to be inserted in these slots were designed to have flanking compatible restriction sites (*MluI* in the 5' and *AscI* in the 3') which allows for directed insertion to either the F or H ORF slot. Hence, the transgenes of interest can all be produced in the same manner and inserted in the desired ORF using a consistent cloning strategy. Also, the transgenes can be subcloned in a single vector (pCG10, a mammalian expression vector) for easy sequence verification and ensuing transfection procedures. This MeV pseudotyping platform offers a robust approach to the often-temperamental cloning procedures accompanied with generating these constructs.

The cloning strategy of the MeV pseudotyping platform was first confirmed via a proof-of-concept experiment. The newly produced MeV ΔF ΔH genomic backbone was reconstituted via the re-addition of the MeV F and H ORFs in their original slots. This was a crucial validation experiment to ensure that the *Paramyxoviridae* rule-of-six was followed and that the original glycoproteins were removed at the appropriate positions. Ensuing MeV ΔF+F ΔH+H reconstitution and viral rescue yielded syncytia formation and viral kinetics similar to the parental MeV (Figure 3.2). Also, the negative control virus MeV ΔF ΔH+EGFP, a glycoprotein negative virus with EGFP inserted as marker to track viral gene expression and spread, demonstrated no viral replication confirmed with the absence of any observable CPE or EGFP (Figure 3.2). These results validate the cloning strategy for this pseudotyping platform.

The first viral glycoprotein donor for pseudotyping MeV using this platform was the G glycoprotein of the vesicular stomatitis virus. Since VSV only has one glycoprotein responsible for viral entry and spread, it could be inserted in one of the available ORF slots while a viral

replication reporter gene, such as EGFP, could be inserted in the other position. Furthermore, the transcriptional gradient of MeV genes effect on the viral kinetics of a MeV-VSV pseudotype could be evaluated by alternating the insertion site of VSV G from the MeV F to the H slot[53]. In addition to this, various chimeras of VSV G and MeV F were generated such as the ectoplasmic domain of VSV G fused to the transmembrane and cytoplasmic domain of MeV F, as well as the ectoplasmic and transmembrane of VSV G fused to the cytoplasmic domain of MeV F. These chimeras were created to increase the likelihood of forming a suitable glycoprotein that can support MeV cellular entry and spread. Utilizing a chimera that possesses the transmembrane domain of MeV F could increase the probability of proper glycoprotein incorporation in the viral envelope whereas the cytoplasmic tail of MeV F has been previously described as a potential viral particle stabilizer through its interaction with the MeV matrix protein[48].

These chimeric glycoproteins in addition to the endogenous VSV G were inserted in either the F or H slot of the MeV ΔF ΔH backbone with the other slot carrying EGFP. Following viral rescue, no CPE was observed and only limited EGFP expression could be detected (Figure 3.4). This was the case for every chimera of VSV G with MeV F as well as the endogenous VSV G. Furthermore, the transcriptional gradient had no impact in producing a better MeV-VSV chimera as no difference was observed if the glycoprotein was inserted in either the F or H slot. Moreover, changes in the viral rescue protocol such as transfection protocol variations (transfection reagent, quantity and ratios of DNA, cell seeding), time of viral harvest, and method of viral passaging (freeze-thaw, infected cell overlay, supernatant transfer, or scraped cells) did not result in added virus production. Co-transfection of the VSV G variants in pCG10 vectors with the corresponding viral rescue also did not result in virus production. Due to these negative

results, a hypothesis was formed that there may not be enough virus following the initial rescue for a viral passage; so, a trans-complementation assay was employed to solve this challenge. Hence, the MeV-VSV constructs were co-transfected with pCG10 plasmids encoding MeV F and H to boost the initial virus production via a phenotypic first viral cycle as the MeV F and H would initially incorporate into the MeV-VSV particle resulting in a normal MeV viral life cycle. As can be seen in Figure 3.5, massive syncytia formation (due simply to the transfection of MeV F and H plasmids) were observed in addition to a large EGFP signal signifying replicating MeV-VSV particles. However, once this rescue was passaged onto new cells, the EGFP signal was limited to what was observed in the original MeV-VSV rescues. Consequently, we were unable to reproduce the results found in the literature[48] as too little or no particles were generated using our system. The difference in results obtained could be attributed to the use of different MeV strains, Edmonston B versus Schwarz, or the different cloning strategy. Still, pseudotyping MeV with VSV gives, at best, a highly attenuated virus (~50-fold decrease in titers compared to MeV[48]).

Pseudotyping MeV with a virus also from the *Paramyxoviridae* family could increase the odds of generating a viable construct as protein sequence homology and the viral life cycle should be more closely conserved within the same virus family. So, pseudotyping MeV with Newcastle disease virus was pursued. NDV, a member of the *Paramyxoviridae* family, possesses two envelope glycoproteins F and HN, which are responsible for viral spread and cellular entry, respectively. Similar to MeV, NDV spreads via syncytia formation. The NDV strain used for this experiment was Hitchner B1, an avirulent strain that harbours a monobasic cleavage site in its F protein which requires external reagents (ex: trypsin) for its activation and, consequently, viral

spread. Therefore, this cleavage site was firstly reverted to a furin polybasic site ordinarily found in the velogenic NDV strains, which can then be readily activated via ubiquitously expressed furin-like proteases[54,55]. While the virulence of NDV is partially regulated via the F furin site [56], it is completely safe to introduce this virulent version of NDV F as a glycoprotein to MeV as the Schwarz MeV backbone was being used and the construct as a whole remains interferon sensitive. Reversion of the monobasic site to its polybasic version was confirmed via co-transfection of the pCG NDV Fv (polybasic) and HN. As can be seen in Figure 3.6, syncytia formation was observed following NDV Fv+HN co-transfection but none could be seen in the NDV F+HN condition. The cytopathic effect of NDV Fv+HN was also very similar to the one observed in the co-transfection of MeV F+H (Figure 3.6).

The NDV Fv and HN glycoproteins were inserted in the F and H slots of MeV ΔF ΔH, respectively. Following viral rescue of the MeV-NDV pseudotype in Vero cells, no syncytia or CPE was observed (Figure 3.7). Additional rescue attempts in DF-1, a chicken embryo fibroblast cell line routinely used for NDV propagation, also yielded negative results (data not shown). As with the MeV-VSV pseudotype troubleshooting, numerous parameters were adjusted to increase the likelihood of producing a viable construct. An RT-PCR assay was employed to attempt to detect viral mRNA, more specifically, NDV HN mRNA. Following viral rescue or blind viral passaging, no detectable amount of NDV HN mRNA was found. Consequently, pseudotyping MeV with NDV may not be feasible. There are several potential factors leading to this negative result; for example, it is possible that the NDV glycoproteins are not incorporating in the MeV particle due to sequence dissimilarity. Moreover, by pseudotyping MeV with NDV, the MeV viral life cycle is altered as the particle will now gain cellular entry via binding to gangliosides and N-linked

glycoproteins[57,58] while budding and release is now dependent on the neuraminidase activity of NDV HN[59] which might not be supported by the MeV particle.

Pseudotyping MeV with a virus not only from the same family, but also one from the same *Morbillivirus* genus, may maximize the likelihood of a successful pseudotype. This was successfully accomplished previously with MeV being pseudotyped with canine distemper virus[49]. This construct was able to evade anti-MeV antibodies, achieved similar titers to MeV, in addition to tolerate a retargeting strategy towards human CD46 and EGFR[50,60]. This pseudotyping candidate was tested in our pseudotyping platform as a positive control for this system. CDV F and H were inserted in the MeV ΔF ΔH backbone in their counterparts ORF slots. Following initial virus rescue, syncytia formation was observed (Figure 3.8). Subsequent passaging yielded additional syncytia formation and titration of the resulting virus displayed similar growth kinetics to the parental MeV (Figure 3.10). An RT-PCR was performed to confirm the exclusive presence of MeV-CDV particles, and no contaminating MeV H mRNA was detected (Figure 3.11). The successful generation of a MeV-CDV pseudotype validates this cloning platform as a straightforward and robust envelope exchange system for oncolytic MeV.

In conclusion, we have developed a rapid and efficient cloning platform for envelope exchange in oncolytic measles virus. Furthermore, the discrepancy in success when selecting a viral glycoprotein donor was highlighted. Pseudotyping MeV with VSV and NDV proved to be ineffective, whereas doing so with CDV was successful, thus replicating the findings found in the literature. Interestingly, taking the results obtained here with those found in the literature, a trend seems to have emerged concerning the correlation between a successful pseudotype with MeV and the genetic relationship of the donor towards MeV. For example, viruses used for

pseudotyping MeV that are more genetically distantly related to MeV, such as VSV, generate, at best, highly attenuated viruses. On the other hand, viruses that are in the same genus as MeV, like CDV, prove to be excellent envelope glycoprotein donors as the resulting viruses display similar replicating kinetics as the original MeV. Therefore, a good candidate to test this hypothesis would be phocine distemper virus (PDV) as it bears similarities to CDV, such as usage of the same cellular receptor for cell entry (CD46)[61], and is also very closely related to MeV. In summary, the MeV pseudotyping platform developed here offers a powerful tool to advance the research in resolving a major obstacle for the systemic administration of oncolytic measles virus in overcoming pre-existing anti-MeV neutralizing antibodies.

CHAPTER 4: INSERTION OF GRANZYME B IN ONCOLYTIC MEASLES VIRUS

4.1 BACKGROUND AND RATIONALE

4.1.1 Human granzyme B: a key player in cell death

The granzyme B-induced cell death has been traditionally viewed as a primary mechanism that is used by cytotoxic lymphocytes (CTL) and natural killer (NK) cells to eliminate harmful target cells including infected and degenerated cells[62,63]. The granzyme B gene (GZMB) encodes a member of the granzyme subfamily of proteins which are in the peptidase S1 group of serine proteases. The encoded preproprotein is predominantly secreted by NK cells and CTLs and is proteolytically processed to generate the active protease which induces apoptosis in target cells upon cleavage of intracellular substrates.

The endogenously found GZMB protein is produced as an enzymatically inactive preproprotein. The prepropeptide is found at the N-terminus of the GZMB protein and its removal is essential for GZMB to be enzymatically active[64]. Its prepeptide consists of a signal sequence 18 amino acids long to direct the GZMB protein to the endoplasmic reticulum where, ultimately, the protein is directed towards the cell's lytic granules[65]. The propeptide, a dipeptide (GE), is removed by cathepsin C, a cysteine protease found in the secretory granule compartment of CTLs[64,66]. Once the dipeptide is removed, GZMB is then fully active. This unique processing sequence ensures that GZMB is shuttled to the lytic granules and is only activated once there so that the cell producing GZMB does not succumb to its activity[64,67].

GZMB is the most abundant serine protease stored in secretory granules of CTLs and NK cells. After recognizing the target cell, the engaged killer cells secrete GZMB along with other

granule proteins, including perforin, into the immunological synapse. From there, GZMB translocates into the cytoplasm of the target cell where GZMB cleaves numerous proteins, such as procaspase-3, resulting in the eventual apoptotic demise of the target cell[68]. GZMB also degrades extracellular matrix (ECM) proteins, such as fibronectin, laminin, and vitronectin[63,69].

4.1.2 Arming oncolytic measles virus

A key advantage with working with oncolytic viruses is that they can be engineered on a genetic level and adapted to the therapeutic needs. Since oncolytic MeV is a replicating system, any transgene encoded within the MeV genetic backbone will also be produced every time the virus replicates in the host. Encoding therapeutic transgenes in MeV changes the paradigm on how the virus is viewed; the virus itself is not only an anti-cancer agent but is also the cargo carrier for a therapeutic payload. This is important as, while oncolytic measles virus is an emerging effective cancer therapeutic, the virus alone may not be able to eliminate the malignancy. By encoding therapeutic transgenes, the immunogenicity of oncolytic viruses can be improved to promote immune cell recruitment at the tumor location for systemic clearance of related malignancies. This was demonstrated with the FDA-approved Talimogene laherparepvec oncolytic virus, a modified HSV type-1 virus encoding multiple copies of granulocyte-macrophage colony-stimulating factor[70]. It was shown in a murine model which had two tumors injected, one in each flank, that if a single tumor was injected with either T-Vec or the virus without GM-CSF, the injected and non-injected tumors shrank significantly more with the T-Vec treatment[71]. In this scenario, the GM-CSF cytokine increases dendritic cell recruitment to the site of infection while increasing their antigen presentation ability resulting in a proinflammatory response

towards the tumor[72]. Moreover, treatment with a GM-CSF encoded virus establishes an improved long-term immunity towards the cancer as was shown with a retargeted MeV encoding GM-CSF in an *in vivo* murine tumor rechallenge model[73]. In this same model, the MeV encoding GM-CSF reduced the tumor volume significantly more in the injected tumor versus the bare MeV. Arming oncolytic MeV with transgenes that increase its immunogenicity gives immediate benefits in reducing the originally infected tumor's volume while conveying a long-term systemic protection towards the cancer's recurrence.

4.1.3 Combining measles virus with granzyme B

Arming oncolytic measles virus with granzyme B could synergise the advantageous characteristics of each element. The specific replication and tumor lysis of MeV combined with the local tumor killing via apoptosis induction of the GZMB protein would improve the immediate impact of the therapeutic. Interestingly, while apoptosis induction is normally non-immunogenic and non-inflammatory, this can be shifted under certain conditions [74]. For example, MeV triggered cell lysis induces immunogenic cell death (ICD) via cytokine release, such as type-I interferons, and syncytium-mediated cell death[75,76]. This coupled with the programmed cell death cascade induced by GZMB could conceivably boost the overall ICD signal by triggering additional cytokine production. Furthermore, immune cell recruitment directed towards the tumor would also improve the probability of complete tumor clearance. Local production and release of GZMB from lysing tumor cells into the tumor microenvironment would induce ECM cleavage and subsequent immune cell homing to the tumor location[63]. Together, we hypothesize that by encoding GZMB in MeV, we may generate synergy to improve direct oncolysis of infected

and neighbouring cancerous cells via a by-stander effect, as well as confer a systemic and long-term immunity towards the targeted malignancy.

4.2 MATERIALS AND METHODS

4.2.1 Generation of MeV granzyme B constructs

Human granzyme B gene (NM_004131.5) was ordered from Cedarlane (HG10345-M, Ontario, Canada) and cloned out using the following primers: fwd 5'-ccctttacgcgtgccaccATGATCATCGGGGGACATGAG-3', and rev 5'-ccctttggcgcgcctaTTAGTAGCGTTTCATGGTTTTCTTTAT-3', thus creating an active human granzyme B (ahGZMB) ORF. The gene was subcloned in the previously described pCG-10MCS plasmid prior to insertion in MeV P-ATU. The uBahGZMB (ubiquitin active human GZMB) transgene was ordered as a gBlock gene fragment from Integrated DNA Technologies (Iowa, United States). The gene was then subcloned in pCG-10MCS plasmid prior to insertion in MeV P-ATU.

4.2.2 Cytopathic effect investigation

Vero cells were seeded at 2.5 x 10^5 cells per well in a 6-well plate and 24 hours later, they were infected at an MOI of 10 for the MeV constructs or treated with staurosporine (Sigma-Aldrich, Missouri, United States) at 100 nM. Images were taken with an AMG EVOS fluorescence microscope (Advanced Microscopy Group, Washington, USA) every 24 hours.

4.2.3 Granzyme B western blot

Protein was extracted from cells that were pelleted, washed once with ice cold PBS, and lysed on ice for 30 minutes with RIPA buffer (Sigma-Aldrich, Missouri, United States) with Roche cOmplete™ protease inhibitor (Roche, Basel, Switzerland). Protein quantification was done using the Bio-Rad Bradford Protein Assay (Bio-Rad, California, United States) according to manufacturer's instructions. Samples were run on 10% Mini-PROTEAN® TGX™ Protein gels (Bio-Rad, California, United States) using the Mini-PROTEAN Electrophoresis gels (Bio-Rad, California, United States) system. The western blot transfers were performed using the Mini Trans-Blot® Cell system (Bio-Rad, California, United States) and the transfer on nitrocellulose membrane was done according to manufacturer's instructions. Blots were blocked with 5% BSA diluted in TBST-T and probed with antibodies towards granzyme B (2C5, sc-8022, Santa Cruz Biotechnology Inc., Texas, United States) at 1:200, and GAPDH (14C10, Cell Signaling Technology, Massachusetts, United States) at 1:1000. Blots were subsequently probed with a goat anti-mouse (GZMB) or rabbit (GAPDH) horseradish peroxidase-conjugated secondary antibody (Cell Signaling Technology, Massachusetts, United States). Bands were visualized on film using the Supersignal West Pico Chemiluminescent Substrate (Thermo Fisher Scientific, Massachusetts, United States).

4.2.4 Caspase-3 real-time assay

For the interval assay, Vero cells were seeded at 2.5 x 10^5 cells per well in a 6-well plate and infected 24 hours post seeding with the indicated virus at an MOI of 1. Following 48 hours of infection, the IncuCyte® Caspase-3/7 Green Apoptosis Assay reagent was added. Subsequently, following 24 hours of this addition, the images and readings were taken with an AMG EVOS fluorescence microscope (Advanced Microscopy Group, Washington, USA) every 24 hours. GFP

readings were taken every 24 hours with the Thermo Scientific ArrayScan XTI (Thermo Scientific, Massachusetts, United States).

For the real-time assay, cells were seeded at 5 x 10^4 cells per well in a 24 well plate and infected 24 hours post seeding with the indicated virus at an MOI of 1. The IncuCyte® Caspase-3/7 Green Apoptosis Assay reagent was added immediately upon infection and GFP readings were done with the IncuCyte ZOOM Live Cell Imaging System (Essen Bioscience, Michigan, USA). Cell lines were kept at 37 °C in a humidified atmosphere with 5% CO2.

4.2.5 RNAseq experiment and analysis

Patient derived peripheral blood mononuclear cells (PBMC; STEMCELL Technologies, British Columbia, Canada) were infected at an MOI of 1 with either MeV P-uBahGZMB, MeV P-encoding firefly luciferase (FLUC), or mock infected with DMEM. RNA was harvested 24 h post-infection using QIAGEN RNeasy Mini Kit (QIAGEN, Hilden, Germany) according to manufacturer's protocol. RNA samples were sent to Fasteris (Fasteris, Switzerland) for RNAseq. Sample transcript purification was done via poly (A)-tail selection, followed by library construction using illumina TruSeq Stranded mRNA Library Prep kit. For the A549 experiment, cells were infected at an MOI of 3 with either MeV P-uBahGZMB, MeV P-FLUC, or mock infected with DMEM. RNA harvest was performed as described above and also sent to Fasteris for subsequent RNAseq analysis.

Data received from Fasteris was in individual transcripts per kilobase million (TPM) format for each attributed human gene. These were compared between the uBahGZMB and the

FLUC constructs to generate a transcriptional ratio and then were subsequently processed in the Ingenuity Pathway Analysis (IPA) software. A transcriptional degree report was produced by the software with the following parameters: For the PBMC experiment, input was adjusted to PBMC cell type, species human, and difference of 1.5log to be considered in the analysis. The output was a heatmap of total disease and regulation pathways comparing the transcriptional upregulation (or downregulation) induced by MeV P-uBahGZMB vs MeV P-FLUC. Further analysis in specific pathways, such as the cytokine canonical pathway, produced bar graphs displaying specific gene cluster transcriptional changes (2.5 log -log(p-value) cut-off). Moreover, a heatmap was generated for the PBMC experiment with regards to the transcriptional fold-change using the Microsoft Excel heatmaps function. A table for the A549 experiment was generated based on the transcriptional fold-change of proteins of interest.

4.3 RESULTS

4.3.1 MeV encoding granzyme B production and characterization

Following the same procedure outlined in the general materials and methods section for harvesting MeV, MeV-GZMB viruses expanded to a viral passage 3 (VP3) titer analogous to MeV (Figure 4.1). Granzyme B production from cells infected with MeV P-ahGZMB was confirmed via western blot (Figure 4.2).

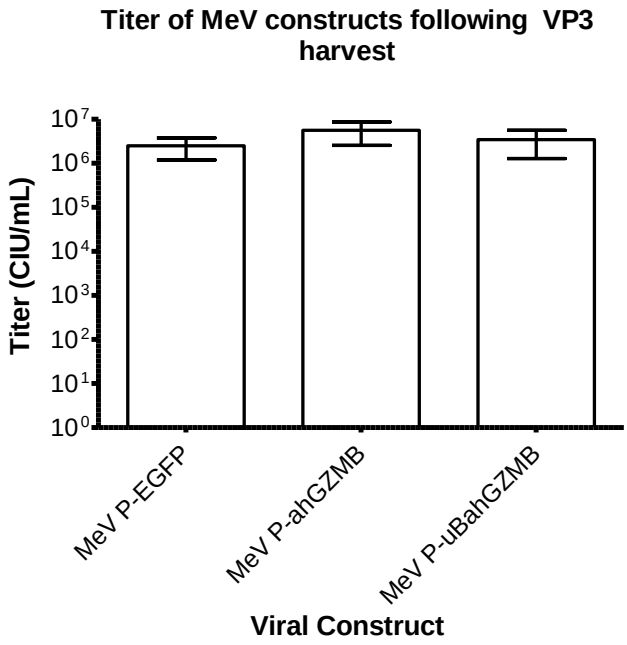

Figure 4.1. MeV P-GZMB constructs grow to similar titers as MeV. Titer cell infectious units (CIU) per ml is displayed here for each construct following the conventional MeV VP3 harvesting procedure. MeV P-EGFP was used here as an analogue of MeV expressing a transgene in its P-ATU cassette. MeV P-ahGZMB and MeV P-uBahGZMB achieved similar titers to the MeV P-EGFP construct. MeV P-EFFP n=4, MeV P-ahGZMB n=4, and MeV P-uBahGZMB n=5, one-way ANOVA mean ± SD.

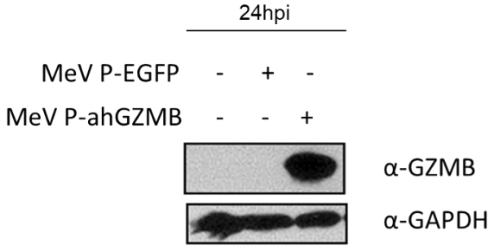

Figure 4.2. GZMB transgene is expressed from MeV P-ahGZMB replication. Western blot validating GZMB expression following Vero cells either mock infected or infected with MeV P-EGFP or MeV P-ahGZMB at an MOI of 1, 24 hours post infection. MeV P-EGFP was used as a negative control and GAPDH as a loading control.

4.3.2 MeV-GZMB infection generates a novel cytopathic effect

Measles virus induces a very particular cytopathic effect, syncytia formation, when spreading from an infected cell, as can be seen on Figure 4.3. Staurosporine is a very strong apoptosis inducer and the characteristic rounding up of apoptotic cells can be seen in cells treated with this drug (Figure 4.3). Interestingly, the MeV P-ahGZMB infected cells displayed a hybrid CPE between typical MeV infection and apoptosis induction from the GZMB production. The infected cells were all connected analogous to syncytia, however, they are also rounded or shrivelled due to the strong apoptosis induction signal from GZMB (Figure 4.3).

4.3.3 MeV-GZMB constructs yield a greater apoptosis induction

Apoptosis induction was measured via a Caspase-3 activity kit (IncuCyte® Caspase-3/7 Green Apoptosis Assay). As can be seen in Figure 4.4, MeV P-ahGZMB induced a larger apoptotic effect compared to that by MeV P-FLUC in Vero cells. Further studies using an IncuCyte real time analysis confirmed this tendency with both MCF7 and U87 cancer cell lines (Figure 4.5). Caspase-3 activation was also evaluated for MeV P-uBahGZMB using a real time IncuCyte analysis. The MeV P-uBahGZMB construct outperformed the MeV P-ahGZMB virus in its apoptosis induction capacity in Vero cells (Figure 4.6).

4.3.3 Enhanced cancer killing ability of MeV P-uBahGZMB

The cancer cell killing ability of MeV P-uBahGZMB was compared to MeV. A549 and HCT-15 cells were infected with a range of MOIs (0.03, 0.3, and 3) with either MeV P-uBahGZMB or MeV P-FLUC. An alamarBlue cell viability assay was performed 144 hours post-infection and results were normalised to mock treatment of DMEM. For the HCT-15 cells, the MeV P-

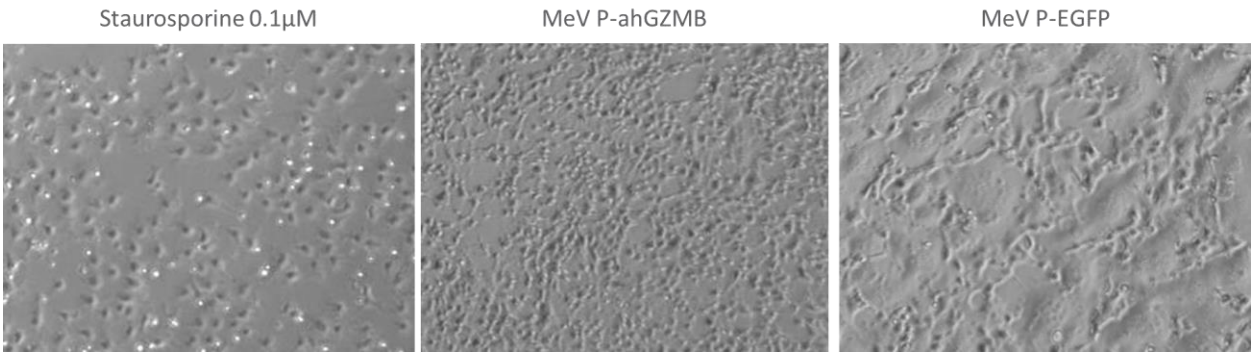

Figure 4.3. MeV expressing GZMB produced hybrid apoptosis-syncytia cytopathic effect. Phase contrast images (10X magnification) of Vero cells 48 hours post-infection at an MOI of 10 or treated with staurosporine at 0.1 µM. The staurosporine is a protein kinase inhibitor that is a strong inducer of apoptosis. Classic apoptosis CPE is seen in the left-most panel with the characteristic rounding of the cells. Typical MeV syncytia formation is seen in the right-most panel from MeV P-EGFP infection. The cytopathic effect of MeV P-ahGZMB in the middle panel demonstrated a hybrid CPE of rounding of the cells from apoptosis induction and syncytia from the measles spread.

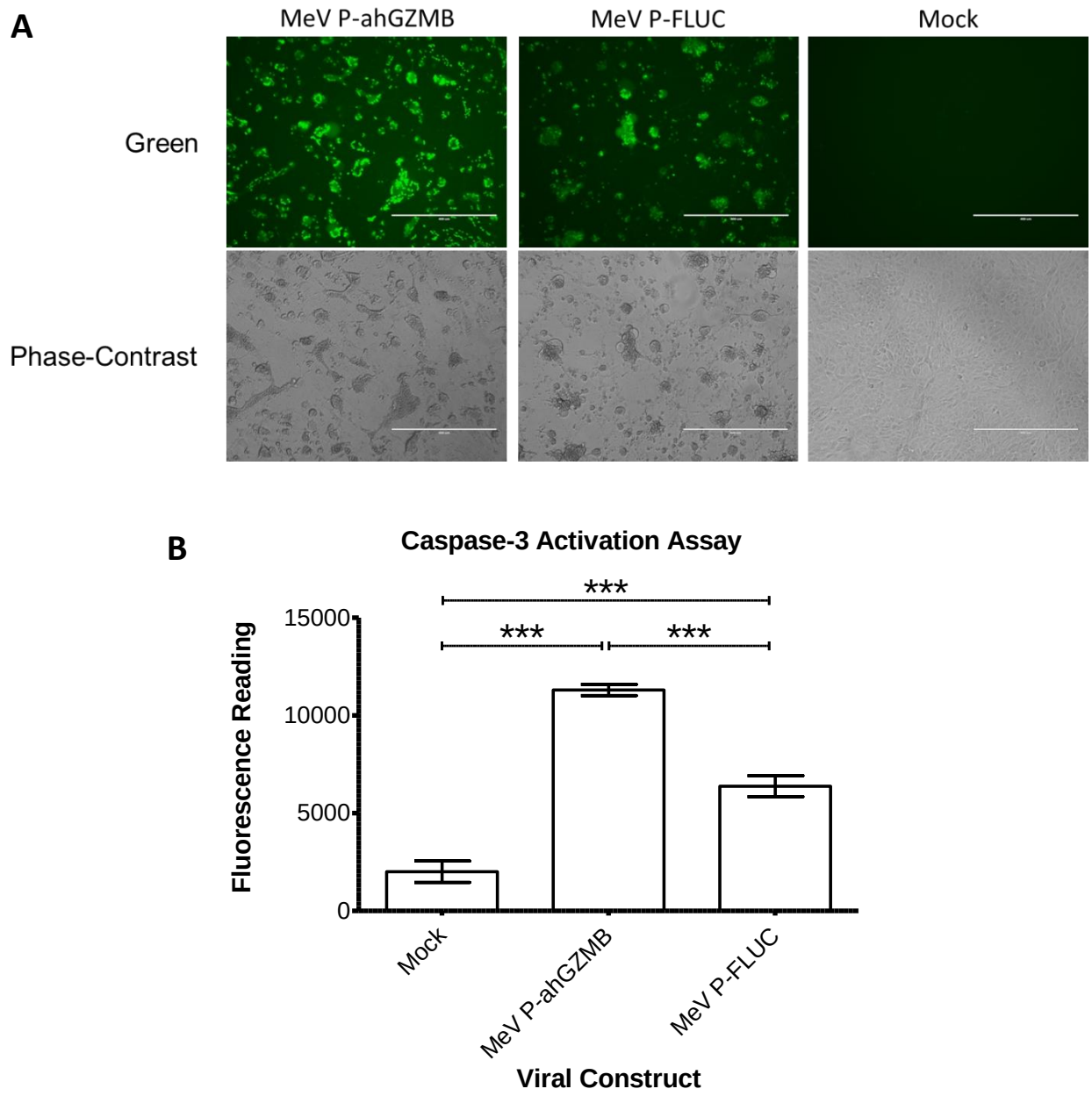

Figure 4.4. MeV expressing GZMB was a stronger activator of caspase-3. A) Vero cells were infected at an MOI of 1 with the indicated virus. Following 48 hours of infection, the IncuCyte® Caspase-3/7 Green Apoptosis Assay Reagent was added. The reagent is activated through cleavage from caspase-3 once the latter is itself cleaved and activated. Subsequently, following 24 hours of this addition, the images and readings were taken. B) The fluorescence reading from the Incucyte reading revealed a significant increase in caspase-3 activation following MeV P-ahGZMB infection versus MeV P-FLUC or mock. (n = 3; mean ± SD; ***P < 0.001, one-way ANOVA).

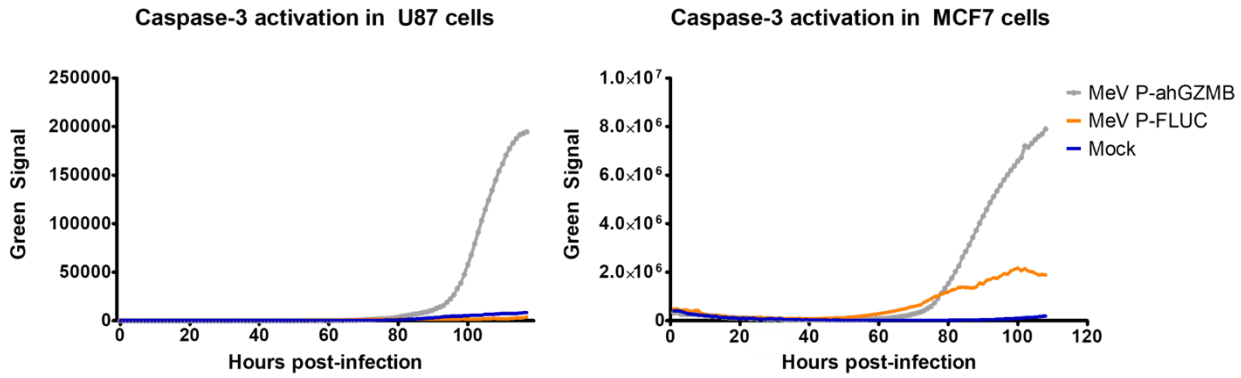

Figure 4.5. MeV P-ahGZMB induced more caspase-3 activation in MCF7 and U87 cancer cells than MeV. Incucyte real time readings of the indicated cell lines at an MOI of 1 for MeV P-ahGZMB, MeV P-FLUC and Mock PBS conditions. The readout is a green fluorescence signal emitting from the IncuCyte® Caspase-3/7 Green Apoptosis Assay reagent. The reagent is activated through cleavage from caspase-3 once the latter is itself cleaved and activated. Cells were seeded at 50,000 cells per well in a 24-well plate and infected 24 hours post seeding. In both cases, MeV P-ahGZMB induced a larger caspase-3 activation than mock or MeV P-FLUC. There was some activation of caspase-3 in MCF7 cells from MeV P-FLUC but very little observed in U87 cells.

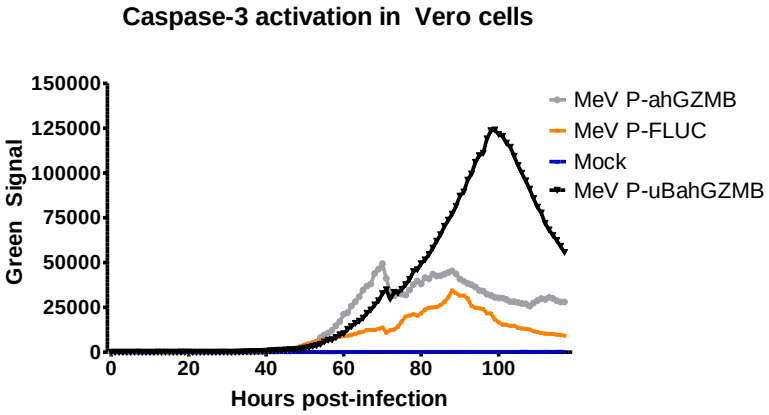

Figure 4.6. MeV P-uBahGZMB outperforms MeV P-ahGZMB in caspase-3 activation in Vero cells. Incucyte real time readings of Vero cells infected at an MOI of 1 for MeV P-ahGZMB, MeV P-uBahGZMB, MeV P-FLUC and Mock PBS conditions. The readout is a green fluorescence signal emitting from the IncuCyte® Caspase-3/7 Green Apoptosis Assay reagent. The reagent is activated through cleavage from caspase-3 once the latter is itself cleaved and activated. Cells were seeded at 50,000 cells per well in a 24-well plate and infected 24 hours post seeding. The MeV P-uBahGZMB induces a much larger caspase-3 activation than MeV P-ahGZMB.

uBahGZMB outperformed MeV P-FLUC at an MOI of 0.3 but failed to do so at the lowest MOI of 0.03 while both constructs nearly eliminated the cells at the highest MOI of 3 (Figure 4.7). For the A549 cells, MeV P-FLUC had an increased cell killing ability at the lowest MOI while the inverse was observed at the highest MOI (Figure 4.7).

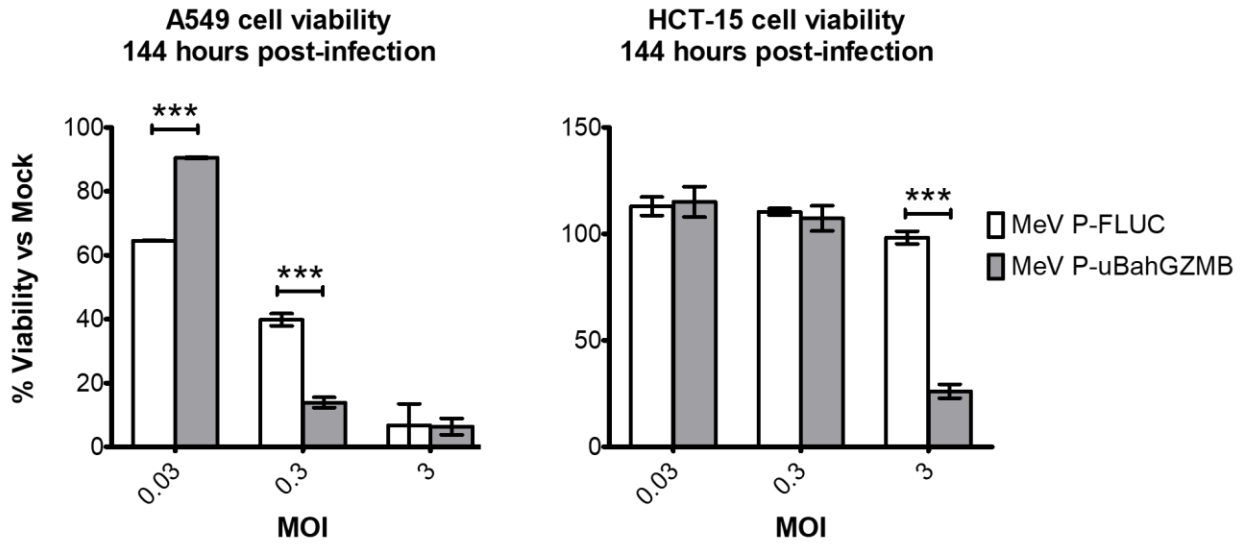

Figure 4.7. MeV P-uBahGZMB has increased cancer cell killing ability in a dose-dependent manner. AlamarBlue readouts 144 hours post-infection of infected cell viability normalised to mock treatment of DMEM. Cells were infected at the indicated MOI 24 hours after cells were seeded. (Left) In A549 cells, MeV P-uBahGZMB outperforms the MeV P-FLUC virus at MOI 0.3 but not 0.03. Cells were killed evenly at the highest MOI. (Right) In HCT-15 cells, the cell line was resistant to the MeV cell death for both constructs up until MOI 3 where the MeV P-uBahGZMB caused significant cell killing. (n = 3; mean ± SD; ***P < 0.001, two-way ANOVA).

4.3.4 Increased inflammation pathway gene expression in PBMCs following infection with MeV P-uBahGZMB

Patient derived PBMCs were infected with either MeV P-uBahGZMB or MeV P-FLUC to evaluate the effect of uBahGZMB on their transcriptional patterns. RNAseq data was obtained and individual transcripts per kilobase million (TPM) values for each ascribed human gene were compared between the uBahGZMB and the FLUC negative control constructs. The expression ratio of uBahGZMB/FLUC transcriptional gene effects was calculated and evaluated with the Ingenuity Pathway Analysis (IPA) software. A heatmap displaying the effect on transcription for pathways involved in the disease and function aspect was generated (Figure 4.8). The size of each pathway or quadrant was determined via the -log (p-value) whereas the heatmap colouring was determined by the z-score (a measure of SD from the mean). Pathways involved in proinflammatory conditions, such as inflammatory response and immune cell signaling, displayed a robust upregulation of transcription.

More in-depth analysis within this heatmap was performed and the cytokine canonical pathway was examined (Figure 4.9). The y axis displayed the -log (p-value) whereas the heatmap colouring of each individual gene cluster was determined by its z-score. Gene clusters involved in proinflammatory circumstances, such as interferon and IL-17 signaling, topped the bar chart in transcriptional upregulation and p-value.

Additional heatmaps were generated for the transcriptional effects in PMBC infected cells (Figure 4.10). The following parameters were used to generate the map: activation of mononuclear leukocytes cluster, must display greater than 1log increase in transcription for MeV

P-uBahGZMB. The heatmap displays the mRNA log-fold increase over mock treated for both MeV P-uBahGZMB and MeV P-FLUC.

4.3.5 Increase in cytokine and chemokine transcription in A549 cells following MeV P-uBahGZMB infection

Gene transcription of A549 cells following infection with either MeV P-uBahGZMB or MeV P-FLUC or mock infected was evaluated following RNAseq analysis. As can be seen in Figure 4.11, the fold change of transcripts over mock for both MeV P-uBahGZMB and MeV P-FLUC for several cytokines and a housekeeping gene (GAPDH) can be compared. MeV P-uBahGZMB generated a stronger upregulation of these genes while GAPDH remained relatively unaffected.

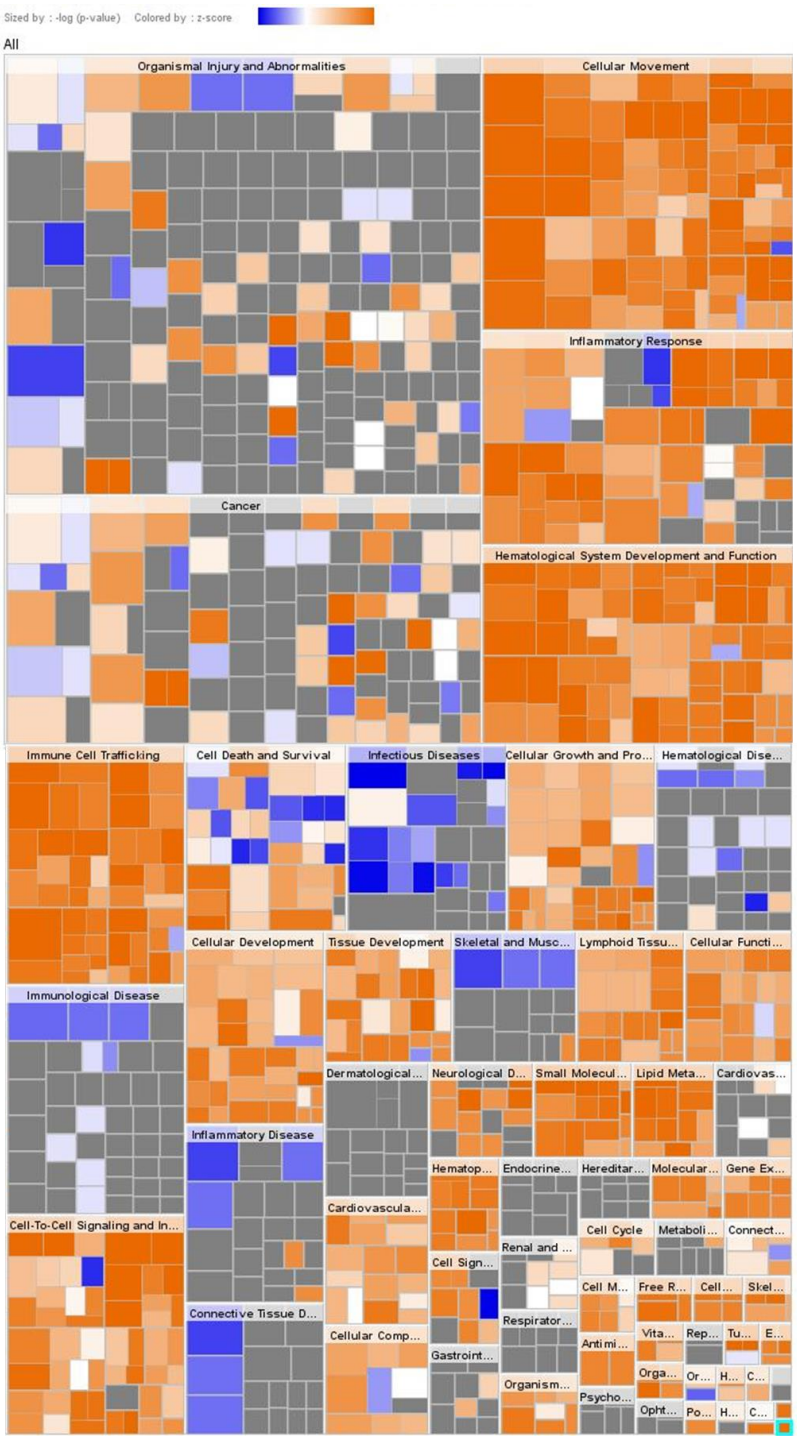

Figure 4.8. MeV P-uBahGZMB triggered translational upregulation of proinflammatory pathways. Heat map of disease and functions pathways comparing the gene transcription of human patient PBMCs infected with either MeV P-uBahGZMB or MeV P-FLUC. The z-score attributed to each gene cluster is a ratio of gene expression induced by MeV P-uBahGZMB over MeV P-FLUC (ex: red means uBahGZMB upregulated a specific gene cluster comparatively to the FLUC construct.) The size of each gene cluster is determined by its -log (p-value). Analysis was done with the Ingenuity Pathway Analysis software.

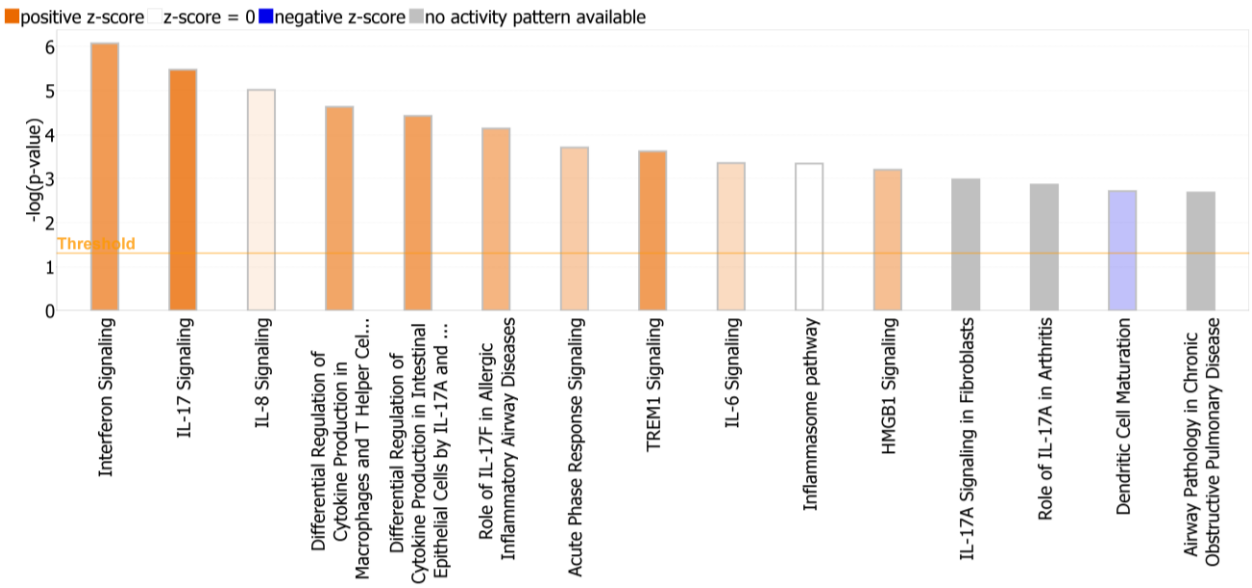

Figure 4.9. MeV P-uBahGZMB upregulated the translation of numerous genes in the cytokine canonical pathways. Bar graph depicting the most influenced pathways in the cytokine canonical pathway category from MeV P-uBahGZMB versus MeV P-FLUC infection of PBMCs (cut-off of 2.5 log for -log(p-value)). The y-axis represents the -log (p-value) while the color of each bar represents the z-score with red being positive and blue negative (ex: red means uBahGZMB upregulated a pathway comparatively to the FLUC construct.) Analysis was done with the Ingenuity Pathway Analysis software.

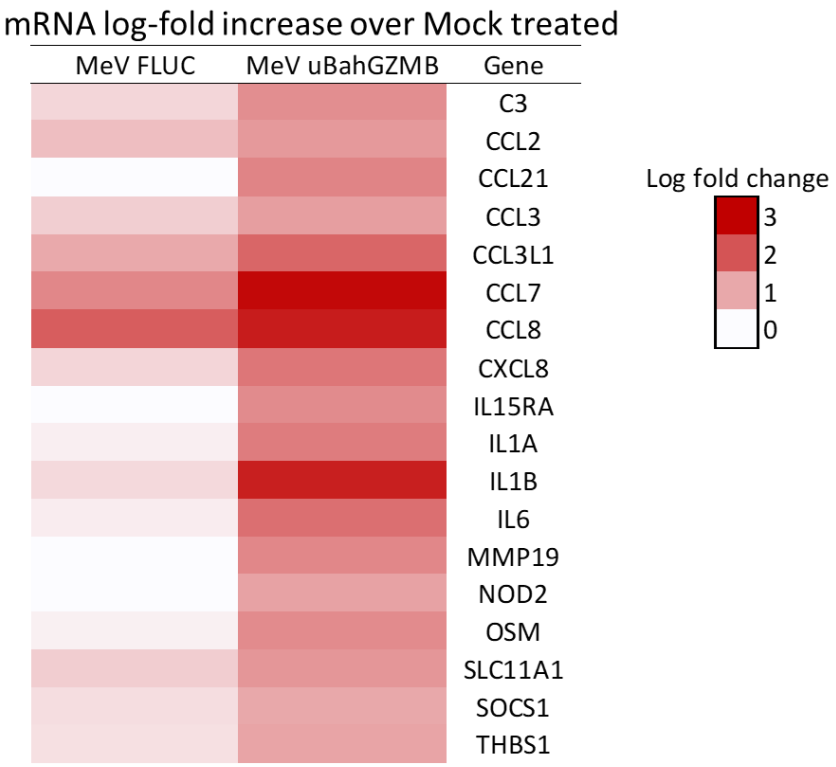

Figure 4.10. MeV P-uBahGZMB upregulated the transcription of proinflammatory cytokines in PBMCs more than MeV P-FLUC. Heat map of individual gene upregulation with the following cut-off criteria: activation of mononuclear leukocytes cluster (234/60736), greater than 1log increase for uBahGZMB (18/234). Fold change of gene expression is shown as log increase over mock infected for both MeV P-FLUC and MeV P-uBahGZMB respectively.

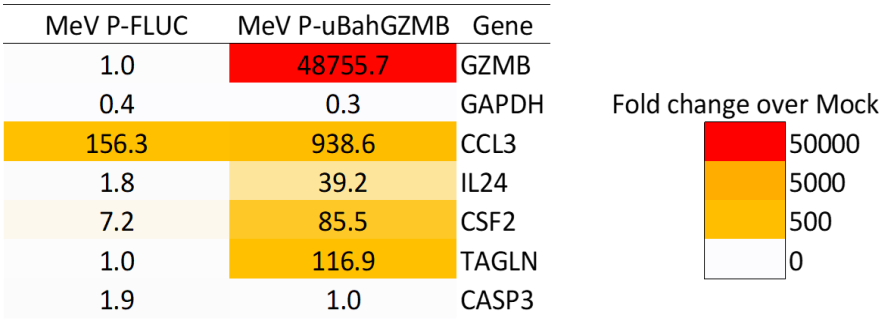

Figure 4.11. MeV P-uBahGZMB upregulated the transcription of proinflammatory cytokines in A549 cancer cells more than MeV P-FLUC. Heatmap displaying transcriptional upregulation of genes of interest following either MeV P-FLUC or MeV P-uBahGZMB infection in A549 cells. Fold increase is shown over mock infected. To note, GAPDH was chosen as a housekeeping gene to demonstrate that baseline levels of gene expression were relatively unchanged.

4.4 DISCUSSION

This chapter highlights the novel insertion of human granzyme B in the oncolytic measles virus genome and its advancements as a cancer therapeutic. This combination aims to take advantage of each element's unique attributes to generate a more powerful anti-cancer therapy. The proposed mechanism of action is as follow: firstly, the oncophilic nature of oncolytic MeV results in selective replication of the virus within the tumor followed by cell lysis and infection of nearby cancer cells. This, in turn, yields a local production of GZMB in infected cells and around the TME due to cell lysis and release of cytoplasmic contents. The presence of GZMB in the TME induces cleavage of ECM components of neighbouring cells resulting in apoptosis initiation and the release of chemokines. Finally, the immunostimulatory environment generated in the TME promotes immune cell recruitment to the tumor and results in a systemic elimination of similar malignancies in addition to a long-term immunity towards that particular cancer. The majority of these putative phases were verified in this project while the remaining mechanisms are outlined as future considerations in order to establish a path to validate the MeV-GZMB oncolytic virus as a potent therapeutic for the treatment of cancer.

The GZMB protein is usually initially produced as an enzymatically inactive preproprotein. Since the GZMB protein will be produced in the cytoplasm of MeV infected cells, the prepropeptide at the N-terminus of the protein cannot be readily removed as is usually the case when processed within CTLs. It was previously reported that the active form of GZMB can be directly produced by substituting the prepropeptide by a methionine[77]. The resulting active human GZMB (ahGZMB) protein is then immediately enzymatically operational following its production, which is ideal for this MeV expression-based system.

The first step in assessing the viability of generating a MeV-GZMB construct is to ensure that the transgene has no negative impact on the viral kinetics of the oncolytic MeV. Previous studies have described the anti-viral properties of GZMB[78–80]; therefore, it is imperative to confirm that GZMB, in this context, possesses a negligible anti-viral effect while maintaining full apoptosis induction capacity. Initial experiments of infecting cells with MeV-GZMB demonstrated very promising results. Under normal circumstances, MeV spread to neighbouring cells via syncytia formation (Figure 4.3). To compare, cells were treated with the staurosporine drug (100 nM), a potent kinase inhibitor and apoptosis inducer[81,82]. Cells treated with the drug displayed the classical CPE of rounding up of the cells from apoptosis (Figure 4.3). Interestingly, cells infected with MeV-GZMB displayed a hybrid CPE; syncytia were observed as the cell's cytoplasms were connected; however, they also appeared to be rounded up and shrivelled, indicating they were also undergoing apoptosis (Figure 4.3). This unique CPE is a strong indication that the GZMB transgene encoded in MeV is functional and has influenced the infected cells.

To substantiate the observed CPE from MeV-GZMB infected cells, the production of GZMB by replicating MeV was assessed by western blot. As can be seen in Figure 4.2, GZMB protein could be detected following infection with MeV-GZMB as opposed to no production in either the mock infected cells or those infected with MeV P-EGFP. Following confirmation of production, GZMBs effect on MeV viral kinetics was assessed. MeV-GZMB achieved similar titers to MeV P-EGFP when the MeV harvesting protocol was followed (Figure 4.1). This confirms that GZMB production from this construct did not hinder the overall replication of MeV. GZMB has been shown to have anti-viral activity via proteolytic cleavage of eukaryotic initiation factor 4 gamma 3, which, some viruses, such as vaccinia virus, are reliant on for viral replication due to its

cap-dependent translation process[78,79]. On the other hand, MeV possesses the capacity to circumvent cap-dependent translation via a mechanism that remains to be determined[83]. It is believed that this adaptation has evolved due to the ability of wildtype MeV to shutdown and redirect host translation for its own viral replication purposes[83]. Altogether, insertion of GZMB in oncolytic MeV did not impair MeV replication so its use as a therapeutic transgene in this system can be further explored.

While verifying expression of GZMB is an essential step, evaluating whether it has any enzymatic activity is equally as important. One of the primary intracellular substrates that GZMB targets is the pro form of caspase-3[68]. Once activated, caspase-3 initiates the classical apoptosis cascade pathway leading to programmed cell death[84,85]. Therefore, caspase-3 activation is not merely a good readout for verifying GZMB activity, but also to confirm apoptosis induction. Cells were either mock infected or infected with MeV P-FLUC or MeV P-ahGZMB. Caspase-3 activation was measured via the IncuCyte® Caspase-3/7 Green Apoptosis Assay kit, which uses a substrate of caspase-3 (DEVD peptide) to evaluate its proteolytic activity. Once the caspase-3 substrate is cleaved, it releases a DNA binding dye that translocates into the cell's nucleus and fluoresces in the green channel once inside the cell. The ahGZMB construct induced a significantly higher fluorescence reading than MeV P-FLUC or mock infected conditions in Vero cells (Figure 4.4). To note, MeV infection by itself promotes apoptosis[86]; nonetheless, by encoding ahGZMB in MeV, the signal was amplified approximately two-fold in this experiment. Subsequent studies using the same assay were performed, namely in the MCF7 and U87 cancer cell lines. Again, the MeV P-ahGZMB construct produced a stronger signal than the MeV P-FLUC, approximately four-fold at

peak in MCF7 cells and two log-fold in U87s. These results confirmed ahGZMB-mediated oncolytic activity in MeV P-ahGZMB infected cells.

The ahGZMB transgene was designed with the aim of producing an enzymatically active form of GZMB as it is expressed. This was achieved by replacing the prepropeptide region at its N-terminus with a single methionine. However, it is possible this single amino acid is attenuating the protein as its N-terminus is not completely free as is typically the case. Therefore, additional engineering of the transgene was performed to maximise its potential potency. An ingenious strategy from Hunter, A., *et al*[87] was adapted to this GZMB system. A ubiquitin tag of 70 amino acids substituted the prepropeptide of human GZMB. This tag is cleaved by ubiquitin carboxy-terminal hydrolase, which is ubiquitously expressed in most tissue types[87]. Following cleavage, the N-terminus is left completely clean and the active form of GZMB is then displayed as is found endogenously. The new construct, termed uBahGZMB, should outperform the ahGZMB if the methionine did in fact interfere with its enzymatic capabilities. Firstly, MeV P-uBahGZMB grew to similar titers to MeV P-ahGZMB and MeV (Figure 4.1). A head-to-head caspase-3 activation assay was performed between the MeV P-uBahGZMB and MeV P-ahGZMB construct. As can be observed in Figure 4.5, the uBahGZMB virus processed caspase-3 considerably more than MeV P-ahGZMB in Vero cells. So, since MeV P-uBahGZMB displayed a more potent apoptosis activation activity than its predecessor, MeV P-uBahGZMB was used for all subsequent experiments.

The cancer cell killing ability of MeV P-uBahGZMB was compared to MeV P-FLUC in an A549 and HCT-15 *in vitro* cancer cell model. The cells were infected with a range of MOIs with either MeV P-uBahGZMB or MeV P-FLUC with a readout using an alamarBlue assay for cell

viability. For the HCT-15, this cell line displays general resistant to MeV induced cell death. No cell death was observed from any condition until the highest MOI of 3 solely with the MeV P-uBahGZMB construct. This result displayed GZMB induced cell death since HCT-15 was seemingly resistant to MeV oncolysis. (Figure 4.6). For the A549 cells, the MeV P-uBahGZMB outperformed MeV P-FLUC at an MOI of 0.3 but failed to do so at the lowest MOI of 0.03 while both constructs nearly eliminated the cells at the highest MOI of 3 (Figure 4.6). These results would indicate a dose-dependent effect for MeV P-uBahGZMB where GZMB impact was only observed at higher MOIs. It is possible that a certain threshold of GZMB must be generated by the virus to have an observable effect over the cell death caused directly by MeV lysis. At the highest MOI in cell lines relatively more susceptible to MeV oncolysis, such as observed here with A549, the ability of MeV to eliminate cancer cells was sufficient and any addition to this is redundant. Nevertheless, while the amount of initial cell death may seem unaffected in certain conditions, the manner in which they are dying is potentially more important.

As cells are stimulated via intrinsic or extrinsic factors, they adapt their transcriptional pathways to adjust their needs. The aim with the MeV P-uBahGZMB construct was ultimately to prompt the host system to generate a proinflammatory response towards the malignancy. By evaluating the transcriptional effects induced by MeV P-uBahGZMB on immune cells and infected cancer cells, its proinflammatory ability can be assessed. Firstly, patient derived PBMCs were incubated with either MeV P-uBahGZMB or MeV P-FLUC. This gives a representative model for the interaction that these viruses would have with the patient's immune system. PBMCs consist predominantly of a mixture of T-cells, B-cells, NK cells, and monocytes who all play a prominent role in adaptive immunity[88,89]. Stimulating these cells into a proinflammatory state

with a virus and then having the same virus replicating in tumor cells may help redirect the patient's immune system towards the tumor itself.

Consequently, transcriptional analysis, specifically RNAseq, was performed on the PBMCs incubated with the genetically altered MeV viral variants. The effects were plotted as MeV P-uBahGZMB versus MeV P-FLUC fold change. The data acquired was analysed with the IPA software to generate total pathway assessments on their transcriptional state. As can be seen on Figure 4.8, a heatmap was generated displaying the transcriptional effects that the uBahGZMB transgene had on the PBMCs. Several relevant proinflammatory pathways, such as the inflammatory response and immune cell trafficking, have upregulated transcriptions. This was the intended impact of the MeV P-uBahGZMB construct as the aim is to generate a more inflammatory version of oncolytic MeV. Further analysis into the inflammatory response pathway led into the cytokine canonical pathway quadrant where individual gene clusters can be evaluated (Figure 4.9). The top hits in this bar chart include interferon and IL-17 signaling. Interferons play a crucial role in anticancer and immune surveillance towards cancer[90], while acute production of IL-17 is attributed to inducing a proinflammatory state of target cells via binding to the IL-17 receptor leading to downstream cytokine and chemokine upregulation[91]. By utilizing the IPA software, a plethora of transcriptional pathway analysis could be undertaken. Nevertheless, the significant trend of upregulating pro-inflammatory genes and pathways by MeV P-uBahGZMB in this PBMC model is very promising.

The transcriptional levels of individual genes were examined following the PBMC incubation with either MeV P-uBahGZMB or MeV P-FLUC versus mock. The genes were filtered to display only those involved with the activation of mononuclear leukocytes and genes that

exhibited an upregulation of 1 log-fold increase or more with the MeV P-uBahGZMB condition. A total of 18 genes fell under these criteria and they were outlined in a heatmap to compare their relative expressions for both virus conditions versus mock (Figure 4.10). The MeV P-uBahGZMB produced a stronger transcriptional upregulation of these genes than the MeV P-FLUC virus. Many of these genes were cytokines and chemokines that play a critical role in the proinflammatory pathway. For example, interleukin-1β (IL1B) is a major component of the inflammatory response[92],and chemokine ligand 7 (CCL7) is a chemoattractant that promotes T-cell and dendritic cell activation[93]. In summary, PBMCs that came in contact with MeV P-uBahGZMB were being readily activated in a proinflammatory state. Therefore, if the PBMCs can be redirected towards the tumor in which the virus is replicating, the host immune response can be guided towards the malignancy.

Direct infection of cancer cells with MeV P-uBahGZMB also generated a strong proinflammatory state. When MeV P-uBahGZMB was compared to MeV P-FLUC in an A549 *in vitro* model, an increase in transcriptional upregulation of proinflammatory genes was also detected (Figure 4.11). An example of this is macrophage inflammatory protein-1α (CCL3) which acts as a potent chemoattractant for lymphocytes to infiltrate tissue[94]. Remarkably, interleukin-24 (IL24) transcription was upregulated approximately 40-fold in A549 cells following MeV P-uBahGZMB infection. This may be valuable as IL24 production is linked with tumor suppressor abilities, such as inhibition to angiogenesis and sensitization to chemotherapy[95]. Interestingly, these transgenes have been previously engineered to be expressed by viruses for the treatment of cancer, for example an oncolytic adenovirus expressing IL24[96], and an autonomous murine parvovirus expressing CCL3[97]. Since GZMB is evidently an upstream inducer of numerous

cytokines and chemokines such as these, multiple proinflammatory pathways can be activated simultaneously which may ensue a multipronged attack towards the cancer.

Genetic engineering of oncolytic measles virus to encode an activatable form of human GZMB produced a cancer therapeutic that is more oncolytic and proinflammatory than the parental oncolytic MeV. The MeV P-uBahGZMB was generated with the aim of creating an oncolytic virus, which displays immunotherapeutic properties, namely, to redirect the patient's immune system towards the malignancy. *In vitro* characterization of this construct validated its pro-apoptosis inducing properties in addition to its increased ability to eliminate cancer cells. Furthermore, transcriptional analysis of PMBCs and cancer cells treated with MeV P-uBahGZMB demonstrated a potent proinflammatory response. However, additional experiments are needed in an immunocompetent *in vivo* cancer model to accurately determine the efficacy of the MeV P-uBahGZMB therapeutic. Regardless, the novel MeV P-uBahGZMB virus offers an exciting avenue of research as an immunostimulatory oncolytic virus.

CHAPTER 5: SYNERGIZING VIRAL SENSITIZERS WITH ONCOLYTIC MEASLES VIRUS FOR ENHANCED TUMOR KILLING

5.1 BACKGROUND AND RATIONALE

5.1.1 Sensitizing cancer cells to virus infection and replication

As described in the previous chapters, cancer cells may have deficiencies in their interferon pathway which allow them to proliferate extensively and uncontrollably; on the other hand, this makes them more susceptible to viral infection. Nevertheless, some cancers remain resistant to oncolytic viruses. Residual innate anti-viral responses remain a major obstacle for the use of oncolytic virotherapies for certain cancer models. Restricted replication and OV spread within heterogenous tumors in addition to virally nonpermissive types of cancer limits the ability of the OV therapy to eliminate the malignancy. These are major impediments that have been highlighted in pre-clinical and clinical trials[98–100]. Therefore, sensitizing cancer cells to oncolytic viruses is at the forefront of the OV research field.

Eliminating or reducing the innate anti-viral response in cancer cells has been investigated from various angles[12]. For example, combining the drug rapamycin with reovirus dampened the innate anti-viral response in a murine melanoma model via mTOR inhibition leading to increased viral replication[101]. Histone deacetylases (HDAC) have also shown to be a target for sensitizing cancer cells to OV replication. Interestingly, targeting HDACs for the treatment of the cancer itself has been previously evaluated. HDACs are major regulatory proteins that control gene transcription via histone deacetylation and chromatin

remodeling[102,103]. Dysregulation of metabolic pathways in certain kinds of cancer guides HDACs to promote gene transcription involved in cellular proliferation, invasiveness, and interferon insensitivity[103–105]. As such, HDAC inhibitors have displayed antineoplastic properties such as cell cycle arrest and apoptosis induction. In addition to this, HDAC inhibitors have demonstrated inhibition of the transcriptional activation of anti-viral ISGs following virus infection leading to increased viral replication and enhanced oncolytic properties[104,106]. A similar strategy was undertaken in sensitising human head and neck cancer cells to VSV with Janus kinase (JAK) 1/2 inhibitors[107]. As a result, a break in the long cascade of antiviral signaling ultimately sensitizes cancer cells to oncolytic viruses.

As such, additional candidates that play a role in antiviral signaling in cancer cells were discovered and pursued to mediate sensitization to oncolytic viruses. Dimethyl fumarate (DMF) had previously shown anticancer properties such as tumor growth and metastasis suppression [108,109]. The group of Diallo, JS., *et al*. demonstrated that combining DMF with oncolytic vesicular stomatitis virus (VSVΔ51) enhanced viral spread in many types of cancers via inhibition of nuclear translocation of nuclear factor κB (NF-κB)[110]. In addition to this, they observed inactivation of STAT1 phosphorylation with IFN stimulation. While the complete mechanism of action remains to be elucidated, the result is a significant decrease in the cancer's cellular response to type I IFN, thus, DMF can be described as an innate antiviral dampener.

Vanadium-based molecules are general inhibitors of protein tyrosine phosphatases[111]. They have been studied in clinicals trials as an anti-diabetic drug, and as a result, their safety in humans has been well documented[112–114]. Further studies revealed the antineoplastic and antimetastatic properties of vanadium-based compounds[115–119]. It was previously reported that

vanadium-based compounds can increase B-cell signaling, splenocyte proliferation, and T-cell activity[120–123]. It was also recently discovered by the Diallo group that vanadium compounds can alter the type I IFN antiviral response to a pro-inflammatory type II IFN response, thereby sensitizing cancer cells to OVs, specifically RNA viruses, to infection and replication[124]. Taken altogether, vanadium-based therapeutics have the potential to significantly alter the patient's adaptive and innate immune system while exhibiting anticancer activity in combination with OVs.

5.1.2 Combining viral sensitizers with oncolytic measles virus

While oncolytic measles virus demonstrates tremendous ability as a cancer therapeutic, some forms of cancer remain resistant to oncolytic viral replication. In a preliminary experiment, it was previously demonstrated that pre-treatment of MeV resistant 786-0 cells with a viral sensitizer (VSe), more specifically, a vanadate compound, increased oncolytic MeV titers[124]. This confirms that previously MeV resistant cell lines can be sensitized to viral replication with pre-treatment of small molecules, such as vanadate. Additionally, in a murine *in vivo* melanoma model, vanadyl sulfate (VS) was shown to increase overall NDV oncolytic ability associated with an increase in NK cell recruitment to the TME[125]. Since NDV belongs to the same *Paramyxoviridae* family as MeV, it is conceivable that VS treatment may also improve oncolytic MeV performance.

An unfortunate caveat with working with oncolytic measles virus is that its replication is very limited in murine cell lines[50,126]. This poses a significant obstacle when developing murine *in vivo* models to best represent human patient settings for oncolytic MeV therapeutics. Though

murine cells do not express a recognised MeV receptor, retargeting MeV or inserting a MeV receptor in the murine cells generally yields limited results[16,51,127,128]. The restrictive replication of MeV within these cells is believed to be due to an intrinsic viral replication blockade subsequent to viral infection[129]. However, no known mechanism has been described to date[50]. Even so, it is possible that viral sensitizers may increase MeV replication in these murine cells via similar mechanisms observed in human cancer cell lines. Consequently, results from these experiments could help elucidate the antiviral mechanisms responsible for restricted oncolytic MeV replication in murine cells thus resulting in the establishment of a better murine *in vivo* model for oncolytic MeV therapy. We hypothesize that viral sensitizer pre-treatment of cancer cells will sensitize them to oncolytic measles virus infection and subsequent oncolysis. This chapter highlights the combinatorial effects of viral sensitizers and oncolytic measles virus for enhanced viral replication and cancer cell killing ability in both human and murine cancer models.

5.2 MATERIALS AND METHODS

5.2.1 Generation and production of murine retargeted MeV

The MeV HmuPA virus was generated as previously described[130]. As a minor modification, the virus used in these experiments was engineered to express EGFP from the P-ATU. Virus rescue was done in Vero α-His cells using the six-his-tagging and retargeting (STAR) MeV rescue system as previously described[131]. Tittering of the virus was done as described in the general materials and methods section, however, Vero α-His cells were used instead.

5.2.2 muPAR expression verification via flowcytometry

Cells were centrifuged 2 min at 5000xg, and supernatant removed. Mouse uPAR-PE antibody was used for murine uPAR detection (FAB531P, R&D Systems, Minnesota, United States) and Rat IgG2A PE as the isotype control (IC006P, R&D Systems, Minnesota, United States). The antibodies used were diluted (1/100) in 1x PBS+0.1% BSA and incubated with the cells for 30 min at 4 °C. Cells were then centrifuged 2 min at 5000xg and supernatant removed. Cells were washed once with 1x PBS and then resuspended in 200uL of 1x PBS. Cells were analysed with a BD Celesta flow cytometer (Beckman Coulter Inc., California, United States). Data was analysed and visualized with FlowJo v10.8 (BD Biosciences).

5.2.4 High throughput VSe and MeV combination analysis

For the human cancer model, BxPC-3 and HT-29 cells were seeded at 25,000 cells per well in a 96-well plate, and then pretreated with VS or DMF 4 hours prior to an infection at an MOI of 0.03 with MeV P-EGFP. Representative images were taken every 24 hours with the AMG EVOS Fluorescence microscope (Advanced Microscopy Group, Washington, USA) and GFP readings taken every 24 hours with the Thermo Scientific ArrayScan XTI (Thermo Scientific, Massachusetts, United States).

For the murine cancer model, 4T1 and TC-1 cells were seeded at 25,000 cells per well in a 96-well plate, and then pretreated with VS or DMF 24 hours prior to an infection at an MOI of 3 with MeV P-EGFP HmuPA. Representative images were taken every 24 hours with the AMG EVOS Fluorescence microscope (Advanced Microscopy Group, Washington, USA) and GFP readings

were taken every 24 hours with the Thermo Scientific ArrayScan XTI (Thermo Scientific, Massachusetts, United States). Alamarblue experiments were done as previously described in the general materials and methods section (2.4).

5.2.6 Compusyn synergy analysis

Cell death data of 4T1 and TC-1 cells was processed with the Compusyn software V1.0 (ComboSyn, Inc.) [132]. A non-constant combination analysis between the combination of MeV + drug versus the single treatment conditions was performed to assess whether the combinatorial effect was synergistic. The following data was excluded from the predictive analysis as they were outliers: 4T1 (400 µM), and TC-1 (64, 160, and 400 µM). A report was generated for each cell line.

5.2.7 *In vivo* murine tumor model

All *in vivo* experiments were approved by the Animal Care and Veterinary Service (University of Ottawa) in compliance with the guidelines of the Canadian Council on Animal Care and the Animals for Research Act. Female C57Bl/6 mice (Charles River Laboratories, Massachusetts, United States) 6-8 weeks old were implanted by subcutaneous injections in the right flank with 1 x 10^6 TC-1 cells resuspended in 100 µl of 1x PBS carrier fluid mixed 1:1 with Matrigel (Corning Matrigel Matrix, Corning Inc., New York, United States). The tumors were allowed to grow to an average size of 100 µl and then the mice were treated on day 1, 3, and 5 with the indicated conditions. Mice were distributed to the different treatment groups according to tumor size for an even tumor average. For the virus injection, 5 x 10^6 ciu MeV P-EGFP HmuPA

in 100 µl of Opti-MEM (Gibco, Thermo Fisher Scientific, Massachusetts, United States) or just the carrier fluid for mock was injected intratumorally. For the viral sensitizer injection, 35 mg/kg of vanadate sulfate diluted in 500 µl of 1x PBS or only 1x PBS for the mock condition was injected intratumorally. The viral sensitizer injection was administered first, and 4 hours later the virus injection was performed. Tumor size was measured every 2 days using a digital caliper. Tumor volume was calculated as: volume = (length^2 × width)/2. Mice were euthanized when tumors had reached 1,500 mm^3.

5.2.8 *Ex vivo* murine tumor model

The *ex vivo* murine model was performed as described previously[124]. Briefly, female C57Bl/6 mice (Charles River Laboratories, Massachusetts, United States) 6-8 weeks old were implanted in the right flank with 1 x 10^6 TC-1 cells resuspended in 100 µl of 1x PBS carrier fluid mixed 1:1 with Matrigel (Corning Matrigel Matrix, Corning Inc., New York, United States) subcutaneously. Mice were euthanized after tumors had reached a size of at least 100 µl. The tumors were excised, cored with a punch biopsy to approximately 2 mm x 2 mm, and deposited in individual wells on a 96-well plate. Each core was kept in 1 ml of DMEM supplemented with 10% FBS, 0.75 µg/ml Amphotericin B, and 50 µg/ml gentamicin. Cores were rested for 30 minutes then pretreated with the indicated concentration of VS and, 4 hours later, infected with 1 x 10^6 ciu MeV P-EGFP HmuPA in specified wells. A total of three cores per condition was done. Images were taken with AMG EVOS Fluorescence microscope (Advanced Microscopy Group, Washington, USA) every 24 hours.

5.3 RESULTS

5.3.1 VSe and MeV combination yields increased BxPC-3 and HT-29 cancer cell killing

Pre-treatment of either BxPC-3 or HT-29 cells with DMF or VS did not yield any visible increase of MeV P-EGFP spread (Figure 5.1). Quantification of MeV spread using an Arrayscan detecting GFP signal confirmed these observations (Figure 5.2-5.3). However, when cell viability was measured via alamarBlue, the combination of either VS+MeV or DMF+MeV outperformed the MeV or VSe monotherapies in cancer cell killing ability (Figure 5.4-5.5).

5.3.2 VSe and MeV synergize for increased viral replication and cancer cell killing ability in TC-1 and 4T1 murine models

As murine cells do not express a recognised MeV receptor, a MeV retargeted to an endogenously expressed murine cell receptor, urokinase-like plasminogen activator (uPA) receptor, was generated. The newly generated virus, also encoding EGFP, termed MeV P-EGFP HmuPA, was successfully rescued, passaged, and purified to titers comparable to MeV. The murine cell lines TC-1, 4T1, and B16 were analysed for muPAR expression via flow cytometry. While TC-1 and 4T1 displayed positive expression of the receptor, B16 did not (Figure 5.6). Infection of these murine cell lines with MeV P-EGFP HmuPA yielded little to no infection, opposite to Vero α-His, which demonstrated high infectibility (Figure 5.7).

Pre-treatment of 4T1 cells with DMF prior to MeV P-EGFP HmUPA infection sensitized the cells to viral replication. However, pre-treatment of 4T1 cells with VS did not have any

observable effect on MeV replication (Figure 5.8). The opposite was observed in TC-1 cells where VS pre-treatment increased MeV permissiveness, but DMF did not (Figure 5.9). B16 cells were

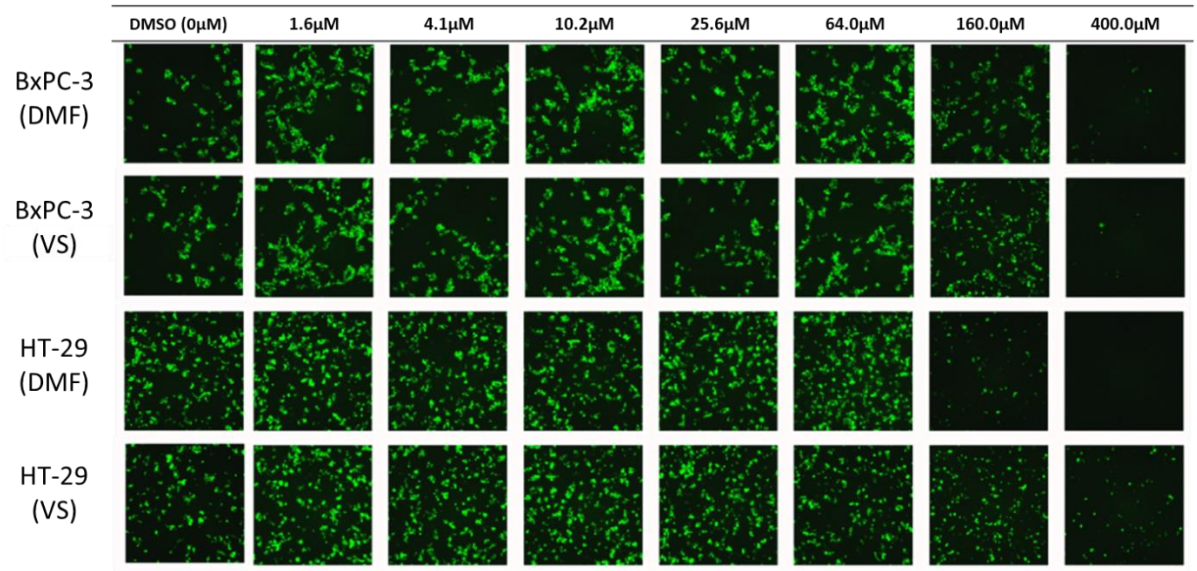

Figure 5.1. No observable difference was detected in MeV P-EGFP replication from BxPC-3 and HT-29 cells treated with viral sensitizers. ArrayScan representative images of BxPC-3 and HT-29 cells, seeded at 25,000 cells/well in 96 well, pretreated with VS or DMF 4 hours prior to an infection at an MOI 0.03 with MeV P-EGFP. Representative images taken 72 hours post-infection. No visible increase in GFP signal is seen in most conditions, however at 400 μM there is reduced MeV P-EGFP replication.

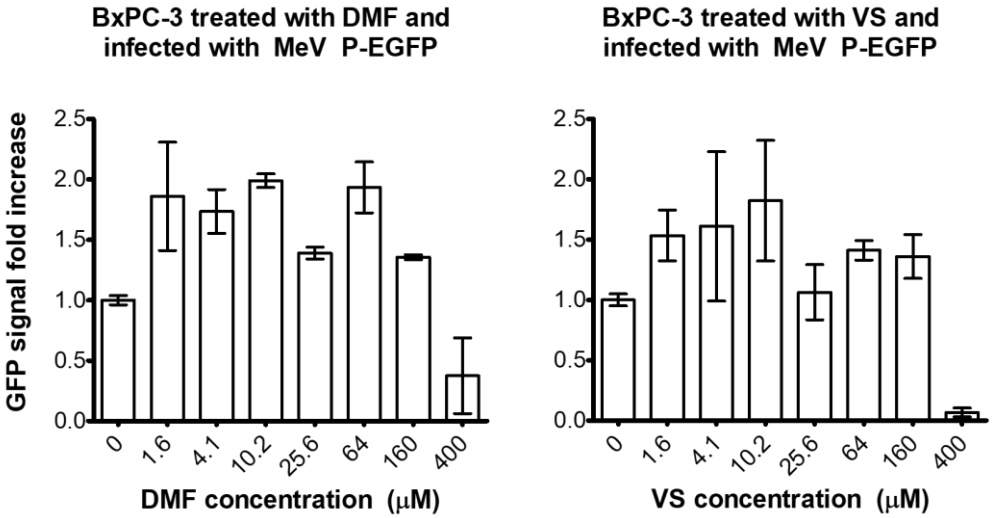

Figure 5.2. DMF and VS did not significantly increase MeV P-EGFP replication in BxPC-3 cells. BxPC-3 cells, seeded at 25,000 cells/well in a 96 well plate, grown for 24 hours, then pretreated with VS or DMF 4h prior to infection with MeV P-EGFP at an MOI 0.03. Readings were done at 72 hours post-infection. No significant difference in GFP reading was observed following VSe treatment. GFP Positive counts determined via ArrayScan. (n = 2; mean ± SD, unpaired t-test).

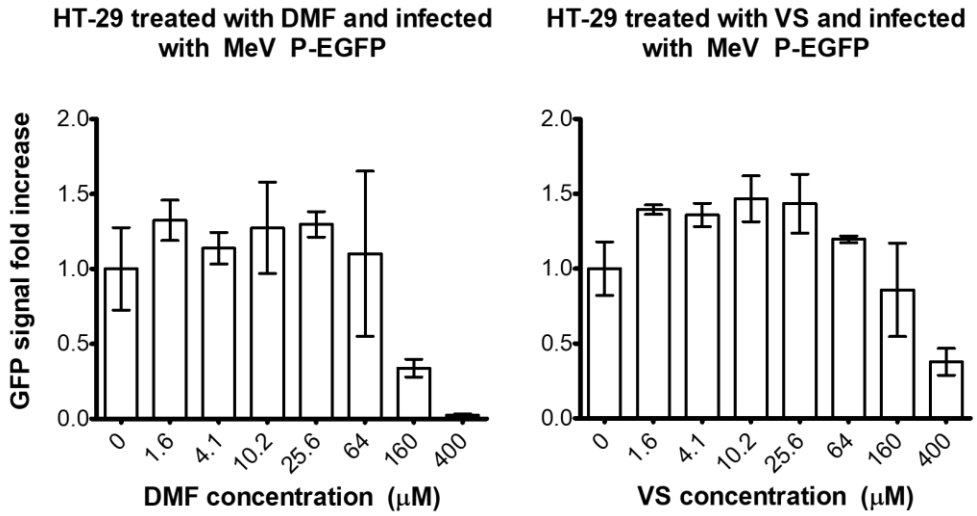

Figure 5.3. DMF and VS did not significantly increase MeV P-EGFP replication in HT-29 cells. HT-29 cells, seeded at 25,000 cells/well in a 96 well plate, grown for 24 hours, and then pretreated with VS or DMF 4h prior to infection with MeV P-EGFP at an MOI 0.03. Readings were done at 72 hours post-infection. No significant difference in GFP reading was observed following VSe treatment. GFP Positive counts determined via ArrayScan. (n = 2; mean ± SD, unpaired t-test).

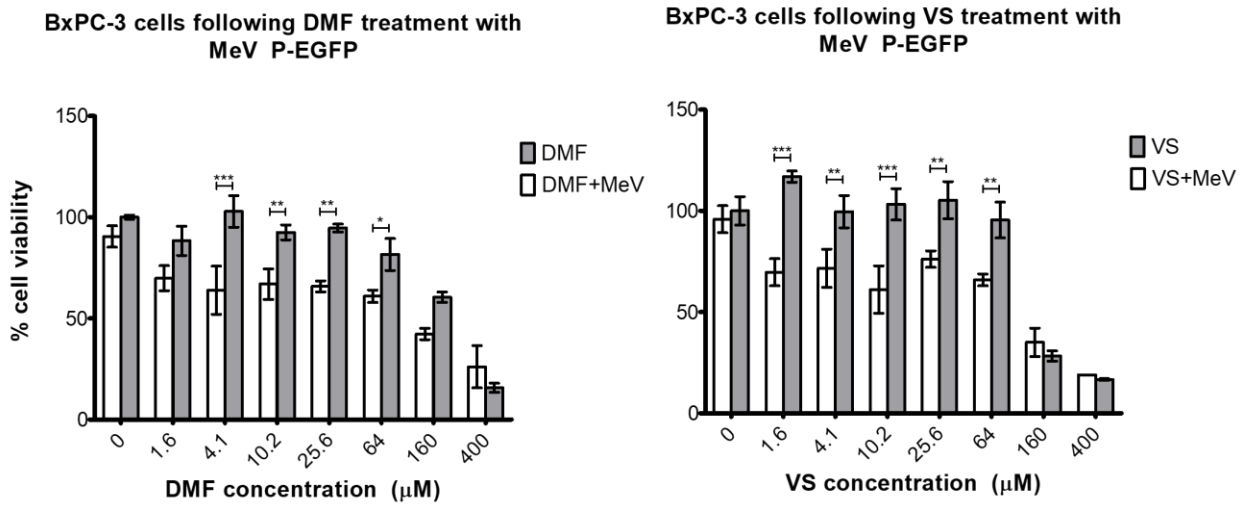

Figure 5.4. DMF and VS sensitize BxPC-3 cells to MeV P-EGFP induced cell killing. AlamarBlue assay on BxPC-3 cells seeded at 25,000 cells/well in a 96-well plate. 24 hours after seeding, the cells were pretreated with DMF or VS 4 hours prior to an infection at an MOI of 0.03 with MeV P-EGFP. Percent cell viability was calculated relative to the mock infected samples. Pre-treatment with either DMF or VS sensitized the cells to MeV P-EGFP induced cell killing. AlamarBlue assay reading done on BioTek reader at 72 hours post-infection. (n = 2; mean ± SD; *P<0.05, **P<0.01, ***P < 0.001, two-way ANOVA).

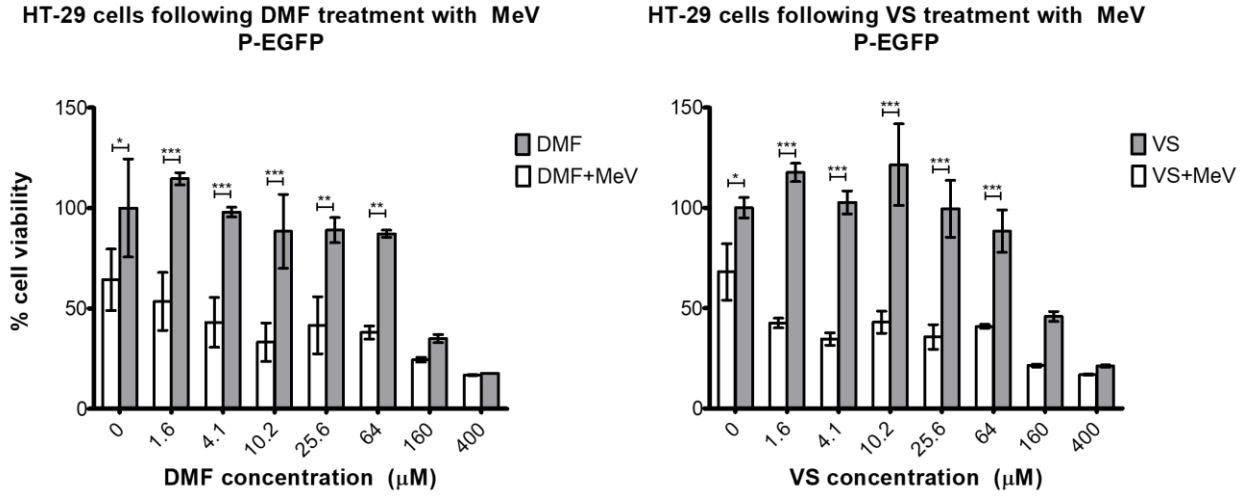

Figure 5.5. DMF and VS sensitize HT-29 cells to MeV P-EGFP induced cell killing. AlamarBlue assay on HT-29 cells seeded at 25,000 cells/well in a 96-well plate. 24 hours after seeding, the cells were pretreated with DMF or VS 4 hours prior to an infection at an MOI of 0.03 with MeV P-EGFP. Percent cell viability was calculated relative to the mock infected samples. Pre-treatment with either DMF or VS sensitized the cells to MeV P-EGFP induced cell killing. AlamarBlue assay reading done on BioTek reader at 72 hours post-infection. (n = 2; mean ± SD; *P<0.05, **P<0.01, ***P < 0.001, two-way ANOVA)

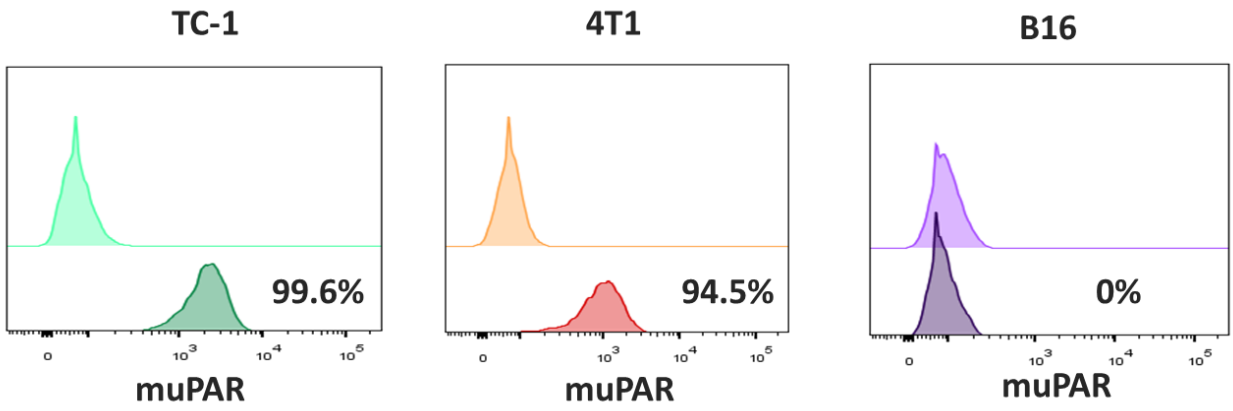

Figure 5.6. TC-1 and 4T1 murine cell lines expressed muPAR whereas B16 did not. Flowcytometry results of the indicated mouse cell line following probing for muPAR. The shift in spectra versus background from the isotype control revealed that muPAR was ectopically expressed on TC-1 and 4T1 cells but not on B16 cells. Data analysed and visualized with FlowJo v10.8 (BD Biosciences).

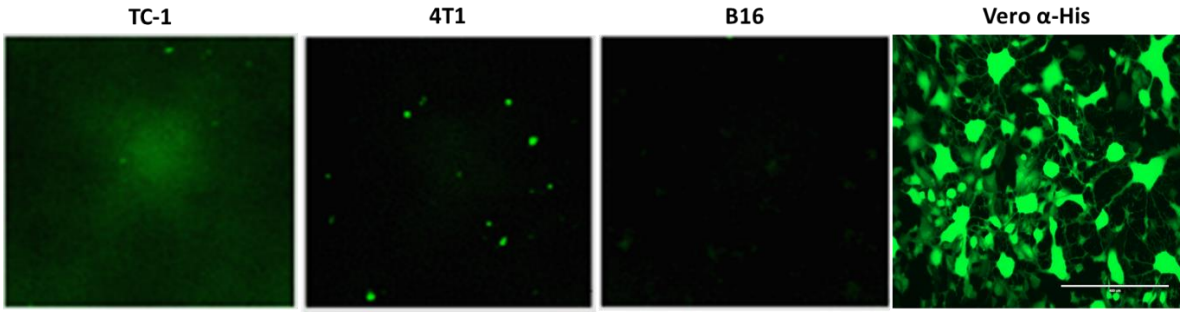

Figure 5.7. MeV P-EGFP HmuPA did not replicate well in murine cells but did replicate normally in Vero α-His cells. Indicated murine cell lines infected with MeV P-EGFP HmuPA at an MOI of 3 for TC-1, 4T1, and B16 cells, while an MOI of 0.1 was used for the Vero α-His cells. Images were taken with a 10X objective at 120 hours post-infection for TC-1, 4T1, and B16, and at 24 hours post-infection for the Vero α-His cells. While there was limited replication in the murine cell lines, the Vero α-His cells were readily infectable. B16 acts as a negative control as it does not have a recognised receptor for MeV P-EGFP HmuPA.

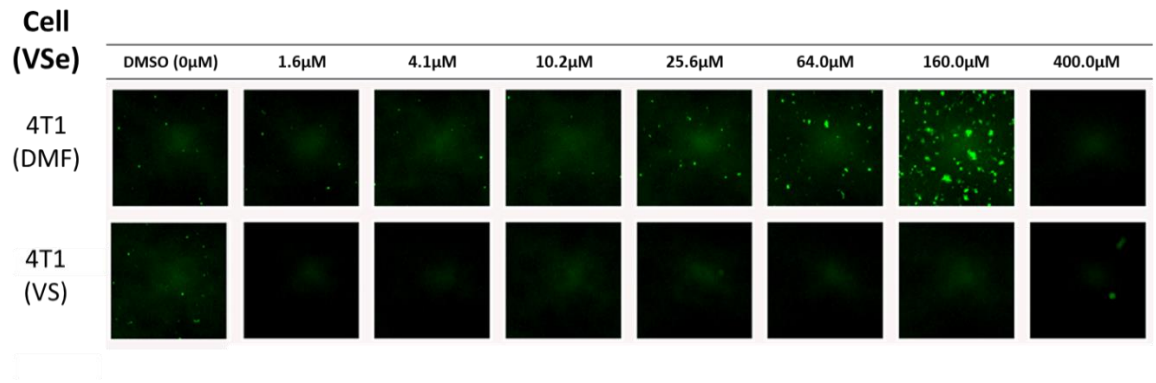

Figure 5.8. DMF, but not VS, sensitizes 4T1 cells to MeV P-EGFP HmuPA replication. ArrayScan images of 4T1 cells seeded at 25,000 cells/well in a 96-well plate. 24 hours after seeding, the cells were pretreated with VS or DMF 24 hours prior to an infection at an MOI 3 with MeV P-EGFP HmuPA. Representative images were taken 120 hours post-infection. A clear increase in MeV P-EGFP HmuPA replication was seen at the higher concentrations of DMF (25.6-160 μM) while no difference is observed in the VS pretreated condition.

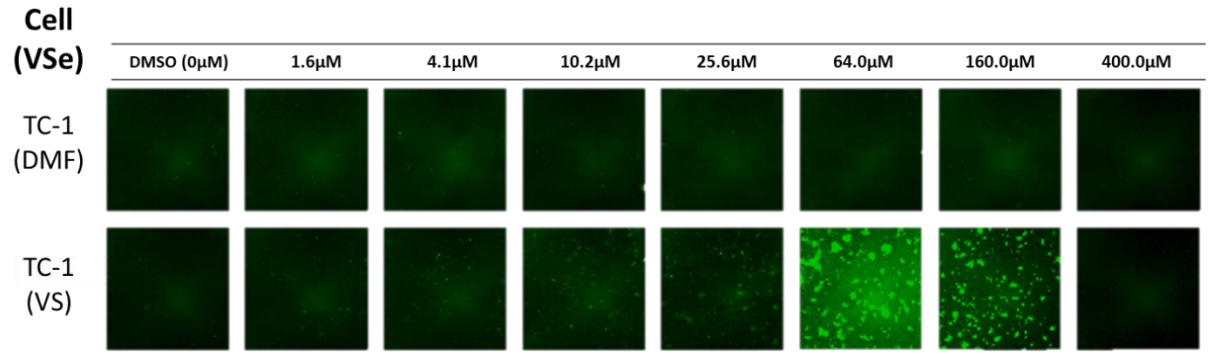

Figure 5.9. VS, but not DMF, sensitizes TC-1 cells to MeV P-EGFP HmuPA replication. ArrayScan images of TC-1 cells seeded at 25,000 cells/well in a 96-well plate. 24 hours after seeding, the cells were pretreated with VS or DMF 24 hours prior to an infection at an MOI 3 with MeV P-EGFP HmuPA. Representative images were taken 120 hours post-infection. A clear increase in MeV P-EGFP HmuPA replication was seen at the higher concentrations of VS while no difference was observed in the DMF pretreated condition.

used as a negative control and no MeV infection was observed regardless of VSe pre-treatment (Figure 5.10). Cell viability was measured via an alamarBlue assay. The increase in MeV replication coincided with an increased cell killing ability for both 4T1 (Figure 5.11) and TC-1 (Figure 5.12) cell lines, with the combination outperforming the MeV monotherapy. Synergy in cancer cell killing ability of DMF+MeV in the 4T1 model as well as VS+MeV in the TC-1 model was confirmed with a sub 1 combination index (CI) score from a Compusyn predictive analysis (Figure 5.11, Table 5.1). A CI score of 1 indicates additive effect and above 1 indicates antagonism.

5.3.3 VS and MeV P-EGFP HmuPA combo was less effective than monotherapies in a C57Bl/6 TC-1 *in vivo* murine model

In order to determine if the encouraging results observed *in vitro* translates to the *in vivo* model, the vanadyl sulfate (35 mg/kg) plus MeV P-EGFP HmuPA (5×10^6 ciu) combination was assessed in a C57Bl/6 TC-1 immunocompetent murine model (Figure 5.14). Following the mice for a total of 39 days (n=4 for PBS+MeV, n=5 for VS+MeV and VS+OPTI, n=3 for PBS+OPTI), the Kaplan-Meier survival curve revealed that the MeV monotherapy outperformed the MeV+VS combination (Figure 5.15). Furthermore, tumor burden was better controlled following singular MeV administration versus the combination, significantly on days 19 and 21 (Figure 5.15). To note, the MeV+VS combination outperformed the VS monotherapy in both survivability and tumor control.

5.3.4 Vanadyl sulfate increased MeV P-EGFP HmuPA viral replication in a TC-1 *ex vivo* model

In order to understand why there were differences of success between the *in vitro* and *in vivo* TC-1 models, an *ex vivo* model was tested. As can be seen on Figure 5.16, 4-hour pre-treatment or cores with VS increased MeV P-EGFP HmuPA spread, as observed by GFP expression, with the highest dose (100 µM) displaying the most drastic effect. The images shown are a representative image of three tumor cores per treatment condition. As expected, there was barely any detectable GFP in the non-VS treated tumor core. Interestingly, when VS and MeV were co-incubated prior to administration, MeV P-EGFP HmuPA infection was completely abrogated.

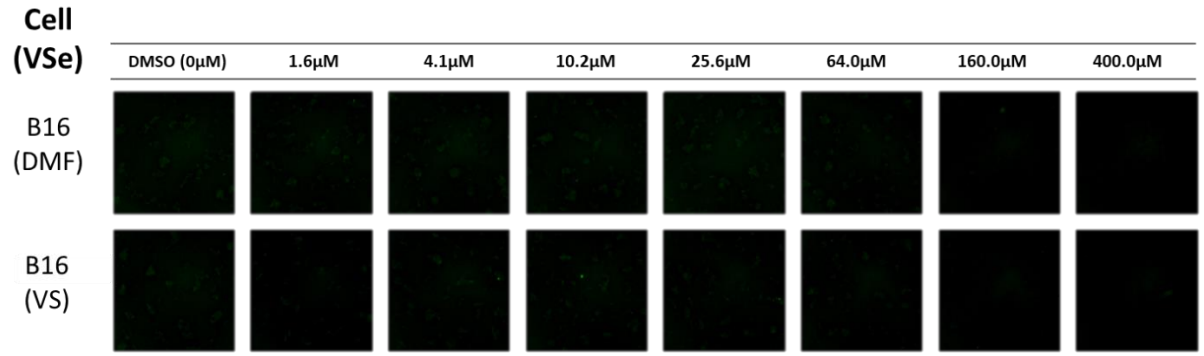

Figure 5.10. Viral sensitizers did not increase MeV P-EGFP HmuPA replication in B16 cells. ArrayScan images of B16 cells seeded at 25,000 cells/well in a 96-well plate. 24 hours after seeding, the cells were pretreated with VS or DMF 24 hours prior to an infection at an MOI 3 with MeV P-EGFP HmuPA. Representative images were taken 120 hours post-infection. There was no increase in infection with the pre-treatment of VSes, as expected since B16 does not possess a recognised receptor for MeV P-EGFP HmuPA

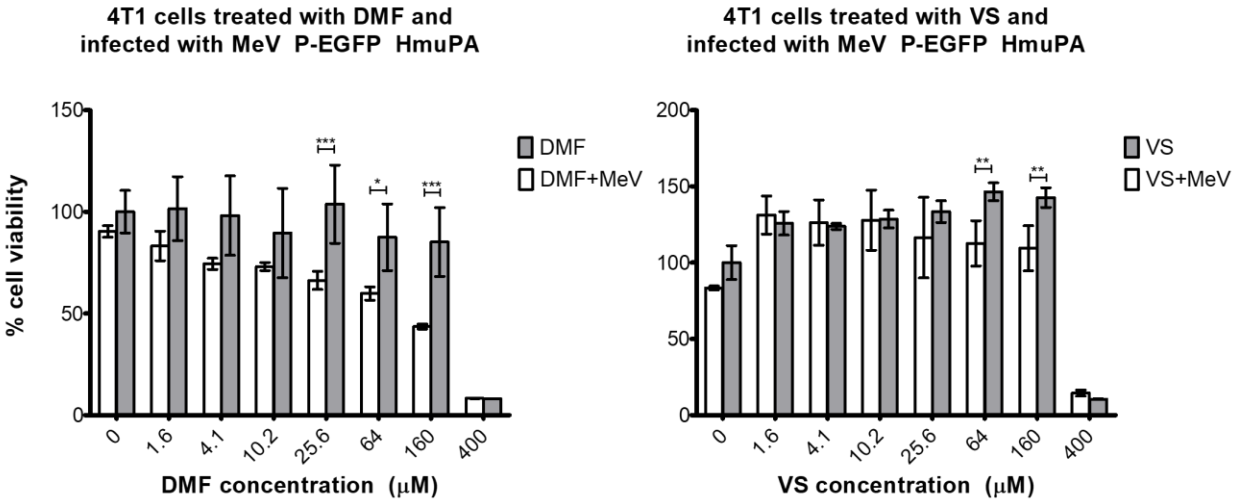

Figure 5.11. DMF, but not VS, sensitizes 4T1 cells to MeV P-EGFP HmuPA-induced cell killing. AlamarBlue assay was performed on 4T1 cells seeded at 25,000 cell/well in a 96-well plate. 24 hours after seeding, the cells were pretreated with DMF or VS 24 hours prior to an infection at an MOI of 3 with MeV P-EGFP HmuPA. Percent cell viability was calculated relative to the mock infected samples. Pre-treatment with DMF sensitized the cells to MeV P-EGFP HmuPA induced cell killing but VS did not. AlamarBlue assay reading done on BioTek reader at 120 hours post-infection. (n = 2; mean ± SD; *P<0.05, **P<0.01, ***P < 0.001, two-way ANOVA)

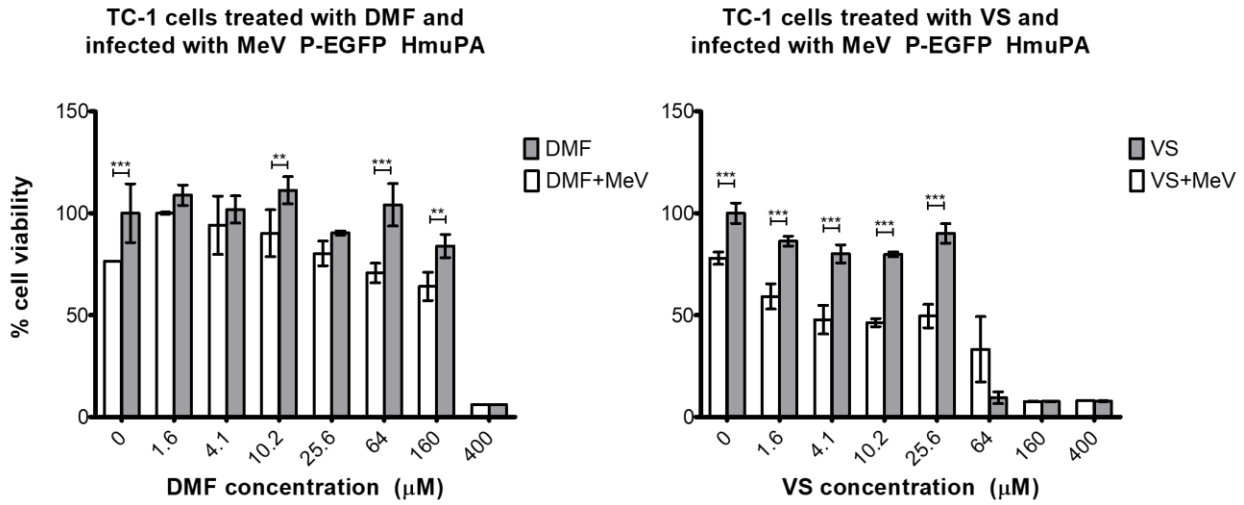

Figure 5.12. VS, but not, DMF sensitizes TC-1 cells to MeV P-EGFP HmuPA-induced cell killing. AlamarBlue assay was performed on TC-1 cells seeded at 25,000 cells/well in a 96-well plate. 24 hours after seeding, the cells were pretreated with DMF or VS 24 hours prior to an infection at an MOI of 3 with MeV P-EGFP HmuPA. Percent cell viability was calculated relative to the mock infected samples. Pre-treatment with VS sensitized the cells to MeV P-EGFP HmuPA induced cell killing but DMF did not. AlamarBlue assay reading done on BioTek reader at 120 hours post-infection. (n = 2; mean ± SD; *P<0.05, **P<0.01, ***P < 0.001, two-way ANOVA)

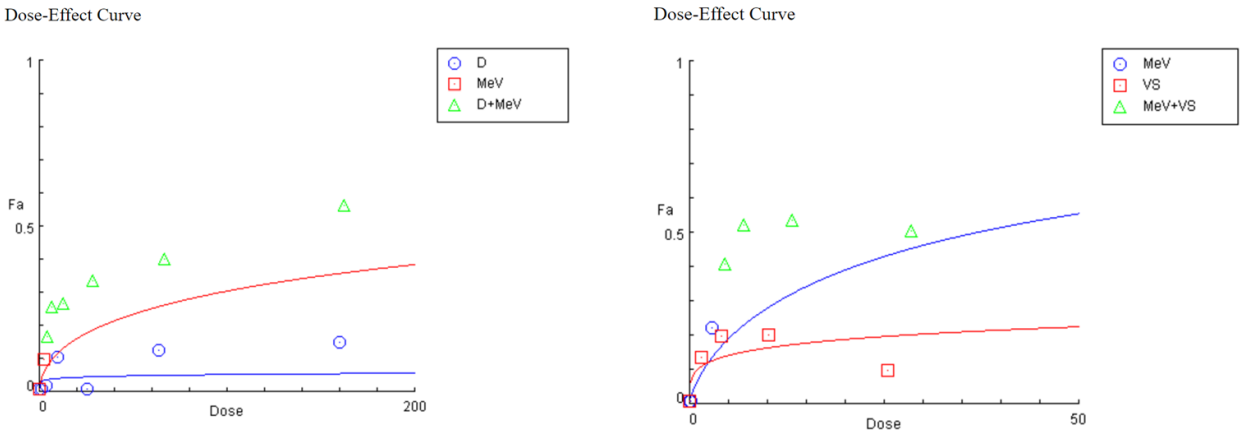

Figure 5.13. Dose-effect on cell death by combinatorial VSe and MeV P-EGFP HmuPA treatment versus the monotherapies in both the TC-1 and 4T1 models. The dose-effect curve depicting the ability to induce cell killing ability (y-axis) in relation to the VSe dose in μM (x-axis). Data was analysed using the Compusyn software. (Left) The dose-effect curve from the cell killing ability in the 4T1 model with DMF (D) and MeV combo. The combination treatment (green) had more effect than both monotherapies. (Right) The dose-effect curve from the cell killing ability in the TC-1 model with VS and MeV combo. The combination treatment (green) had more effect than both monotherapies.

Table 5.1. DMF and MeV in the 4T1 model and VS and MeV P-EGFP HmuPA in the TC-1 model acted in synergy in their cancer cell killing ability. Combination index score for VSe + MeV condition in cell killing ability. Data was analysed using the Compusyn software. The combination index was determined via a predictive algorithm, where a score lower than 1 indicates synergy in that condition. (Top) Data from the 4T1 cell killing ability of DMF + MeV P-EGFP HmuPA. (Bottom) Data from the TC-1 cell killing ability of VS + MeV P-EGFP HmuPA.

CI Data for Non-Constant Combo: DMF+MeV

Dose DMF (μM)	Dose MeV (MOI)	Effect	CI
1.6	3	0.168	0.136
4.1	3	0.256	0.048
10.2	3	0.269	0.042
25.6	3	0.338	0.022
64	3	0.402	0.013
160	3	0.564	0.004

CI Data for Non-Constant Combo: MeV+VS

Dose VS (μM)	Dose MeV (MOI)	Effect	CI
1.6	3	0.409	0.137
4.1	3	0.523	0.072
10.2	3	0.537	0.067
25.6	3	0.505	0.082

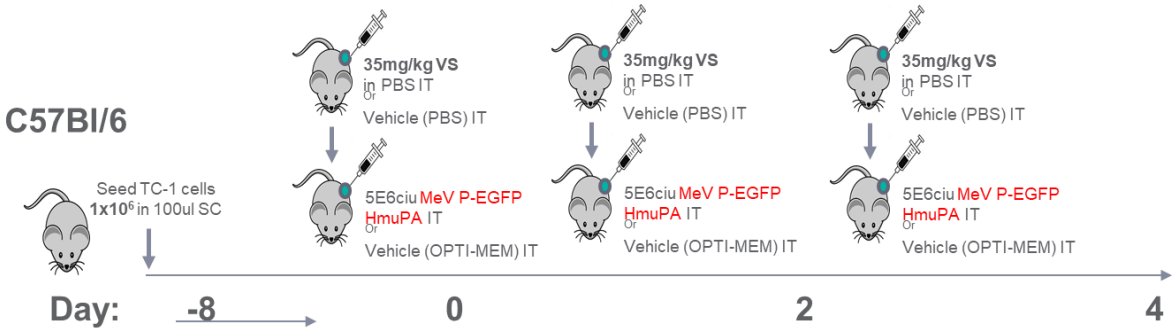

Group	Treatment 1	Treatment 2 (4h later)	#Animals
1	PBS	OPTI-MEM	5
2	VS	OPTI-MEM	5
3	PBS	MeV P-EGFP HmUPA	5
4	VS	MeV P-EGFP HmuPA	5

Figure 5.14. Experimental outline of TC-1 C57Bl/6 syngeneic *in vivo* murine model to assess the efficacy of vanadyl sulfate and MeV P-EGFP HmuPA combination treatment. The top of the figure depicts the treatment regimen for the mice. The mice were seeded with TC-1 cells and 8 days later the treatment was started. There was a total of three treatments every 2 days. The group outline is depicted in the table at the bottom of the figure with the treatment conditions.

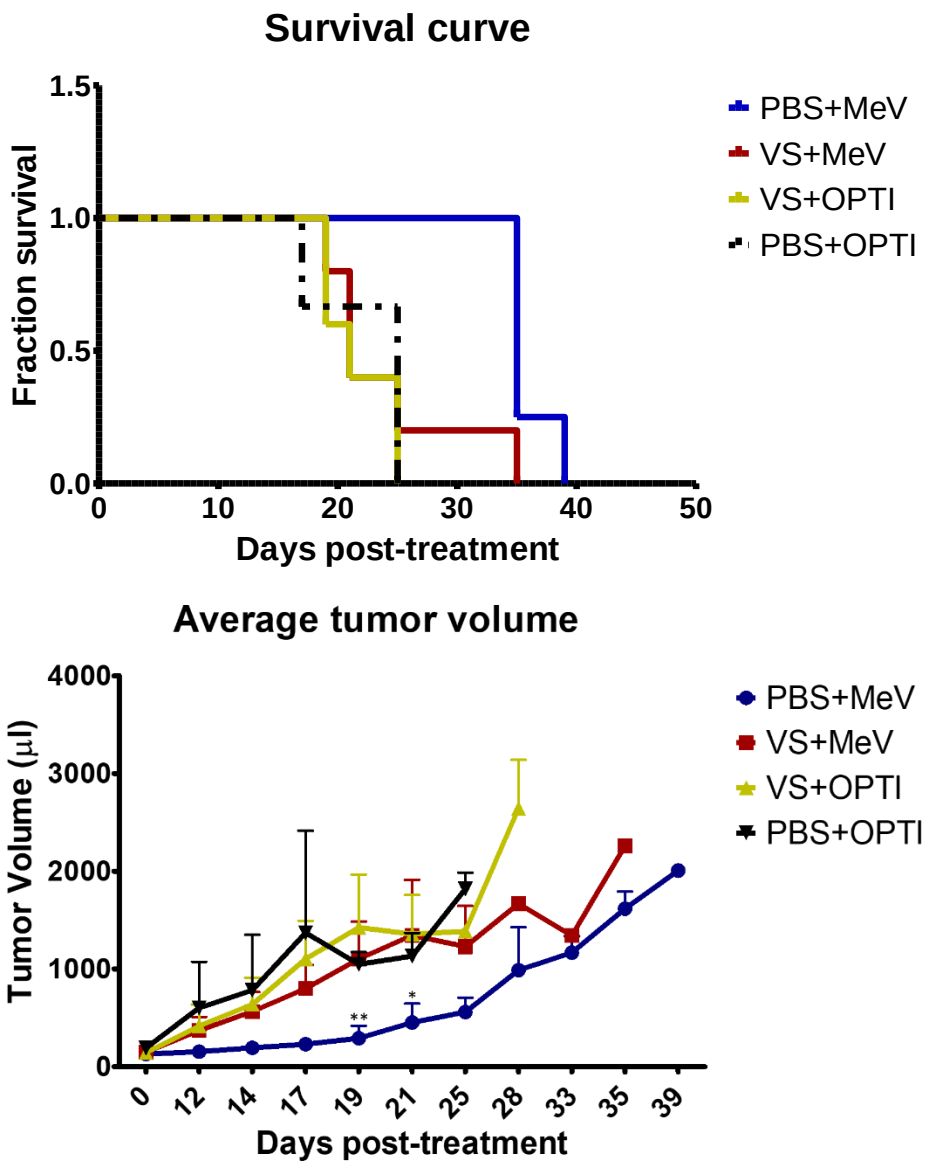

Figure 5.15. The VS and MeV combination did not increase survival or reduce tumor volume in a TC-1 C57Bl/6 *in vivo* murine model. The mice were either mock treated (PBS) or treated with vanadyl sulfate (VS) intratumorally. 4 hours following the drug treatment, the mice were injected with mock treated (OPTI) or infected with MeV P-EGFP HmuPA (MeV) intratumorally. Mice were subjected to three total treatments on day 0, 2, and 4. 18 out of the 20 tumors grew. One mouse perished during MeV IT injection by an unidentified cause. (Top) Kaplan-Meier survival curve of each group of mice following their respective treatments. No significant results are observed in the survival curve graph. (Bottom) The average tumor volume over the course of the experiment of each group of mice following their respective treatment. Some significance observed comparing average tumor volume of PBS+MeV versus VS+MeV on days 19 and 21. (n=4 for PBS+MeV, n=5 for VS+MeV and VS+OPTI, n=3 for PBS+OPTI, mean+SD, log rank Mantel+Cox test for the survival curve and two-way ANOVA for the average tumor volume, *P<0.05, **P<0.01).

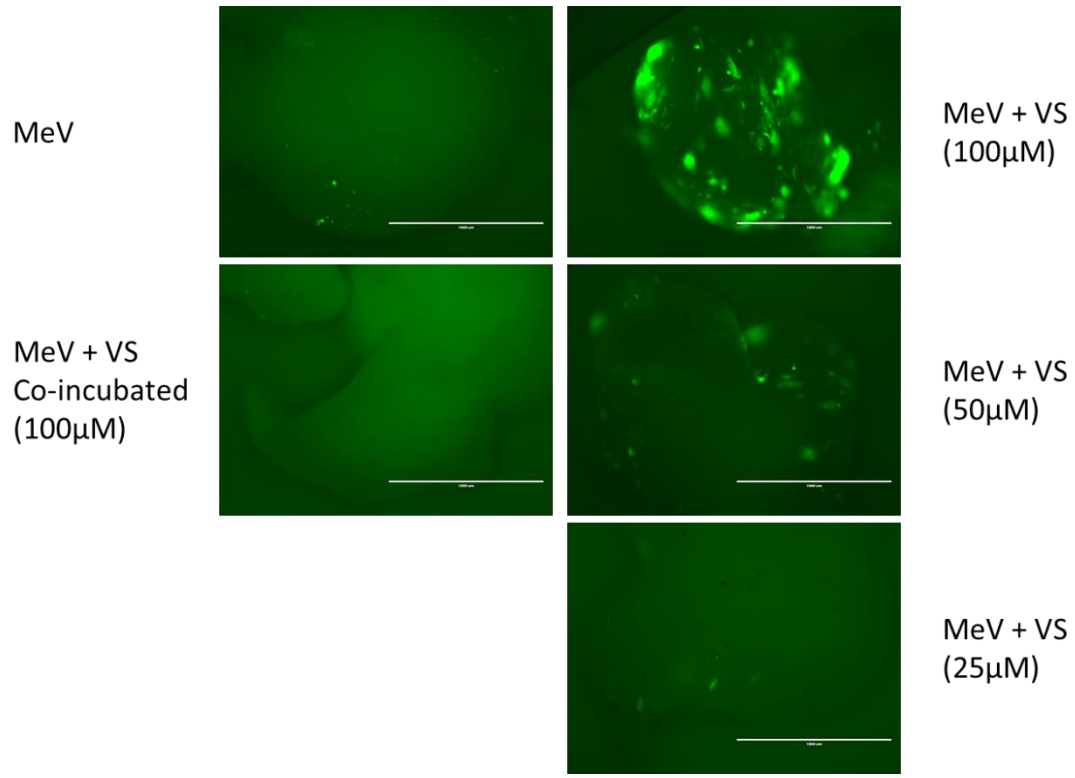

Figure 5.16. Vanadyl sulfate sensitizes TC-1 *ex vivo* tumor cores to MeV P-EGFP HmuPA replication when administered prior to infection. Representative images from a total of three tumor cores per treatment group. Images taken 144 hours post-infection of TC-1 explanted tumor. The tumor was subsequently cored and pre-treated with VS at the indicated concentration 4 hours prior to infection with MeV P-EGFP HmuPA. A clear increase in GFP signal is observed with increasing concentration of VS. On the bottom left panel, the VS formulation was incubated with MeV P-EGFP HmuPA prior to infection. No GFP signal is visible suggesting virus neutralization.

5.4 DISCUSSION

This chapter highlights the effects of viral sensitizers, namely dimethyl fumarate and vanadyl sulfate, on the replication and cancer cell killing ability of oncolytic measles virus. The aim of this study was to validate the use of these viral sensitizers in combination with oncolytic MeV in specific human and murine cancer models. Since certain cancer models remain resistant to oncolytic MeV, sensitizing them to viral replication would result in a significantly improved therapeutic strategy.

The first arm of this project consisted of evaluating whether DMF and VS sensitize MeV resistant human cancer cells to oncolytic MeV replication and oncolysis. BxPC-3 and HT-29 cancer cells were chosen based on their tolerance towards MeV infection but resistance to total MeV oncolysis at lower MOIs. Pre-treatment of cells with a VSe 4 hours prior to virus infection was determined previously as a suggested treatment regimen[110,124]. Following MeV P-EGFP infection, Arrayscan images were taken and total GFP signal was measured every 24 hours. As can be seen on Figure 5.1, after 72 hours there was no obvious difference in GFP signal in the treatment groups with the exception of the lack of signal in the highest concentration of VSes stemming from cytotoxicity from the drugs. Follow up quantification of these results confirmed a lack of significant increase of GFP signal in the treatment conditions compared to the DMSO control (Figure 5.2-5.3). An alamarBlue assay was performed to assess whether the combination treatment induced a higher rate of cell death. For the BxPC-3 cells, after 72 hours the virus alone reduced the viability to approximately 90%; however, with pre-treatment of DMF (4.1-64 µM) or VS (1.6-64 µM) in combination with MeV, the cell viability was reduced to the 60-70% range (Figure 5.4). The drug doses seemed well tolerated up until the 160 µM where cytotoxic effect

from the drug itself was observed. For the HT-29 cells, after 72 hours the virus alone reduced the viability to approximately 65%; however, with pre-treatment of DMF (1.6-64 μM) or VS (1.6-64 μM) in combination with MeV, cell viability was reduced to around 40% (Figure 5.5). As with BxPC-3, the HT-29 tolerated the drug concentration up until the 160 μM where cytotoxic effect from the drug itself was observed. Interestingly, in the case for both cell lines, a higher concentration of VSe did not result in additional MeV induced cell killing, indicating that the drug's effect was sufficient at lower doses. Also, while an increase in MeV replication was not observed in these conditions, an increase in cell killing ability was evident. This may be due to an oversaturation of initial MeV particles; a lower initial MOI could permit us to observe an increase in MeV titers with the combination of VSes. To note, as described in the introduction, one of the major benefits of VS is its immune cell activation properties, which, in this *in vitro* model, cannot be assessed. Nonetheless, it is very interesting to see VS and DMF performing similarly in this scenario. This suggests a similar mechanism of action in sensitizing BxPC-3 and HT-29 cells to oncolytic MeV infection, either through a shared or redundant pathway, via innate antiviral pathway shutdown. The results obtained here with the combination of VS and MeV were very similar to what was previously observed in the combination treatment of VS and NDV in the sense that the fold change in titer was non-significant but the impact on viability was[125]. Regardless, additional experiments, such as IFN-β expression, NF-κB nuclear translocation (for DMF), and antiviral ISG regulation, are needed to fully elucidate the mechanism of action in sensitizing human cancer cells to MeV replication. Also, *in vivo* immunocompetent models should be performed to evaluate the adaptive immunity activity of VS in combination with MeV.

To this end, murine cancer cells were tested in conjunction with VS or DMF with oncolytic measles virus with the goal of developing an immunocompetent *in vivo* model to evaluate the proinflammatory properties of VSes when used with MeV. In addition to this, murine cells are inherently nonpermissive to MeV infection; therefore, by sensitizing them to MeV infection, a MeV permissive murine *in vivo* model can be established. Firstly, as murine cells do not express a MeV receptor, the oncolytic MeV construct was retargeted to the commonly expressed urokinase-like plasminogen activator (uPA) receptor and additionally engineered to express EGFP as a viral replication marker. Flow cytometry analysis on candidate murine cell lines was performed to confirm uPA receptor expression. Interestingly, TC-1 and 4T1 cells express uPA receptor where as B16 cells do not (Figure 5.6). Consequently, B16 cells were used as a negative control. Initial infection of these murine cells at an MOI of 3 with the MeV P-EGFP HmuPA virus yielded very little replication (Figure 5.7). However, infection of Vero α-His cells with the same virus demonstrated a massive EGFP signal and the typical CPE of syncytia formation (Figure 5.7). These results confirmed a post-entry replication blockade activity in these murine cell lines towards MeV.

The 4T1, TC-1 and B16 cells were pre-treated with either VS or DMF 24 hours prior to viral infection in an attempt to maximize their potential effects[110]. Following MeV P-EGFP HmUPA infection, Arrayscan images were taken and total GFP signal was measured every 24 hours. The negative control B16 cells did not show any significant GFP signal in any condition (Figure 5.10) as was expected since it is lacking a recognised receptor for MeV P-EGFP HmUPA. On the other hand, 4T1 cells saw a significant increase in GFP signal 120 hours post-infection when pre-treated with DMF (Figure 5.8). Specifically, the GFP signal was as its peak when the

cells were conditioned with 160 µM of DMF. Interestingly, the increase in GFP signal was not observed when 4T1 cells were pre-treated with any dose of VS. Conversely, TC-1 cells conditioned with VS demonstrated greater permissiveness to MeV infection with a peak GFP signal at 64 µM (Figure 5.9), whereas no increase in GFP signal was observed when TC-1 cells were pre-treated with any dose of DMF. Taken together, these results are quite remarkable as they suggest that murine cell lines may utilize different mechanisms that block MeV replication. Since DMF and VS do not exert the same mechanism of action in conveying viral replication permissiveness, the underlying replication blockade of both 4T1 and TC-1 could be determined via transcriptional and proteomic analysis. If the post-entry MeV replication blockade mechanism of action is elucidated, murine cell lines may be specifically engineered for MeV permissiveness. Continued research in this aspect of the project is entirely warranted as the establishment of MeV permissive murine cancer cell lines would be a major advancement for the oncolytic MeV field.

Cell viability assays were performed to determine whether there is an increase in associated cell death with the increase in MeV P-EGFP HmuPA replication. In the conditions where no increase in GFP signal was observed, 4T1 with VS and TC-1 with DMF, there was no observable difference in cell viability. However, in the conditions where increased GFP signal was detected, there was an attributed amount of cell death (Figure 5.11-5.12). The 4T1 cells tolerated DMF up until the 400 µM dose whereas the TC-1 cells tolerated VS up until the 64 µM dose. MeV alone had negligeable impact on cell viability, except when combined with DMF in the 4T1 model, in which case cell viability was reduced to approximately 40 % at the 160 µM dose. When the TC-1 cells were treated with VS, cell viability was reduced to approximately 45% at the

10.2 µM dose when combined with MeV infection. The cell viability results obtained were analysed via a Compusyn predictive analyses simulation and the activity of VSe + MeV was deemed synergistic for both cell line conditions as the CI rating was below 1 (Table 5.1). Taken together, there seems to be a correlation in MeV replication sensitization and cell death in the TC-1 with VS and 4T1 with DMF conditions. As previously mentioned, additional insight in the mechanism of action of VSes concerning MeV replication sensitization in these murine models may lead to improved efficacy via optimization of the therapeutic regimen. For example, administration of multiple doses of VSes during the course of the MeV infection may further improve spread and subsequent cancer cell killing ability.

With the encouraging results obtained in the *in vitro* models, an immunocompetent murine *in vivo* model was designed. Since VS has previously demonstrated adaptive immunity modulation abilities, TC-1 treated with VS (35 mg/kg) + MeV P-EGFP HmuPA (5 x 10^6 ciu) model was chosen as the *in vivo* experiment. A syngeneic C57Bl/6 TC-1 murine model was established, and groups of mice were apportioned to compare the monotherapies (VS or MeV) versus mock treated and combination therapy. The treatment regimen was designed based on previous work, briefly, tumors were treated with the drug or vehicle and four hours later infected with the virus or the vehicle alone[124,125]. From TC-1 implantation, 1 x 10^6 TC-1 cells were implanted sub-cutaneous in the right-flank; 18 out of the 20 tumors grew. One mouse perished during MeV IT injection by an unidentified cause. As can be seen in Figure 5.15, the average tumor volume growth seems unaffected in both VS treatment conditions but a slight delay in growth is observed in the MeV monotherapy (significantly on days 19 and 21 comparatively to the combination treatment). The survival curve illustrates these findings as the combination therapy

of VS+MeV underperforms relative to both monotherapies, though, none of the groups offers any significant survival benefit (Figure 5.15). These results were quite surprising as it would seem VS administration is having a negative impact on the oncolytic activity of MeV which is contrary to what was observed *in vitro*. A theory to explain this trend is that the VS formulation, which is very acidic, is neutralizing and inactivating the very pH sensitive MeV[133]. In the *in vitro* model, the VS formulation was added into buffered cell media whereas in the *in vivo* model, VS was administered prior to MeV infection three times in a span of 4 days. This cycle of VS administration and virus neutralization may abrogate any effect MeV has on the tumor. Additional insight on treatment regimens and VS formulation is required to optimize the *in vivo* models for MeV combination therapy.

The mixed results obtained from the *in vitro* and *in vivo* TC-1 models required further understanding into the VS + MeV P-EGFP HmuPA therapeutic combination. Therefore, an *ex vivo* TC-1 model was generated. Tumors were explanted once the tumor size reached 100 µl and cored into 2mm x 2mm sections from TC-1 implanted ($1x10^6$ ciu) C57Bl/5 mice and were treated with VS at various concentrations 4 hours prior to MeV P-EGFP HmuPA ($1x10^6$ ciu/core) infection. For one of the samples, the VS mixture was co-incubated with the virus prior to infection to mimic their interaction in a live system. As can be seen in Figure 5.16, the tumor core that was infected with MeV alone had minimal GFP expression even after 144 hours post-infection. However, when the cores were pre-treated with VS, an increase in MeV, as indicated by an increase in GFP expression, is observed as a positive-correlation with a VS dose from 25-100 µM. TC-1 sensitization to MeV replication by VS is therefore achievable in a 3D tumor system. Interestingly, the virus that was co-incubated with the VS formulation prior to infection

displayed no infection thus substantiating the theory of MeV inactivation via contact with the VS formulation in the *in vivo* model. Taken together, these results confirm the positive effect of VS for MeV replication sensitization in murine TC-1 cancer cells and highlight the importance of establishing a suitable treatment regimen for this system.

In summary, oncolytic MeV replication and cancer cell killing ability can be significantly improved with the use of viral sensitizers. In HT-29 and BxPC-3 human cancer cell lines, while no difference in MeV replication was detected following pre-treatment of DMF or VS, increased cell killing ability of the MeV + VSe combination was observed. Remarkably, for the murine cell lines, the viral sensitization effect was only evident with specific VSes. In 4T1 cells, DMF sensitized the cells to MeV replication and cell killing ability, whereas for TC-1 cells, it was VS that sensitized the cells to MeV replication and cell killing ability. The increases in cell killing ability were subsequently confirmed to be in synergistic fashion. Unfortunately, the syngeneic TC-1 *in vivo* model for VS + MeV combination therapy fell short, underperforming versus the monotherapies. However, subsequent *ex vivo* experiments corroborated the theory that the treatment regimen and VS formulation were possibly at fault leaving the prospect of therapy optimization for future experiments. Additional mechanistic insights in VSe induced MeV sensitization of human and, potentially more significantly, murine cancer cells could lead to the development of novel cancer models expanding the field of oncolytic measles virus research. The combinatorial use of viral sensitizers and oncolytic MeV offers a promising avenue in producing a therapeutic approach capable of overpowering treatment resistant cancers.

CHAPTER 6: GENERAL DISCUSSION AND CONCLUDING REMARKS

The overall aim of this thesis was to improve oncolytic measles virus as a cancer therapeutic. Cancer is a very heterogeneous disease with numerous distinct and intricate complexities. Therapies to overcome it require tailored approaches and innovative thinking. The use of attenuated viruses as a treatment option for cancer is in itself cunning. This approach led to the foundation of a novel research field, oncolytic viral therapy, and gave hope that alternative strategies in combatting cancer are not only possible but, in some cases, may develop into the predominant therapeutic recommendation. Nevertheless, as is often the case in research, as more is learned, new questions arise. For instance, several types of cancer present resistance to oncolytic virus treatment by limiting their replication with residual anti-viral mechanisms, while others cannot be eliminated with the virus alone. Also, in some cases, the viral therapy itself inherently poses some drawbacks. This thesis highlights advancements in the development of an oncolytic measles virus therapeutic to overcome existing obstacles that cancer offers.

Firstly, an immediate and important hindrance for the systemic administration of oncolytic measles virus is the presence of pre-existing neutralizing antibodies. Envelope exchange, or pseudotyping, MeV conceals the virus from neutralization. Here, we described the generation of a robust genetic platform for pseudotyping MeV. Also, we demonstrated the complexities involved with pseudotyping MeV, more specifically, the rigidity of MeV in accepting foreign envelope glycoproteins to produce new virions. For example, pseudotyping MeV with

VSV or NDV did not results in the generation of a viable construct, but, doing so with CDV yielded a virus with analogous replication kinetics to MeV. Still, in coming to this observation, we propose a course of action for future MeV pseudotyping endeavours: pseudotyping attempts of MeV ought to be attempted with viruses from the same genus, such as phocine distemper virus. To this end, we have developed a direct and effective genetic platform for envelope exchange of oncolytic measles virus which allows for efficient testing of future pseudotyping candidates.

Secondly, a common issue emphasized by pre-clinical studies of oncolytic viruses is that the virus alone tends to not be potent enough to eradicate the malignancy. A major benefit of oncolytic MeV is that it can be genetically engineered to act as a delivery vector for complimentary genes in addition to its potent and specific oncolytic activity. Here, we describe an oncolytic measles virus engineered to express the human granzyme B transgene. This novel construct displayed increased apoptosis induction capacity, cancer cell killing ability, and immunogenicity than the original virus. When infecting cancer cells and while in the presence of patient derived immune cells, the MeV P-uBahGZMB virus induced the upregulation of a plethora of proinflammatory cytokines and chemokines ideal for the recruitment of the patient's immune system to the tumor location. Moreover, by directing the patient's immune system to attack the initially targeted malignancy, it is likely that systemic clearance and long-term protection to the cancer is promoted. Though, pre-clinical *in vivo* studies using this MeV-GZMB virus is needed to confirm its intended effects. Nonetheless, we have demonstrated the generation and characterization of a novel proinflammatory oncolytic measles virus.

Finally, many types of cancers remain resistant to oncolytic viral therapy due to residual antiviral activity. This poses a significant issue for OV therapy as limited virus replication within

the tumor will reduce the efficacy of the cancer therapeutic. As a result, viral sensitizers were explored as an exogenous additive to OV therapy. Compounds, such as vanadyl sulfate and dimethyl fumarate, sensitize cancer cells to viral replication by abrogating their antiviral capabilities. Moreover, they also play a role in adaptive immunity by promoting the activation and proliferation of immune cells. Here, we demonstrated that a combinatorial therapy of MeV with either VS or DMF increases the viral replication and cancer cell killing ability in certain human and murine cancer models. The latter offers the opportunity, with further investigation, for the development of a novel MeV permissive murine cancer cell line which would benefit the oncolytic MeV research field greatly. Hence, additional studies are necessary to elucidate the exact mechanisms of action of these VSes in inducing MeV sensitization to cancer cells. Also, further research is required to establish a working syngeneic *in vivo* murine model for the combination treatment of VS and MeV. However, as a whole, this project has given valuable insights on the opportunities and benefits of combining viral sensitizers with oncolytic measles virus to develop an enhanced cancer therapeutic regimen.

In summary, this thesis illustrates current challenges facing oncolytic measles therapy for the treatment of cancer and demonstrates three distinct and innovative approaches in surmounting them. With every advancement in generating a better oncolytic virus therapeutic, we are nearing a tipping point where the fight with cancer will be in our favour. Unrelenting contributions and collaborations from scientists around the world have brought this field to this point. Herein lies my contribution: arming, pseudotyping, and enhancing the efficacy of oncolytic measles virus for a better cancer therapeutic.

REFERENCES

1. Brenner DR, Weir HK, Demers AA, et al. Projected estimates of cancer in Canada in 2020. *CMAJ*. 2020;192(9):E199-E205. doi:10.1503/cmaj.191292

2. Anand P, Kunnumakara AB, Sundaram C, et al. Cancer is a preventable disease that requires major lifestyle changes. *Pharmaceutical Research*. 2008;25(9):2097-2116. doi:10.1007/s11095-008-9661-9

3. Hanahan D, Weinberg RA. Hallmarks of Cancer: The Next Generation. *Cell*. 2011;144(5):646-674. doi:10.1016/J.CELL.2011.02.013

4. Katsoulidis E, Kaur S, Platanias LC. Deregulation of interferon signaling in malignant cells. *Pharmaceuticals*. 2010;3(2):406-418. doi:10.3390/ph3020406

5. Fuertes MB, Woo SR, Burnett B, Fu YX, Gajewski TF. Type I interferon response and innate immune sensing of cancer. *Trends in Immunology*. 2013;34(2):67-73. doi:10.1016/j.it.2012.10.004

6. Critchley-Thorne RJ, Simons DL, Yan N, et al. Impaired interferon signaling is a common immune defect in human cancer. *Proceedings of the National Academy of Sciences of the United States of America*. 2009;106(22):9010-9015. doi:10.1073/pnas.0901329106

7. Schoggins JW, Rice CM. Interferon-stimulated genes and their antiviral effector functions. *Current Opinion in Virology*. 2011;1(6):519-525. doi:10.1016/j.coviro.2011.10.008

8. Samuel CE. Antiviral actions of interferons. *Clinical Microbiology Reviews*. 2001;14(4):778-809. doi:10.1128/CMR.14.4.778-809.2001

9. Cattaneo R, Miest T, Shashkova E v., Barry MA. Reprogrammed viruses as cancer therapeutics: Targeted, armed and shielded. *Nature Reviews Microbiology*. 2008;6(7):529-540. doi:10.1038/nrmicro1927

10. Msaouel P, D. Iankov I, Dispenzieri A, Galanis E. Attenuated Oncolytic Measles Virus Strains as Cancer Therapeutics. *Current Pharmaceutical Biotechnology*. 2012;13(9):1732-1741. doi:10.2174/138920112800958896

11. Msaouel P, Opyrchal M, Dispenzieri A, et al. Clinical Trials with Oncolytic Measles Virus: Current Status and Future Prospects. *Current Cancer Drug Targets*. 2017;18(2):177-187. doi:10.2174/1568009617666170222125035

12. Leber MF, Neault S, Jirovec E, et al. Engineering and combining oncolytic measles virus for cancer therapy. *Cytokine and Growth Factor Reviews*. 2020;56:39-48. doi:10.1016/j.cytogfr.2020.07.005

13. Palosaari H, Parisien J-P, Rodriguez JJ, Ulane CM, Horvath CM. STAT Protein Interference and Suppression of Cytokine Signal Transduction by Measles Virus V Protein. *Journal of Virology*. 2003;77(13):7635-7644. doi:10.1128/jvi.77.13.7635-7644.2003

14. Barilla-LaBarca ML, Liszewski MK, Lambris JD, Hourcade D, Atkinson JP. Role of Membrane Cofactor Protein (CD46) in Regulation of C4b and C3b Deposited on Cells. *The Journal of Immunology*. 2002;168(12):6298-6304. doi:10.4049/jimmunol.168.12.6298

15. Buettner R, Huang M, Gritsko T, et al. Activated signal transducers and activators of transcription 3 signaling induces CD46 expression and protects human cancer cells from complement-dependent cytotoxicity. *Molecular Cancer Research*. 2007;5(8):823-832. doi:10.1158/1541-7786.MCR-06-0352

16. Dörig RE, Marcil A, Chopra A, Richardson CD. The human CD46 molecule is a receptor for measles virus (Edmonston strain). *Cell*. 1993;75(2):295-305. doi:10.1016/0092-8674(93)80071-L

17. Andtbacka RHI, Kaufman HL, Collichio F, et al. Talimogene laherparepvec improves durable response rate in patients with advanced melanoma. *Journal of Clinical Oncology*. 2015;33(25):2780-2788. doi:10.1200/JCO.2014.58.3377

18. Ledford H. Cancer-fighting viruses win approval. *Nature*. 2015;526(7575):622-623. doi:10.1038/526622a

19. Wong HH, Lemoine NR, Wang Y. Oncolytic viruses for cancer therapy: Overcoming the obstacles. *Viruses*. 2010;2(1):78-106. doi:10.3390/v2010078

20. Lund GA, Tyrrell DLJ, Bradley RD, Scraba DG. The molecular length of measles virus RNA and the structural organization of measles nucleocapsids. *Journal of General Virology*. 1984;65(9):1535-1542. doi:10.1099/0022-1317-65-9-1535

21. Guseva S, Milles S, Blackledge M, Ruigrok RWH. The Nucleoprotein and Phosphoprotein of Measles Virus. *Frontiers in Microbiology*. 2019;0(AUG):1832. doi:10.3389/FMICB.2019.01832

22. Kolakofsky D, Pelet T, Garcin D, Hausmann S, Curran J, Roux L. Paramyxovirus RNA Synthesis and the Requirement for Hexamer Genome Length: the Rule of Six Revisited. *Journal of Virology*. 1998;72(2):891-899. doi:10.1128/jvi.72.2.891-899.1998

23. Devaux P, Cattaneo R. Measles Virus Phosphoprotein Gene Products: Conformational Flexibility of the P/V Protein Amino-Terminal Domain and C Protein Infectivity Factor Function. *Journal of Virology*. 2004;78(21):11632-11640. doi:10.1128/jvi.78.21.11632-11640.2004

24. Iwasaki M, Takeda M, Shirogane Y, Nakatsu Y, Nakamura T, Yanagi Y. The Matrix Protein of Measles Virus Regulates Viral RNA Synthesis and Assembly by Interacting with the Nucleocapsid Protein. *Journal of Virology*. 2009;83(20):10374-10383. doi:10.1128/jvi.01056-09

25. Mühlebach MD, Mateo M, Sinn PL, et al. Adherens junction protein nectin-4 is the epithelial receptor for measles virus. *Nature*. 2011;480(7378):530-533. doi:10.1038/nature10639

26. Dhiman N, Jacobson RM, Poland GA. Measles virus receptors: SLAM and CD46. *Reviews in Medical Virology*. 2004;14(4):217-229. doi:10.1002/rmv.430

27. Yanagi Y, Takeda M, Ohno S. Measles virus: Cellular receptors, tropism and pathogenesis. *Journal of General Virology*. 2006;87(10):2767-2779. doi:10.1099/vir.0.82221-0

28. Nanda SK, Baron J, Royall E, Robinson L, Falciani F, Baron MD. Infection of bovine dendritic cells by rinderpest or measles viruses induces different changes in host transcription. *Virology*. 2009;395(2):223-231. doi:10.1016/j.virol.2009.09.031

29. Kato SI, Nagata K, Takeuchi K. Cell tropism and pathogenesis of measles virus in monkeys. *Frontiers in Microbiology*. 2012;3(JAN):14. doi:10.3389/fmicb.2012.00014

30. Heneen WK, Nichols WW, Levan A, Norrby E. Studies on syncytia formation in a cell line (LU 106) of human origin after treatment with measles virus. *Hereditas*. 1967;57(3):369-372. doi:10.1111/j.1601-5223.1967.tb02121.x

31. Brindley MA, Takeda M, Plattet P, Plemper RK. Triggering the measles virus membrane fusion machinery. *Proceedings of the National Academy of Sciences of the United States of America*. 2012;109(44):17750. doi:10.1073/pnas.1210925109

32. Griffin DE, Pan CH. Measles: Old vaccines, new vaccines. *Current Topics in Microbiology and Immunology*. 2009;330:191-212. doi:10.1007/978-3-540-70617-5_10

33. Ungerechts G, Springfeld C, Frenzke ME, et al. An immunocompetent murine model for oncolysis with an armed and targeted measles virus. *Molecular Therapy*. 2007;15(11):1991-1997. doi:10.1038/sj.mt.6300291

34. Allen C, Vongpunsawad S, Nakamura T, et al. Retargeted oncolytic measles strains entering via the EGFRvIII receptor maintain significant antitumor activity against gliomas with increased tumor specificity. *Cancer Research*. 2006;66(24):11840-11850. doi:10.1158/0008-5472.CAN-06-1200

35. Bucheit AD, Kumar S, Grote DM, et al. An oncolytic measles virus engineered to enter cells through the CD20 antigen. *Molecular Therapy*. 2003;7(1):62-72. doi:10.1016/S1525-0016(02)00033-3

36. Martin A, Staeheli P, Schneider U. RNA Polymerase II-Controlled Expression of Antigenomic RNA Enhances the Rescue Efficacies of Two Different Members of the Mononegavirales Independently of the Site of Viral Genome Replication. *Journal of Virology*. 2006;80(12):5708-5715. doi:10.1128/jvi.02389-05

37. Radecke F, Spielhofer P, Schneider H, et al. Rescue of measles viruses from cloned DNA. *EMBO Journal*. 1995;14(23):5773-5784. doi:10.1002/j.1460-2075.1995.tb00266.x

38. Spearman C. The method of 'right and wrong cases' ('constant stimuli') without gauss's formulae. *British Journal of Psychology, 1904-1920*. 1908;2(3):227-242. doi:10.1111/j.2044-8295.1908.tb00176.x

39. Kärber G. Beitrag zur kollektiven Behandlung pharmakologischer Reihenversuche. *Naunyn-Schmiedebergs Archiv für Experimentelle Pathologie und Pharmakologie*. 1931;162(4):480-483. doi:10.1007/BF01863914

40. Laksono BM, Vries RD de, McQuaid S, Duprex WP, Swart RL de. Measles Virus Host Invasion and Pathogenesis. *Viruses*. 2016;8(8). doi:10.3390/V8080210

41. Mina M, Kula T, Leng Y, et al. Measles virus infection diminishes preexisting antibodies that offer protection from other pathogens. *Science (New York, NY)*. 2019;366(6465):599-606. doi:10.1126/SCIENCE.AAY6485

42. Petrova V, Sawatsky B, Han A, et al. Incomplete genetic reconstitution of B cell pools contributes to prolonged immunosuppression after measles. *Science immunology*. 2019;4(41). doi:10.1126/SCIIMMUNOL.AAY6125

43. Baker JP. The First Measles Vaccine. *Pediatrics*. 2011;128(3):435-437. doi:10.1542/PEDS.2011-1430

44. Griffin D. Measles Vaccine. *Viral immunology*. 2018;31(2):86-95. doi:10.1089/VIM.2017.0143

45. Galanis E, Atherton PJ, Maurer MJ, et al. Oncolytic measles virus expressing the sodium iodide symporter to treat drug-resistant ovarian cancer. *Cancer Research*. 2015;75(1):22-30. doi:10.1158/0008-5472.CAN-14-2533

46. Russell SJ, Federspiel MJ, Peng KW, et al. Remission of disseminated cancer after systemic oncolytic virotherapy. *Mayo Clinic Proceedings*. 2014;89(7):926-933. doi:10.1016/j.mayocp.2014.04.003

47. Hudacek AW, Navaratnarajah CK, Cattaneo R. Development of measles virus-based shielded oncolytic vectors: Suitability of other paramyxovirus glycoproteins. *Cancer Gene Therapy*. 2013;20(2):109-116. doi:10.1038/cgt.2012.92

48. Spielhofer P, Bächi T, Fehr T, et al. Chimeric Measles Viruses with a Foreign Envelope. *Journal of Virology*. 1998;72(3):2150-2159. doi:10.1128/jvi.72.3.2150-2159.1998

49. Miest TS, Yaiw KC, Frenzke M, et al. Envelope-chimeric entry-targeted measles virus escapes neutralization and achieves oncolysis. *Molecular Therapy*. 2011;19(10):1813-1820. doi:10.1038/mt.2011.92

50. Bah ES, Nace RA, Peng KW, Muñoz-Alía MÁ, Russell SJ. Retargeted and Stealth Modified Oncolytic Measles Viruses for Systemic Cancer Therapy in Measles-Immune Patients. *Molecular cancer therapeutics*. 2020;19(10):2057. doi:10.1158/1535-7163.MCT-20-0134

51. Muñoz-Alía MÁ, Nace RA, Tischer A, et al. Mev-stealth: A cd46-specific oncolytic measles virus resistant to neutralization by measles-immune human serum. Bukreyev A, ed. *PLOS Pathogens*. 2021;17(2):e1009283. doi:10.1371/journal.ppat.1009283

52. Finkelshtein D, Werman A, Novick D, Barak S, Rubinstein M. LDL receptor and its family members serve as the cellular receptors for vesicular stomatitis virus. *Proceedings of the National Academy of Sciences of the United States of America*. 2013;110(18):7306-7311. doi:10.1073/pnas.1214441110

53. Wignall-Fleming EB, Hughes DJ, Vattipally S, et al. Analysis of Paramyxovirus Transcription and Replication by High-Throughput Sequencing. *Journal of Virology*. 2019;93(17). doi:10.1128/jvi.00571-19

54. Toyoda T, Sakaguchi T, Imai K, et al. Structural comparison of the cleavage-activation site of the fusion glycoprotein between virulent and avirulent strains of newcastle disease virus. *Virology*. 1987;158(1):242-247. doi:10.1016/0042-6822(87)90261-3

55. Glickman RL, Syddall RJ, Iorio RM, Sheehan JP, Bratt MA. Quantitative basic residue requirements in the cleavage-activation site of the fusion glycoprotein as a determinant of virulence for Newcastle disease virus. *Journal of Virology*. 1988;62(1):354-356. doi:10.1128/jvi.62.1.354-356.1988

56. Leeuw OS de, Koch G, Hartog L, Ravenshorst N, Peeters BPH. Virulence of Newcastle disease virus is determined by the cleavage site of the fusion protein and by both the stem region and globular head of the haemagglutinin–neuraminidase protein. *Journal of General Virology*. 2005;86(6):1759-1769. doi:10.1099/VIR.0.80822-0

57. Chu Z, Gao X, Liu H, et al. Newcastle disease virus selectively infects dividing cells and promotes viral proliferation. *Veterinary Research*. 2019;50(1):27. doi:10.1186/s13567-019-0644-0

58. Cheng X, Wang W, Xu Q, et al. Genetic Modification of Oncolytic Newcastle Disease Virus for Cancer Therapy. *Journal of Virology*. 2016;90(11):5343-5352. doi:10.1128/jvi.00136-16

59. Huang Z, Panda A, Elankumaran S, Govindarajan D, Rockemann DD, Samal SK. The Hemagglutinin-Neuraminidase Protein of Newcastle Disease Virus Determines Tropism and Virulence. *Journal of Virology*. 2004;78(8):4176. doi:10.1128/JVI.78.8.4176-4184.2004

60. Muñoz-Alía MA, Casasnovas JM, Celma ML, Carabaña J, Liton PB, Fernandez-Muñoz R. Measles Virus Hemagglutinin epitopes immunogenic in natural infection and vaccination are targeted by broad or genotype-specific neutralizing monoclonal antibodies. *Virus Research*. 2017;236:30-43. doi:10.1016/j.virusres.2017.04.018

61. Kennedy JM, Earle JAP, Omar S, et al. Canine and Phocine Distemper Viruses: Global Spread and Genetic Basis of Jumping Species Barriers. *Viruses*. 2019;11(10). doi:10.3390/V11100944

62. Ida H, Utz PJ, Anderson P, Eguchi K. Granzyme B and natural killer (NK) cell death. *Modern Rheumatology*. 2005;15(5):315-322. doi:10.1007/s10165-005-0426-6

63. Boivin WA, Cooper DM, Hiebert PR, Granville DJ. Intracellular versus extracellular granzyme B in immunity and disease: Challenging the dogma. *Laboratory Investigation*. 2009;89(11):1195-1220. doi:10.1038/labinvest.2009.91

64. Pham CTN, Ley TJ. Dipeptidyl peptidase I is required for the processing and activation of granzymes A and B in vivo. *Proceedings of the National Academy of Sciences*. 1999;96(15):8627-8632. doi:10.1073/PNAS.96.15.8627

65. Woodsworth DJ, Dreolini L, Abraham L, Holt RA. Targeted Cell-to-Cell Delivery of Protein Payloads via the Granzyme-Perforin Pathway. *Molecular Therapy Methods & Clinical Development*. 2017;7:132. doi:10.1016/J.OMTM.2017.10.003

66. Sutton VR, Waterhouse NJ, Browne KA, et al. Residual active granzyme B in cathepsin C–null lymphocytes is sufficient for perforin-dependent target cell apoptosis. *The Journal of Cell Biology*. 2007;176(4):425. doi:10.1083/JCB.200609077

67. Grifliths GM, Isaaz S. Granzymes A and B Are Targeted to the Lytic Granules of Lymphocytes by the Mannose-6-Phosphate Receptor. *The Journal of Cell Biology*. 1993;120(4):885-896.

68. Metkar SS, Wang B, Ebbs ML, et al. Granzyme B activates procaspase-3 which signals a mitochondrial amplification loop for maximal apoptosis. *The Journal of Cell Biology*. 2003;160(6):875. doi:10.1083/JCB.200210158

69. Buzza MS, Zamurs L, Sun J, et al. Extracellular Matrix Remodeling by Human Granzyme B via Cleavage of Vitronectin, Fibronectin, and Laminin *. *Journal of Biological Chemistry*. 2005;280(25):23549-23558. doi:10.1074/JBC.M412001200

70. Conry RM, Westbrook B, McKee S, Norwood TG. Talimogene laherparepvec: First in class oncolytic virotherapy. *Human Vaccines & Immunotherapeutics*. 2018;14(4):839. doi:10.1080/21645515.2017.1412896

71. Liu BL, Robinson M, Han Z-Q, et al. ICP34.5 deleted herpes simplex virus with enhanced oncolytic, immune stimulating, and anti-tumour properties. *Gene Therapy 2003 10:4*. 2003;10(4):292-303. doi:10.1038/sj.gt.3301885

72. Kaufman HL, Ruby CE, Hughes T, Slingluff CL. Current status of granulocyte–macrophage colony-stimulating factor in the immunotherapy of melanoma. *Journal for ImmunoTherapy of Cancer*. 2014;2(1):11. doi:10.1186/2051-1426-2-11

73. Grossardt C, Engeland CE, Bossow S, et al. Granulocyte-Macrophage Colony-Stimulating Factor-Armed Oncolytic Measles Virus Is an Effective Therapeutic Cancer Vaccine. *https://home-liebertpub-com.proxy.bib.uottawa.ca/hum*. 2013;24(7):644-654. doi:10.1089/HUM.2012.205

74. Tesniere A, Panaretakis T, Kepp O, et al. Molecular characteristics of immunogenic cancer cell death. *Cell Death & Differentiation 2008 15:1*. 2007;15(1):3-12. doi:10.1038/sj.cdd.4402269

75. Matveeva O v, Guo ZS, Shabalina SA, Chumakov PM. Oncolysis by paramyxoviruses: multiple mechanisms contribute to therapeutic efficiency. *Molecular Therapy Oncolytics*. 2015;2:15011. doi:10.1038/MTO.2015.11

76. Donnelly OG, Errington-Mais F, Steele L, et al. Measles virus causes immunogenic cell death in human melanoma. *Gene therapy*. 2013;20(1):7. doi:10.1038/GT.2011.205

77. Caldas H, Jaynes FO, Boyer MW, Hammond S, Altura RA. Survivin and Granzyme B–induced apoptosis, a novel anticancer therapy. *Molecular Cancer Therapeutics*. 2006;5(3):693-703. doi:10.1158/1535-7163.MCT-05-0423

78. Trapani JA, Sutton VR. Granzyme B: pro-apoptotic, antiviral and antitumor functions. *Current Opinion in Immunology*. 2003;15(5):533-543. doi:10.1016/S0952-7915(03)00107-9

79. Marcet-Palacios M, Duggan BL, Shostak I, et al. Granzyme B Inhibits Vaccinia Virus Production through Proteolytic Cleavage of Eukaryotic Initiation Factor 4 Gamma 3. *PLoS Pathogens*. 2011;7(12):1002447. doi:10.1371/JOURNAL.PPAT.1002447

80. Velotti F, Barchetta I, Cimini FA, Cavallo MG. Granzyme B in Inflammatory Diseases: Apoptosis, Inflammation, Extracellular Matrix Remodeling, Epithelial-to-Mesenchymal Transition and Fibrosis. *Frontiers in Immunology*. 2020;11:1. doi:10.3389/FIMMU.2020.587581

81. Belmokhtar CA, Hillion J, Ségal-Bendirdjian E. Staurosporine induces apoptosis through both caspase-dependent and caspase-independent mechanisms. *Oncogene 2001 20:26*. 2001;20(26):3354-3362. doi:10.1038/sj.onc.1204436

82. Malsy M, Bitzinger D, Graf B, Bundscherer A. Staurosporine induces apoptosis in pancreatic carcinoma cells PaTu 8988t and Panc-1 via the intrinsic signaling pathway. *European Journal of Medical Research 2019 24:1*. 2019;24(1):1-8. doi:10.1186/S40001-019-0365-X

83. Sato H, Masuda M, Kanai M, Tsukiyama-Kohara K, Yoneda M, Kai C. Measles Virus N Protein Inhibits Host Translation by Binding to eIF3-p40. *Journal of Virology*. 2007;81(21):11569. doi:10.1128/JVI.00570-07

84. Walsh JG, Cullen SP, Sheridan C, Lüthi AU, Gerner C, Martin SJ. Executioner caspase-3 and caspase-7 are functionally distinct proteases. *Proceedings of the National Academy of Sciences*. 2008;105(35):12815-12819. doi:10.1073/PNAS.0707715105

85. Brentnall M, Rodriguez-Menocal L, de Guevara RL, Cepero E, Boise LH. Caspase-9, caspase-3 and caspase-7 have distinct roles during intrinsic apoptosis. *BMC Cell Biology 2013 14:1*. 2013;14(1):1-9. doi:10.1186/1471-2121-14-32

86. Wang B, Yan X, Guo Q, et al. Deficiency of caspase 3 in tumor xenograft impairs therapeutic effect of measles virus Edmoston strain. *Oncotarget*. 2015;6(18):16019. doi:10.18632/ONCOTARGET.3496

87. Hunter AM, Kottachchi D, Lewis J, Duckett CS, Korneluk RG, Liston P. A Novel Ubiquitin Fusion System Bypasses the Mitochondria and Generates Biologically Active Smac/DIABLO *. *Journal of Biological Chemistry*. 2003;278(9):7494-7499. doi:10.1074/JBC.C200695200

88. Autissier P, Soulas C, Burdo TH, Williams KC. Evaluation of a 12-color flow cytometry panel to study lymphocyte, monocyte, and dendritic cell subsets in humans. *Cytometry Part A*. 2010;77A(5):410-419. doi:10.1002/CYTO.A.20859

89. Acosta Davila JA, Hernandez De Los Rios A. An Overview of Peripheral Blood Mononuclear Cells as a Model for Immunological Research of Toxoplasma gondii and Other Apicomplexan Parasites. *Frontiers in Cellular and Infection Microbiology*. 2019;0:24. doi:10.3389/FCIMB.2019.00024

90. Saleiro D, Platanias LC. Interferon signaling in cancer. Non-canonical pathways and control of intracellular immune checkpoints. *Seminars in Immunology*. 2019;43:101299. doi:10.1016/J.SMIM.2019.101299

91. Zhao J, Chen X, Herjan T, Li X. The role of interleukin-17 in tumor development and progression. *Journal of Experimental Medicine*. 2020;217(1). doi:10.1084/JEM.20190297

92. Lopez-Castejon G, Brough D. Understanding the mechanism of IL-1β secretion. *Cytokine & Growth Factor Reviews*. 2011;22(4):189. doi:10.1016/J.CYTOGFR.2011.10.001

93. Liu Y, Cai Y, Liu L, Wu Y, Xiong X. Crucial biological functions of CCL7 in cancer. *PeerJ*. 2018;6(6). doi:10.7717/PEERJ.4928

94. Baba T, Mukaida N. Role of macrophage inflammatory protein (MIP)-1α/CCL3 in leukemogenesis. *Molecular & Cellular Oncology*. 2014;1(1). doi:10.4161/MCO.29899

95. Persaud L, Jesus D de, Brannigan O, et al. Mechanism of Action and Applications of Interleukin 24 in Immunotherapy. *International Journal of Molecular Sciences*. 2016;17(6). doi:10.3390/IJMS17060869

96. Zhao L, Gu J, Dong A, et al. Potent Antitumor Activity of Oncolytic Adenovirus Expressing mda-7/IL-24 for Colorectal Cancer. *https://home.liebertpub.com/hum*. 2005;16(7):845-858. doi:10.1089/HUM.2005.16.845

97. Wetzel K, Struyf S, Damme J van, et al. MCP-3 (CCL7) delivered by parvovirus MVMp reduces tumorigenicity of mouse melanoma cells through activation of T lymphocytes and NK cells. *International Journal of Cancer*. 2007;120(6):1364-1371. doi:10.1002/IJC.22421

98. Martinez-Quintanilla J, Seah I, Chua M, Shah K. Oncolytic viruses: overcoming translational challenges. *The Journal of Clinical Investigation*. 2019;129(4):1407-1418. doi:10.1172/JCI122287

99. Kaufman HL, Kohlhapp FJ, Zloza A. Oncolytic viruses: a new class of immunotherapy drugs. *Nature Reviews Drug Discovery 2015 14:9*. 2015;14(9):642-662. doi:10.1038/nrd4663

100. Zheng M, Huang J, Tong A, Yang H. Oncolytic Viruses for Cancer Therapy: Barriers and Recent Advances. *Molecular Therapy Oncolytics*. 2019;15:234. doi:10.1016/J.OMTO.2019.10.007

101. Comins C, Simpson GR, Rogers W, et al. Synergistic antitumour effects of rapamycin and oncolytic reovirus. *Cancer Gene Therapy 2018 25:5*. 2018;25(5):148-160. doi:10.1038/s41417-018-0011-8

102. Chen HP, Zhao YT, Zhao TC. Histone Deacetylases and Mechanisms of Regulation of Gene Expression (Histone deacetylases in cancer). *Critical reviews in oncogenesis*. 2015;20(1-2):35. Accessed August 8, 2021. /pmc/articles/PMC4809735/

103. Gallinari P, Marco S di, Jones P, Pallaoro M, Steinkühler C. HDACs, histone deacetylation and gene transcription: from molecular biology to cancer therapeutics. *Cell Research 2007 17:3*. 2007;17(3):195-211. doi:10.1038/sj.cr.7310149

104. Suraweera A, O'Byrne KJ, Richard DJ. Combination Therapy With Histone Deacetylase Inhibitors (HDACi) for the Treatment of Cancer: Achieving the Full Therapeutic Potential of HDACi. *Frontiers in Oncology*. 2018;0(MAR):92. doi:10.3389/FONC.2018.00092

105. Li Y, Seto E. HDACs and HDAC Inhibitors in Cancer Development and Therapy. *Cold Spring Harbor Perspectives in Medicine*. 2016;6(10). doi:10.1101/CSHPERSPECT.A026831

106. Nakashima H, Nguyen T, Chiocca EA. Combining HDAC inhibitors with oncolytic virotherapy for cancer therapy. *Oncolytic Virotherapy*. 2015;4:183. doi:10.2147/OV.S66081

107. Escobar-Zarate D, Liu Y-P, Suksanpaisan L, Russell S, Peng K-W. Overcoming cancer cell resistance to VSV oncolysis with JAK1/2 inhibitors. *Cancer gene therapy*. 2013;20(10):582. doi:10.1038/CGT.2013.55

108. Saidu NEB, Noé G, Cerles O, et al. Dimethyl Fumarate Controls the NRF2/DJ-1 Axis in Cancer Cells: Therapeutic Applications. *Molecular Cancer Therapeutics*. 2017;16(3):529-539. doi:10.1158/1535-7163.MCT-16-0405

109. Kastrati I, Siklos MI, Calderon-Gierszal EL, et al. Dimethyl Fumarate Inhibits the Nuclear Factor κB Pathway in Breast Cancer Cells by Covalent Modification of p65 Protein. *The Journal of Biological Chemistry*. 2016;291(7):3639. doi:10.1074/JBC.M115.679704

110. Selman M, Ou P, Rousso C, et al. Dimethyl fumarate potentiates oncolytic virotherapy through NF-κB inhibition. *Science Translational Medicine*. 2018;10(425):1613. doi:10.1126/SCITRANSLMED.AAO1613

111. Irving E, Stoker AW. Vanadium Compounds as PTP Inhibitors. *Molecules : A Journal of Synthetic Chemistry and Natural Product Chemistry*. 2017;22(12). doi:10.3390/MOLECULES22122269

112. Fugono J, Yasui H, Sakurai H. Improvement of diabetic states in streptozotocin-induced type 1 diabetic rats by vanadyl sulfate in enteric-coated capsules. *Journal of Pharmacy and Pharmacology*. 2010;57(5):665-669. doi:10.1211/0022357055993

113. Thompson KH, Lichter J, LeBel C, Scaife MC, McNeill JH, Orvig C. Vanadium treatment of type 2 diabetes: A view to the future. *Journal of Inorganic Biochemistry*. 2009;103(4):554-558. doi:10.1016/J.JINORGBIO.2008.12.003

114. Sekar N, Li J, Shechter Y. Vanadium Salts as Insulin Substitutes: Mechanisms of Action, a Scientific and Therapeutic Tool in Diabetes Mellitus Research. *http://dx.doi.org/103109/10409239609108721*. 2008;31(5):339-359. doi:10.3109/10409239609108721

115. Evangelou AM. Vanadium in cancer treatment. *Critical Reviews in Oncology/Hematology*. 2002;42(3):249-265. doi:10.1016/S1040-8428(01)00221-9

116. Bishayee A, Waghray A, Patel MA, Chatterjee M. Vanadium in the detection, prevention and treatment of cancer: The in vivo evidence. *Cancer Letters*. 2010;294(1):1-12. doi:10.1016/J.CANLET.2010.01.030

117. Naso LG, Martínez VR, Ferrer EG, Williams PAM. Antimetastatic effects of VOflavonoid complexes on A549 cell line. *Journal of Trace Elements in Medicine and Biology*. 2021;64:126690. doi:10.1016/J.JTEMB.2020.126690

118. Dankhoff K, Ahmad A, Weber B, Biersack B, Schobert R. Anticancer properties of a new non-oxido vanadium(IV) complex with a catechol-modified 3,3'-diindolylmethane ligand. *Journal of Inorganic Biochemistry*. 2019;194:1-6. doi:10.1016/J.JINORGBIO.2019.02.005

119. Amante C, Sousa-Coelho AL de, Aureliano M. Vanadium and Melanoma: A Systematic Review. *Metals 2021, Vol 11, Page 828*. 2021;11(5):828. doi:10.3390/MET11050828

120. Tsave O, Petanidis S, Kioseoglou E, et al. Role of Vanadium in Cellular and Molecular Immunology: Association with Immune-Related Inflammation and Pharmacotoxicology Mechanisms. *Oxidative Medicine and Cellular Longevity*. 2016;2016. doi:10.1155/2016/4013639

121. Ha D, Joo H, Ahn G, et al. Jeju ground water containing vanadium induced immune activation on splenocytes of low dose γ-rays-irradiated mice. *Food and Chemical Toxicology*. 2012;50(6):2097-2105. doi:10.1016/J.FCT.2012.03.041

122. Valko M, Morris H, Cronin M. Metals, Toxicity and Oxidative Stress. *Current Medicinal Chemistry*. 2005;12(10):1161-1208. doi:10.2174/0929867053764635

123. Wang K, Cui H, Deng Y, et al. Effect of Dietary Vanadium on the Ileac T Cells and Contents of Cytokines in Broilers. *Biological Trace Element Research 2011 147:1*. 2011;147(1):113-119. doi:10.1007/S12011-011-9274-8

124. Selman M, Rousso C, Bergeron A, et al. Multi-modal Potentiation of Oncolytic Virotherapy by Vanadium Compounds. *Molecular Therapy*. 2018;26(1):56-69. doi:10.1016/j.ymthe.2017.10.014

125. McAusland TM, Vloten JP van, Santry LA, et al. Combining vanadyl sulfate with Newcastle disease virus potentiates rapid innate immune-mediated regression with curative potential in murine cancer models. *Molecular Therapy Oncolytics*. 2021;20:306. doi:10.1016/J.OMTO.2021.01.009

126. Yanagi Y, Hu H-L, Seya T, Yoshikura H. Measles virus infects mouse fibroblast cell lines, but its multiplication is severely restricted in the absence of CD46. *Archives of Virology 1994 138:1*. 1994;138(1):39-53. doi:10.1007/BF01310037

127. Evlashev A, Valentin H, Rivailler P, Azocar O, Rabourdin-Combe C, Horvat B. Differential permissivity to measles virus infection of human and CD46-transgenic murine lymphocytes. *Journal of General Virology*. 2001;82(9):2125-2129. doi:10.1099/0022-1317-82-9-2125

128. Horvat B, Rivailler P, Varior-Krishnan G, Cardoso A, Gerlier D, Rabourdin-Combe C. Transgenic mice expressing human measles virus (MV) receptor CD46 provide cells exhibiting different permissivities to MV infections. *Journal of Virology*. 1996;70(10):6673-6681. doi:10.1128/JVI.70.10.6673-6681.1996

129. Vincent S, Tigaud I, Schneider H, Buchholz CJ, Yanagi Y, Gerlier D. Restriction of Measles Virus RNA Synthesis by a Mouse Host Cell Line: trans -Complementation by Polymerase Components or a Human Cellular Factor(s) . *Journal of Virology*. 2002;76(12):6121-6130. doi:10.1128/JVI.76.12.6121-6130.2002

130. Jing Y, Tong C, Zhang J, et al. Tumor and vascular targeting of a novel oncolytic measles virus retargeted against the urokinase receptor. *Cancer Research*. 2009;69(4):1459-1468. doi:10.1158/0008-5472.CAN-08-2628

131. Nakamura T, Peng KW, Harvey M, et al. Rescue and propagation of fully retargeted oncolytic measles viruses. *Nature Biotechnology*. 2005;23(2):209-214. doi:10.1038/nbt1060

132. Chou TC. Theoretical basis, experimental design, and computerized simulation of synergism and antagonism in drug combination studies. *Pharmacological Reviews*. 2006;58(3):621-681. doi:10.1124/pr.58.3.10

133. Loewe, Häussler, Grein, et al. Forced Degradation Studies to Identify Critical Process Parameters for the Purification of Infectious Measles Virus. *Viruses*. 2019;11(8):725. doi:10.3390/v11080725

CONTRIBUTIONS OF COLLABORATORS

The generation of MeV P-EGFP HmuPA in addition to the flowcytometry experiments was done with Dr. Carole Achard. The RNAseq experiments was done with Dr. Adrian Pelin from the Dr. John Bell lab. Experimental design of the pseudotyping project was conceived with Dr. Sascha Bossow. *In vivo* and *ex* vivo work was done with Andrew Chen. Supervision and project design was done by Dr. Guy Ungerechts, Dr. Jean-Simon Diallo, and Dr. Mathias Leber. Thesis editing was done by Dr. Mathias Leber, Dr. Nafisa Neault, and Dr. Rozanne Arulanandam.

APPENDIX

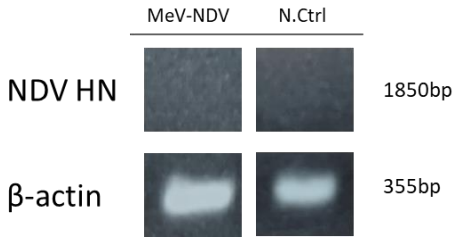

Figure S3.1. MeV-NDV pseudotype rescue does not produce any detectable viral mRNA via RT-PCR. PCR was done on VP1 virus samples. RNA was harvested from Vero cells 48 hours post-infection (blind passaging) followed by RT-PCR processing using the SuperScript III First-Strand Synthesis System by Invitrogen SOP. N.Ctrl was an MeV-NDV rescue without MeV L Co-transfection. β-actin was used as a housekeeping gene. Expected amplicon size is shown on the right of the figure.